Membrane-Targeting Approaches for Enhanced Cell Destruction with Irreversible Electroporation

A DISSERTATION
SUBMITTED TO THE FACULTY OF
UNIVERSITY OF MINNESOTA
BY

Chunlan Jiang

IN PARTIAL FULFILLMENT OF THE REQUIREMENTS
FOR THE DEGREE OF
DOCTOR OF PHILOSOPHY

Advisor: John C. Bischof

May 2014

© Chunlan Jiang 2014

Acknowledgements

This dissertation would not have been possible without the support (both professional and personal) of a great number of people. I wish to thank, first and foremost, my advisor Professor John Bischof for his inspiration and guidance throughout this endeavor. I learned a lot during my time here in the University of Minnesota from his critical thinking and genuine attitude towards research. I am extremely grateful to him for providing such wonderful support to my graduate career despite his busy schedules.

I was also very fortunate to work in a friendly and supportive team in the Bioheat and Mass Transfer Lab. I would like to express my gratitude for Zhenpeng Qin, who introduced me to this lab and provided lots of help and useful discussions that helped me started this work. I would also like to thank Dr. Mithun Shenoi, Dr. Jeunghwan Choi, and Dr. Michael Etheridge for their technical help and general directions throughout this project. In addition, Pong Patana-anake, Dushyant Mehra, and Connie Chung offered significant experimental support at various stages in this work.

My graduate program also offered me the opportunity to collaborate with a variety of research teams investigating therapeutic and imaging technologies involved with the use of pre-clinical animal models. I would like to thank Professor Paul Iaizzo and Dr. Ryan Goff, Professor Shai Ashkenazi and Qi Shao, and Professor Bin He and Leo Mariappan for giving me the chance to gain broader experiences in the biomedical scientific research field and for the enjoyment from the success of our collaborative projects. I would also like to thank for the financial support during the first years of my program by Ethicon Endo-Surgery. Both Gary Long and Peter Shires from Ethicon have provided insightful discussions and technical support at the early stage of this work.

I am also very grateful to Professor Rafael Davalos from the Virginia Tech-Wake Forest University for reviewing the manuscript of Chapter 1 and provided many important suggestions which enhanced this thesis.

Last, but certainly not least, I would like to thank my family and friends for helping me maintain a balanced life beyond school. Thanks to my parents for everything they have given me. Thanks to my sister for listening to me and help me make wiser life choices. Thanks to my friends for all the good times we shared together.

Dedication

I would like to dedicate this thesis to my parents, *Jiyue Shi and Mingyu Jiang*, who have given endless love and support to me. Their strong personalities, hard-working spirit, and selfless love to the family are what I would learn for a lifetime.

Abstract

Irreversible Electroporation (IRE) has gained increasing popularity in the cancer treatment field during the past decade due to many advantages over other focal therapies. Despite early success in pre-clinical and clinical IRE trials, in vivo studies have shown that IRE suffers from an inability to destroy large volumes of cancer tissue without repeating treatment and/or increasing the applied electrical dose to dangerous levels. There are approaches to expand the treatment volume by IRE with the addition of chemotherapeutic or cytotoxic agents. While these studies demonstrated improved cell killing, the focus was on enhancing the ability of chemotherapeutic drugs or cytotoxic agents to enter and kill the cancer cells rather than enhancing the efficacy of IRE itself.

Therefore, the aim of this work is to investigate the ability to increase the destructive capability of IRE without relying on cytotoxic drugs. Specifically, mechanisms that directly modify membrane properties should reduce the voltage threshold for lethal permeabilization and therefore increase the efficacy of cell killing and therefore the volume treated after a given IRE level. Two methods to achieve these changes are proposed in this study: 1) addition of surfactant (e.g. Dimethyl sulfoxide, or DMSO) to directly interact with membrane lipids thereby changing membrane line tension and surface tension, and 2) use of pulse timing (i.e. introduction and persistence of defects in the membrane between pulses).

Here then we began by Investigation of IRE enhancement in vitro to understand the impacts of our proposed mechanisms and their ideal working parameters. We found that the best enhancement effect was achieved with addition of 5% v/v DMSO, which resulted in a significant increase of 75% more cell destruction compared to baseline IRE.

Similarly with pulse timing, when dividing the pulses into three trains with 30s delays in between, an enhancement of 67% more cell destruction was achieved compared to baseline IRE.

Next we tested our IRE enhancement approaches in an in vivo dorsal skin fold chamber (DSFC) model of prostate cancer with optimal parameters selected from our in vitro experiments. The results reproducibly showed that more than 120% and 101% enhancement in the treatment volume were achieved by the addition of DMSO and pulse timing, respectively, with two independent injury assessment methods (histological and perfusion defect).

Finally, we translated one of the enhancement approaches (pulse timing) to an in vivo hind limb model of prostate cancer and demonstrated that more than 33% additional tumor destruction and 2 weeks longer tumor growth delay could be achieved compared to baseline IRE treatment without relying on any cytotoxic drugs or agents.

Because DMSO is commercially available and regularly used at low concentrations (<10% v/v) in clinic, this approach could easily be integrated into current IRE procedures to increase the treatment efficacy. In addition, introducing pulse timing delays in IRE also increases the destructive potential of IRE without the introduction of any foreign agents into the body. Further opportunities exist in improving the adjuvant delivery methods, optimizing the pulse timing delivery approach and understanding the fundamental mechanisms of IRE. Nevertheless, we suggest that the simple and safe nature of our proposed approaches compared with cytotoxic drugs may help to translate IRE into the clinic.

Tables of Contents

List of Tables

List of Figures

Chapter 1. *A Review of Basic to Clinical Studies of Irreversible Electroporation Therapy*

Contributing Authors: Chunlan Jiang, Rafael Davalos, and John C. Bischof

The following chapter is under review in publication:
C. Jiang, R. Davalos, and J. C. Bischof, “A Review of Basic to Clinical Studies of Irreversible Electroporation Therapy,” IEEE Trans. on Biomed. Eng., 2014.

1.1 Introduction

Electroporation, also known as electropermeabilization, is a technique that utilizes high magnitude electric pulses (1000s of Volts/cm) to induce permeability increase in cell membranes. While some of the molecular events that take place at the membrane level have not been fully elucidated, there is general agreement in the literature [1], [2] that nm-sized metastable structural defects are created when the plasma membrane is exposed to the external pulsed electric field. These defects are thought to be the source of the increased permeability from electroporation first used for material (i.e. DNA, protein, molecule) transfer into cells and then later as a therapeutic modality to treat diseases as reviewed below.

The first observation of electroporation was reported in the 1950s on electrically stimulated membranes, and was described as “membrane breakdown” [3]. Soon thereafter, the non-thermal killing effect of strong electric field pulses was discovered and reported by Sale in a study on micro-organisms [4]. Many studies followed into the early 1990s demonstrating the utility of electroporation in molecular biology, mainly as a method to introduce foreign molecules into living cells. Although further exploration and

optimization studies continue, electroporation is now sufficiently mature for commercial application for molecular and gene transfer *in vitro*, as has been reviewed by Jaroszeski [5]–[7].

The introduction of electroporation to cancer therapy originated from one of its drug delivery applications. Specifically, electroporation was used to assist uptake of chemo drug molecules into tumor cells [8]. The pairing of electroporation and chemo drug delivery quickly gained popularity and is an independent treatment termed electrochemotherapy (ECT). ECT has been translated to clinical practice [9]–[12] with reported objective response rates ranging from 72 to 100% [13], [14]. As a result ECT is one of the most well-established clinical applications of electroporation today [15].

In 2005, the concept of using electroporation as a monotherapy (i.e. without cytotoxic drugs or in conjunction with thermal effects) to destroy tissue was proposed by Davalos, Mir, and Rubinsky [16]. The term “irreversible electroporation (IRE)” was used to distinguish between cell destruction rather than reversible permeabilization used in previous embodiments of electroporation for molecular biology applications. In this study, IRE alone showed the ability to destroy undesirable tissues in the body in a manner similar to more traditional focal thermal therapies such as radiofrequency (RF) heating or cryosurgery. The advantages over thermal therapy were immediately realized due to IRE’s potential to (1) reduce collateral thermal effects (i.e. over-treatment) and (2) lack of the influence of local blood perfusion on treatment outcome (i.e. no blood sink or source to heat transfer). The new application of IRE as an independent cancer therapy and its unique advantages quickly triggered widespread interest from the scientific community. Much effort has since been invested to study its efficacy as a cancer

therapy, both *in vitro* [17]–[20] and *in vivo* [21]–[25]. A wide variety of cell [17]–[20], organ [26]–[28], and animal [21], [24], [29] models have been used to characterize the destructive potential of IRE for different cancer types. These studies have provided valuable experimental results and treatment planning protocols (IRE threshold, pulse parameters, etc.) including probe delivery (probe design, placement, intra-operative imaging methods, etc.), injury evaluation (methods and timing), and treatment efficacy. While reviews of IRE are now beginning to be published [1], [2], [30], [31], [31], [32], a systematic summary and categorization of basic to clinical IRE studies allowing ready access and comparison between protocols and parameters has not yet been provided for researchers and clinicians who are new to the field.

Therefore, the main purpose of this chapter is to give a critical review of the *in vitro,* translational, and clinical work based on major experimental studies on IRE therapy in the past decade, and provide organized data and facts to assist further research, optimization, and clinical applications with IRE.

1.2 Proposed Mechanisms of IRE

This topic has been well evaluated in many well-written reviews [32]–[35]. For completeness and discussion of later *in vitro* and *in vivo* results, a brief overview of mechanisms is given here.

Electroporation is essentially a membrane phenomenon that involves behavior of the lipid plasma membrane under the intense stimulation of external electric field (1000s V/cm). The early observation of “membrane breakdown” in electrically stimulated membranes dates back more than half a century ago [3]. However, it was not until the

1970s that insights into IRE mechanisms began to accumulate with the development of experimental platforms. Using a natural vesicular membrane system, Neumann [36] detected the release of catecholamines induced by intense electric field and confirmed the transient change of membrane permeability during electroporation. In a subsequent series of studies [37]–[42], it was suggested that the site of interaction between the electric field and the cell subjects was the cell membrane. These findings stimulated great interest in modeling the membrane lipid system and developing membrane based mechanisms for electroporation.

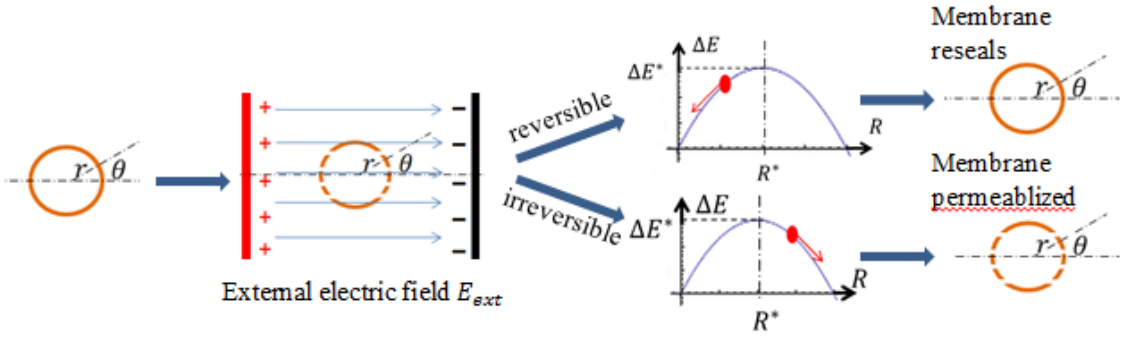

Figure 1.1. *Illustration of electroporation process and outcome.*

The potential distribution surrounding an isolated spherical cell (Figure 1.1) with a non-conducting membrane in an external electric field E_{ext} can be described by Laplace equation, and has the following solution for the transmembrane voltage (U):

$$U = 1.5 \cdot r \cdot E_{ext} \cdot cos\theta \tag{1.1}$$

where r is the radius of the cell, and θ is the angle between the site on the cell membrane where U is measured and the direction of E_{ext}. The relationship between U

and E_{ext} in Eqn (1.1) has been validated by Kinosita's experiments on electroporation with electric field-sensitive fluorescent dyes [43], [44]. Following this approximation, for a typical eukaryotic cell with a radius of $r = 10\mu m$, it takes an external field strength of 667V/cm to achieve a transmembrane voltage of 1V [33]. Note that Eqn (1.1) applies only to the scenario when the cell to cell distance is much greater than the radius of a single cell (as in dilute cell suspension) and membrane charging time is negligible. More comprehensive discussions on electric field-induced transmembrane potential can be found in [34], [45]–[47]. When the cell density and charging time are considered, Eqn (1.1) needs to be generalized into Eqn (1.2)

$$U = f \cdot r \cdot E_{ext} \cdot cos\theta \cdot (1 - e^{-\frac{t}{\tau}}) \quad \text{where } \tau = r \cdot C_m \cdot (\frac{1}{\sigma_i} + \frac{1}{2\sigma_e})) \tag{1.2}$$

in which a coefficient f (mV/(V/cm)) is introduced to reflect the influence of cell packing density, i.e. the ratio of cell radius to cell separation distance, and the membrane charging time constant τ_c determined by C_m (specific membrane capacitance), σ_i and σ_e (intracellular and extracellular specific conductivities).

The integrity of the membrane after electroporation is dependent on various parameters, but primarily on the transmembrane voltage. In the important case of cell membranes, reversible poration is usually found for $\mathrm{U} \leq 1\mathrm{V}$ [33]. Temporary poration allows ions and molecules that are normally impermeable to the cell membrane to pass through, but these pathways usually reseal after electroporation and eventually lead to cell survival. For transmembrane voltage greater than 1V, and usually with longer pulsing,

electroporation may cause permanent membrane destruction (irreversible). Although the cell injury can be caused directly or indirectly from the pulsing, the creation of extended lethal membrane defects is presently believed to be responsible for cell killing after IRE.

There have been several different types of theoretical models explaining membrane stability at elevated transmembrane voltage. In earlier studies, it was suggested that membrane rupture is caused by an electromechanical collapse due to the compression of the entire membrane [48]. However, according to this model, there is a deterministic "breakdown voltage" for each specific cell type, which is contradictory to the stochastic nature of IRE from experiments. Based on the earlier studies by Litster [49] and [50] on stability of spontaneous pores on membranes, Weaver [51] proposed an energy based pore formation model for membrane rupture during electroporation. In this model, the free energy for pore formation is dependent on both the membrane properties and the applied external electric field

$$\Delta E(R,\, U) = 2\pi R \cdot \lambda \, - \, \pi R^2 \cdot (\sigma + aU^2) \tag{1.3}$$

where $\Delta E(R,\, U)$ is the free energy to create a pore of radius R, λ and σ are the edge line tension and surface tension of the membrane, respectively, and a represents the contrast of dielectric constants of water and lipid. This model accounts for factors of both the applied external electric field and the membrane's intrinsic physical properties, such as line tension and surface tension, which could also influence the outcome of electroporation [52] (Figure 1.2). Furthermore, it allows for estimation of the pore formation rate with calculations described in [33], [53], [54].

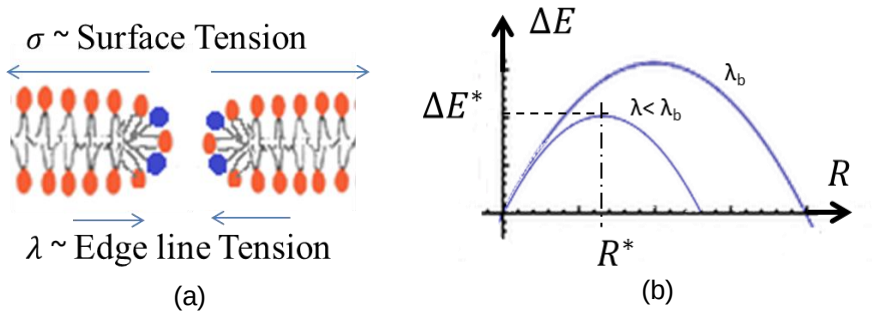

Figure 1.2. *Reported IRE influencing factors: (a) competing factors (surface tension and edge line tension) during pore formation, (b) nucleation based energy model and critical pore radius & energy with baseline (λ_b) or decreased edge line tension*

The mechanisms whereby cells die post IRE continue to be actively investigated. Several mechanisms with experimental support have been proposed and are reviewed here. One mechanism is lethal membrane disruption from repetitive electrical pulsing. This lethal event is predicted in existing electroporation theories [1], [2], [33], [35], [53] considering the creation of aqueous pores. Direct visualization of the transient pore formation process has been elusive due to the combination of time scale and spatial resolution limit of the imaging methods. However, many attempts based on indirect or "fix-then-process" approaches have been made to observe the membrane defect induced by electroporation. Using electron microscope, Chang et. al. [55] were able to observe numerous "pore-like" structures from rapid frozen electroporation treated sample (Figure 1.3a). The observed pore structure sizes ranged from 20 nm to as large as 120 nm in diameter. Because direct poration is difficult to detect, researchers have often resorted to indirect measurements which may support either poration or permeabilization. For instance, sharp changes in electrical conductivity can reflect alteration of membrane permeability (Figure 1.3c), and can be used to detect the occurrence of electroporation [56]–[59]. Dye uptake and volumetric response of cells

(Figure 1.3b) have also been used to evaluate pore formation during electroporation [17]–[19], [60]. In addition, for the non-vital defects that completely reseal after electroporation, many secondary events, such as electro-conformational protein denaturation [34], osmotic imbalance, flush in/out of ions, depletion of ATP [61], or uptake of toxic/foreign molecules [14], could occur before complete defect reseal and may eventually result in cell death. Numerous studies have reported the “delay” of injury development after electroporation [28], [61], [62]. Electrochemotherapy also takes advantage of the permeability change during electroporation to introduce cytotoxic drugs to kill cancer cells [14]. Studies have shown that the secondary events mentioned above could potentially cause more injury than primary membrane defect [61].

In summary, the current understanding of IRE is that it occurs on the site of the plasma membrane. There tends to be general agreement of the pore formation process although how the membrane recovers is poorly understood and an area of ongoing research. Cell death may be due to lysis but predominately due to loss of homeostasis as the amount of mass transfer during electroporation is too difficult to overcome in cases where the membrane reveals.

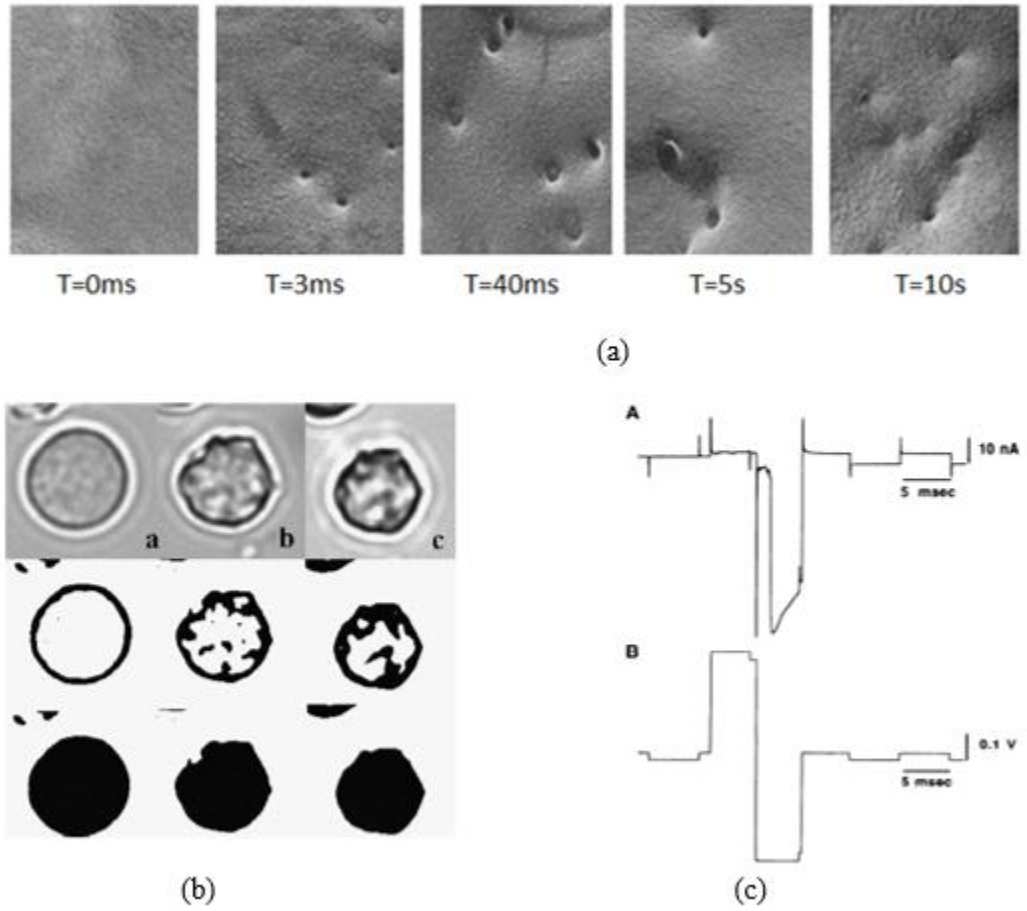

Figure 1.3. *Experimental observations of electroporation: (a) observation of numerous "pore-like" structures from rapid frozen electroporation treated sample under electron microscope* [55]*, (b) volumetric response of cells during electroporation* [60]*, and (c) sharp changes in electrical conductivity reflecting alteration of membrane permeability* [57]*. Reprinted with the permissions from Elsevier.*

1.3 In Vitro Studies of IRE

The majority of research on *in vitro* electroporation was conducted before IRE was proposed as a tissue destruction modality. The *in vitro* model systems, such as cell suspension in cuvettes and microfluidic channels, are similar to those systems that have been studied for molecular biology applications, such as genetic transfection and *in vitro*

drug testing. With the development over the past several decades, much knowledge and insights have been gained from these studies. However, the goal of most molecular biology applications is to increase the uptake of desired molecules while minimizing cell injury. Therefore, it is beyond the scope of this paper to include all the results from *in vitro* electroporation studies. Readers may refer to [7], [63], [64] for reviews on progresses in these fields. In this paper, only the studies with irreversible electroporation (i.e. cell destruction) as the goal, or those that provided insights on electroporation mechanisms and are relevant to cell destructive applications are included.

1.3.1 In Vitro Models

The *in vitro* model systems for IRE that have been studied and published in literature can be classified into three categories based on the type of membrane studied [33], [65]. These categories include (1) artificial membrane systems, including lipid bilayer sheet membrane [66], [67] or vesicles [36], (2) isolated single cells [57], [68], and (3) cell suspension in cuvettes or microfluidic channels [17]–[20]. The artificial membrane models ignore the inter and intra cellular structures and therefore cannot account for how these structures may affect cell death pathways. However, due to their simplicity, artificial membrane models are easy to manipulate and image and therefore have contributed to numerous insights on the membrane level, such as direct observation of membrane surface change and measurements of defect formation timing and size [36], [37], [39]–[41], [66]. Single cell models isolate the individual cells from their extracellular environment, but provide access for cell behavior observation and direct measurements of electrical properties on the cellular level. Early experimental studies chose larger cells (e. g. muscle cells and oocytes) due to the ease of manipulation [57], [69], [70]. Nowadays, with the development of micro-fluidic devices, researchers are able to

conduct electroporation on regular sized cells (micrometer scales) using micropipette tips and microelectrodes [71]–[76]. The cell suspension model is the most widely used experimental system for *in vitro* cell destruction studies. It allows observation of a group of cells under external electrical stimulations. Here membrane or extracellular properties can be adjusted by changing or adding components in the medium, allowing optimization of IRE conditions [17]–[19], [52]. The drawback of this model is that suspension data reflects cell population behavior, not individual cells which require a more specialized microfluidic setup.

1.3.2 Electroporation Time Frame

The generation of transmembrane potential in a large lipid vesicle (~40μm) or a single cell (~50 μm) depends on ion concentration of the surrounding medium, but is in the range of micro-seconds [31], [56], [77], [78] from modeling. Electric defects occurring in the lipid domain are expected to reseal in milliseconds to seconds, as is the case for bilayer lipid membrane (BLM) or lipid vesicles [37]. Experimentally, kinetics of electroporation of cell membranes have been monitored by permeability, conductivity, fluorescence imaging, and rapid freezing electron microscopy (EM) methods [43], [44], [55], [79]–[85]. With permeability and conductivity measurements, a sub-microsecond pore initiation is recorded and confirmed by leakage experiment [82], [86]. Pore expansion happens in the 100 μs time range and begins to reseal (incompletely) within milliseconds. However, EM did not detect pore-like structures until 10 ms after the pulse was terminated [55], and the defects also lasted longer (up to 10 seconds) than what was expected for reversible electroporation voltage range (as was used in their paper). Another EM study observed pore structures 15mins or as long as 24 hours after IRE treatment in tissue [87]. One possible explanation is that the large pore-like imprints

imaged by the EM result from secondary effects during recovery period after pulsing, similar to ideas suggested by Tsong [77].

Therefore, both theoretical estimations and experimental measurements indicate that electroporation induced membrane events occur with a membrane charging time that is less than microseconds. The amount of time it takes for a membrane to bear IRE pores range from microseconds to milliseconds. After the external electrical simulation is withdrawn, it may take the membrane seconds to hours to recover if lethal damage has not been induced on the cell (Figure 1.4). Importantly, each of the time frames above depends strongly on the cell/membrane type and applied electric voltage.

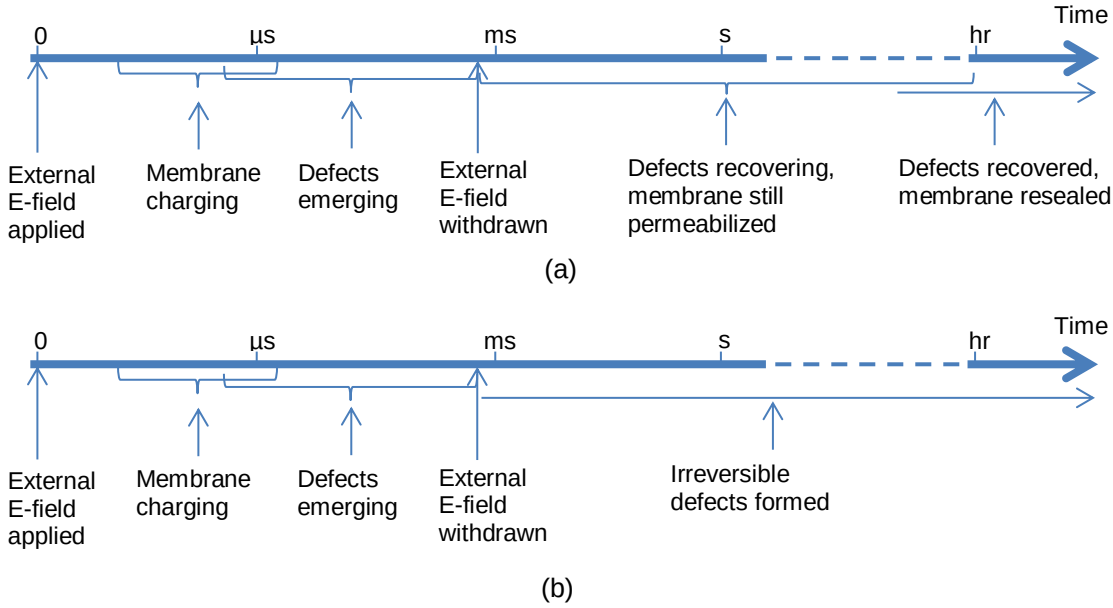

Figure 1.4. *Illustration of the time frames of reversible (a) and irreversible (b) electroporations.*

1.3.3 Injury Mechanisms and Evaluation

As was discussed above, defect formation does not necessarily result in cell death. The critical cellular injury comes from either direct membrane destruction (irreversible pore, rupture, etc) that deployed cytoskeleton (and/or extracellular matrix connection to the cell through proteins), or secondary effect such as osmolarity imbalance, loss of critical organelles, or influx of cytotoxic molecules that eventually result in cell death. Therefore, it is important to examine existing *in vitro* injury evaluation methods and discuss their advantages and disadvantages.

The classic membrane integrity dye assay (PI, Hoechst, Trypan blue, etc.) is simple and inexpensive to perform, and can detect direct membrane defects. Since most IRE injuries are associated with membrane defects and/or permeability change, membrane integrity assay is a great fit for post IRE injury evaluation. However, two questions need to be carefully considered and addressed before using membrane integrity assays. Firstly, when is the dye introduced? As mentioned previously both reversible and irreversible defects are present in the membrane during IRE. If the dye is introduced before IRE, the “dead” cell count will be biased since cells with reversible defects are included in the counting even though they may eventually survive. If the dye is introduced after IRE, how long is the waiting period before assessment? Although it is difficult to measure the time for reversible defects to recover i.e. it can take seconds to hours, a reasonable estimation is on the scale of seconds to minutes. And it is important for researchers to keep this waiting period constant and report it with their experimental results. Secondly, how long is the dye incubation time? For instance, it is possible that after prolonged incubation, the secondary injury from IRE will result in cell lysis that would tend to increase cell death by dye count over time. Moreover, the timing of such

processes are unpredictable and may result in inconsistent viability results if the waiting period is varied. Therefore, the timing of dye application and incubation time need to be carefully controlled and considered when comparing results obtained from one study to another using membrane integrity dye assays.

NAD(P)H-dependent cellular oxidoreductase enzymatic (MTT, XTT, CCK, etc.) assays are a class of colorimetric assays that measure the activity of cellular enzymes which reduce the tetrazolium based dyes via NAD(P)H-dependent metabolic activities, therefore reflect the number of viable cells present. The advantage of this type of assay is that it can detect a dead (or dying) cell under conditions others cannot. For instance, the dye assay can only detect cell death when the membrane is compromised whereas NAD(P)H can detect cell death when it is still intact. However, NAD(P)H-dependent assay does not have the capability to differentiate between metabolically dormant and dead cells. Also, environmental conditions that affect the cell metabolic activity can alter the cell viability results as well.

ATP, or adenosine triphosphate, is a molecule found in and produced by living cells. It is a direct indication of biological activity and thus cell or tissue health. ATP level can be quantified by measuring the light emitted through its reaction with luciferase reagents using a luminometer. The amount of light produced is directly proportional to the amount of living cells present in the sample. ATP assay can suffer from similar limitations of the NAD(P)H-based assays in that it is unable to differentiate metabolically mute cells from dead ones and can also vary with the environmental conditions.

Table 1.1. *Summary of in vitro IRE Studies*

	Model	System	Electric Field (V/cm)	Pulse Parameters			Injury Evaluation[#]	Ref
				Number	Duration (µs^)	Freq. (Hz)		
Cancer Cells	HepG2 (liver)	Cuvette	1500	30	300	0.1	a, c	[19]
	M109 (lung)	µChannel	300~400	n/a	100ms~300ms	n/a*	a	[18]
	DC-3F (lung)	Cuvette	1200	8	99	n/s*	c, e	[61]
	Lewis (lung)	Cuvette	1400	8	99	n/s	c, e	[58]
	PC3 (prostate)	Cuvette	250~2000	10~3840	100µs	10	a	[17]
	THP-1 (leukemia)	Cuvette	1500~7500	1	2ms or 5ms	n/a	a	[20]
	K-562 (leukemia)	Cuvette	1200	8	99	n/s	c, e	[58]
	Sp2 (myeloma)	µSlide	2~3k	1	20	n/a	a, g	[88]
Other Cells	Cardiac cell (Frog)	Single cell	0.4 V[A]	1	10ms	n/a	d	[57]
	Cardiac cell (Pig)	Single cell	3.6[B]	2	10ms	0.2	b	[68]
	RBC (mouse)	µChannel	1100~1200	n/a	100ms~300ms	n/a	f	[18]
	WBC (mouse)	µChannel	400~500	n/a	100ms~300ms	n/a	a	[18]

* n/a- not applicable, n/s- not specified

[#] a- Membrane integrity dye (PI, Hoechst, Trypan blue, etc.),
b- Voltage sensitive dye (di-8-ANEPPS, etc.),
c- NAD(P)H dependent cellular oxidoreductase enzymes (MTT, XTT, CCK, etc.),
d- Electrical properties (current, voltage breakdown),
e- ATP assay,
f- RBC ghosts,
g- Volumetric assay

^ unless otherwise noted

A-Pipette tip suction, B-chamber field

1.3.4 IRE Parameters and Outcomes

This section is an attempt to tabulate and compare the IRE parameters between the *in vitro* studies that have been published to date. Due to the wide variations of experimental configurations and evaluation methods, the choice of IRE parameters varies greatly among studies reviewed in Table 1.1. The applied electric field can range from hundreds to thousands of Volt/cm. The pulse number can range from 1 to more than 3800, and pulse duration can range from under 100 µs to 300ms. Most studies did

not report their pulsing frequency. In terms of injury assessment, more than half the studies have chosen membrane dye or NAD(P)H-based assay (or both) as their viability assay. Some studies have adopted the viability assay that is more specific to their chose of cell line (eg. the RBC ghost assay).

TABLE 1. *Trypan blue test results of PC3 cell viability after nonthermal IRE at range of fields and number of pulses*

	No. Alive/No. Dead (% alive)			
	Trial 1	Trial 2	Trial 3	Mean ± SD % Alive
Control	80/0 (100.0)	90/0 (100.0)	50/0 (100.0)	100
IRE:				
2,000 V/cm, 10, 100 μsec pulses	65/25 (72.2)	74/25 (74.7)	33/19 (63.5)	70 ± 6
1,500 V/cm, 17, 100 μsec pulses	53/30 (63.9)	35/50 (41.2)	32/19 (62.7)	56 ± 12
1,000 V/cm, 60, 100 μsec pulses	35/60 (36.8)	23/60 (27.7)	10/45 (18.2)	27 ± 9
750 V/cm, 106, 100 μsec pulses	7/50 (12.3)	7/83 (7.8)	11/60 (15.5)	12 ± 4
500 V/cm, 240, 100 μsec pulses	0/80	0/90	0/50	0.0
250 V/cm, 960, 100 μsec pulses	0/80	0/90	0/50	0.0
125 V/cm, 3,840, 100 μsec pulses	0/80	0/90	0/50	0.0

TABLE 2. *Flow cytometry results of PC3 cell viability after nonthermal IRE at range of fields and number of pulses*

	No. Alive/No. Dead (% alive)			
	Trial 1	Trial 2	Trial 3	Mean % Alive
Control	10/0 (100)	10/0 (100)	10/0 (100)	100
IRE:				
2,000 V/cm, 10, 100 μsec pulses	8/2 (80)	8/2 (80)	8/2 (80)	80
1,500 V/cm, 17, 100 μsec pulses	6/4 (60)	6/4 (60)	6/4 (60)	60
1,000 V/cm, 60, 100 μsec pulses	3/7 (30)	3/7 (30)	3/7 (30)	30
750 V/cm, 106, 100 μsec pulses	1/9 (10)	1/9 (10)	1/9 (10)	10
500 V/cm, 240, 100 μsec pulses	0/10	0/10	0/10	0
250 V/cm, 960, 100 μsec pulses	0/10	0/10	0/10	0
125 V/cm, 3,840, 100 μsec pulses	0/10	0/10	0/10	0

Figure 5. *Test results of PC3 cell viability after non-thermal IRE at range of fields and number of pulses* [17]. *Reprinted with permission from Elsevier.*

Probably the first systematic study to determine the parameters needed for IRE of cancer cells was performed *in vitro* by Rubinsky's group using a cuvette and cell suspension setup [17]. In this study, the researchers tested IRE electric field strengths in the range of 125V/cm to 2000V/cm, and pulse number from 1 to 3840 (Figure 5). The pulse duration was kept constant in this study at 100 µs. A total of 90 pulses at 250 V/cm for 100 µs separated by 100 milliseconds were found to completely destroy prostate cancer cells without inducing thermal damage. What is surprising about this study is that within the constraint of applying electroporation with no thermal damage,

lower electrical fields are actually more effective for cell destruction with IRE alone than higher electrical fields. Also, this study did not provide data on the influence of each individual parameter (i.e. varying electric field, pulse number, and pulse duration independently while keeping the other two constant). Nevertheless, this was the beginning of systematic study of IRE parameters for cell destruction.

A more recent overview of electroporation parameters on IRE has been presented by Weaver et. al. [31]. Here, combinations spanning three orders of magnitude in pulse strength (i.e. E-field) and nine orders of magnitude in pulse duration were discussed. For instance, higher field strengths (1~10kV/cm) and longer pulses (μs~ms) tends to necrosis, while even higher field strengths (10~100kV/cm) and shorter pulses (<μs) tends to apoptosis (an emerging concept called supra electroporation). Finally, lower field strength and short pulses tend to lead to survival. However, this appears to be in conflict with Rubinsky's paper [17]. This suggests the need for simultaneously varying all three parameters in a single cell type to more fully explore biological response to electroporation parameter space (see Appendix A3).

To begin asses these three parameters independently, our group recently performed a study on cell viability *in vitro* in a prostate cancer cell line (LNCaP Pro 5) and a cardiac cell line (HL-1) using the cuvette cell suspension setup (Figure 1.6) [89]. We observed that due to the stochastic nature of IRE injury, even extremely strong electric field cannot guarantee complete death of the entire cell population with low cumulative pulse time (i.e. "CPT", pulse number multiplied by individual pulse duration). For instance in the HL-1 case, the viability first starts to drop below 90% when electrical field exceeded 750V/cm. This number can be considered as a lower threshold for this cell type.

Complete cell death (greater than 90%) can be achieved when the E-field is above 1250V/cm given sufficient CPT. This E-field can be considered as an upper threshold. When the E-field is above this level, the user can be confident that complete cell death can be achieved as long as a sufficient CPT is given. If the strength of E-field is not a concern, the higher the E-field is beyond 1250V/cm, a smaller CPT is needed to achieve complete death. There is a grey zone between 750V/cm and 1250V/cm. In this zone, the cells are injured but may not actually die as a result of IRE treatment. It is worth noting that in our study, when the E-field is lower than 500V/cm, simply increasing the CPT (either pulse number or duration) does not lead to higher cell injury. This appears to be contradictory to the findings from Rubinsky's study [17], in which complete cell death (100%) can be achieved for E-field as low as 125V/cm. However, the pulse number range in our study (up to 90) is far less than that in Rubinsky's study (up to 3840). It will be interesting to investigate further on whether low E-field (lower than 500V/cm) can induce complete cell death from IRE given sufficient CPT, and how this can be related to clinical applications.

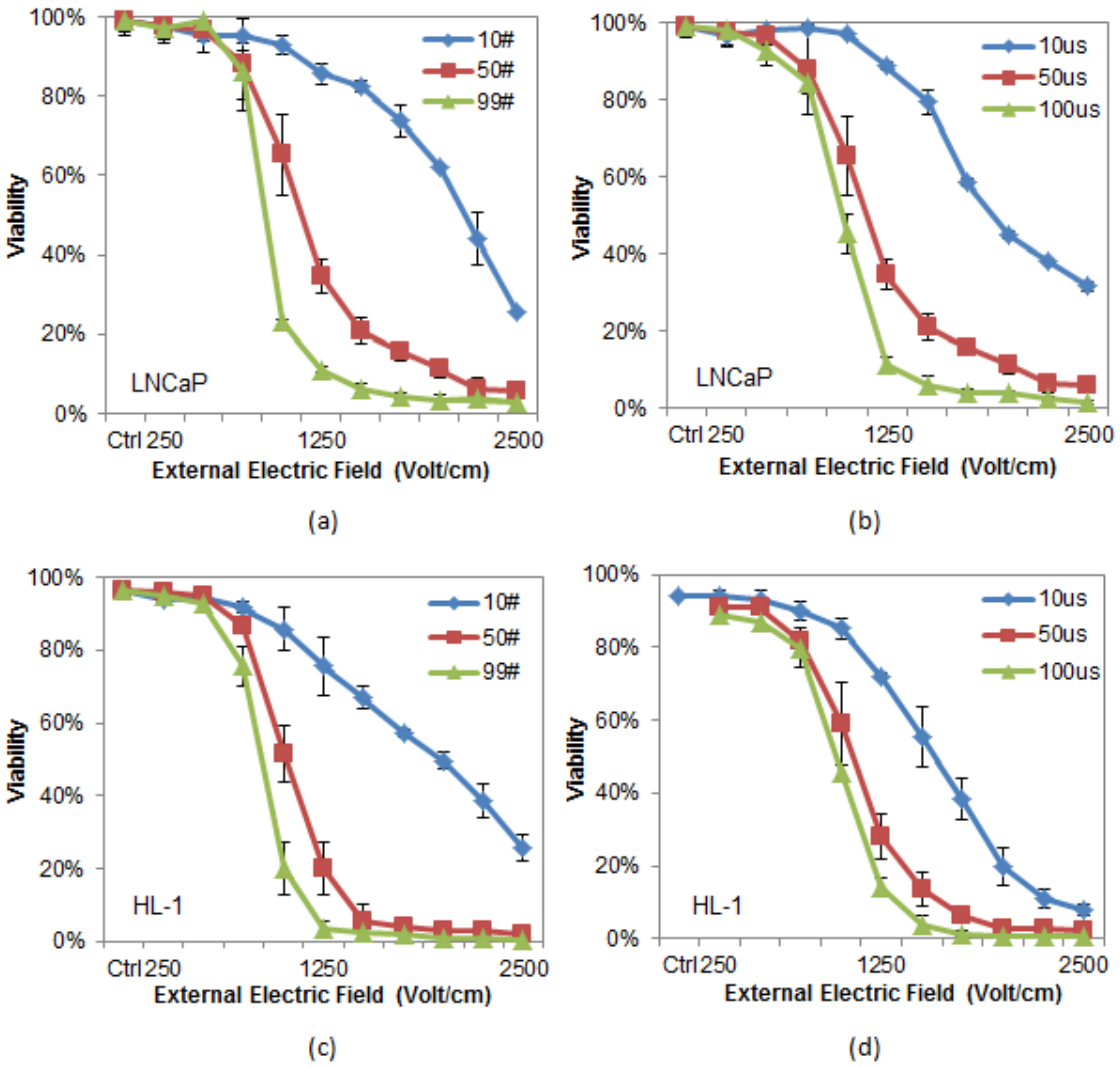

Figure 1.6. *Test results of cell viabilities after IRE: (a) LNCaP Pro5 viability as a function of changing electric field and pulse number, pulse duration is 50μs, (b) LNCaP Pro5 viability as a function of changing electric field and pulse duration, pulse number is 50, (c) HL-1 viability as a function of changing electric field and pulse number, pulse duration is 50μs, and (d) HL-1 viability as a function of changing electric field and pulse duration, pulse number is 50. Injury assessment method for (a) and (b) is CCK-8 cell viability assay, for (c) and (d) is double dye staining assay (Hoescht and PI). Pulse frequency for each case is 10Hz. Each data point represents the average of n≥3 measurements ± SD.*

In summary, despite some variations, general trends do appear to hold from these studies. For example, the majority of field strengths used in *in vitro* IRE studies fall

between 1000~2000 V/cm, which is above the theoretical threshold calculation of 667V/cm to induce IRE injury as discussed with Eqn(1.1) and in previous work by Weaver and others [33]. Although the timing and delivery pattern of the pulses can change, once the electric field is above the threshold for IRE, it generally takes at least 800 μs of CPT (a combination of pulse number and duration) to achieve sufficient cell death.

Table 1.2. *Summary of in Vivo IRE Studies*

	Model		Probe Design		Field (V/cm) or Potential(V)	Pulse Parameters			Injury Evaluation	Outcomes	Ref.
			Type *	Number /Dist. (mm)		Number	Duration (µs)^	Freq. (Hz)^			
Normal Tissue	***Liver***	Rat	P	2/4	1000	1	20ms	n/a	H	Threshold: 300~500V/cm Lesion size: 48.6~59.6 mm^2	[21]
									V	Vascular block: transient 15~20mins	
		Rat	P	2/5	1500	8	100	10	H	Lesion: qualitative	[58]
									E	σ increase: 43+-1%	
		Rat	N	2/5 or 2/10	500V or 1000V	8	100	10	MRI	Lesion: hyperintense	[90]
									H	Lesion: qualitative	
		Rabbit	N	2/8	860V ~1360V	8	100	1	H	Threshold: 637±43V/cm	[91]
		Porcine	N	4/15 or 2/25	2500V	8	100	10	H	Threshold: 600V/cm.	[24]
									US	Lesions: hypointense during, then hyperintense 24hrs after IRE	
		Porcine	P	various	1000	99	100	0.25~4	H	Threshold: 423±147V/cm.	[92]
			N	2/5	1500				D	>50% decellularized	
		Rabbit and Porcine	NK	1	2500V	90	100	n/s	H, US, and TTC	Lesion: qualitative	[93]
									US	Pores sizes from 80-490nm	
	Brain	Rat	N	2/1	50~400V	90~180	200	250k or 500k	H, MRI	Lesion: qualitative	[94]
									V	Hi-Frequency reduces muscle contraction	
		Dog	N	2/5	500V or 1000V	90	50	4	MRI, US	Threshold 495~510V/cm Lesion size: 0.25~0.6cm^3	[23]
									MRI	Lesion: hyperintense	
		Dog	N	2/5	500~1500V	80	50	0.5, 1, or 4	H, CT	Lesion: qualitative	[95]
									MRI	Lesion size: 0.131 (T1) and 0.12cm^2 (T2) immed after IRE, hyperintense for both	
		Dog	N	1 or	500~2000V	90	50	4	H	Lesion: qualitative	[26]

				2/5~10						
								MRI	Lesion size: 0.259cm^2 (500V), 0.599cm^2 (1000), 1.665 cm^2 (1500V). Lesion is hypointese under T1-MRI and hyperintense under T2-MRI.	
	Lung	Porcine	N	2/9 or 2/15	1500V or 2500V	90	70	4 or ECG synchronized	H, CT ECG	Threshold 500V/cm. Lesion size:776.4cm^3. Distance for IRE to cause heart damage: 1.7cm.	[96]
	Kidney	Porcine	NK	2/9~15	1700V~2500V	90	70	4	H, CT	CT imaging hypodense.	[27]
		Porcine	NK	1 or 2/15	2700V (single) or 2700V (paired)	90	70 or 100	n/s	H	Lesion size: 0.38~2cm^3 (paired), 0.68~5.6cm^3 (single). Sizes decrease over time.	[28]
		Porcine	NK	1	2700V	90	70ms	1.5	A	No acute vascular damage by IRE from real-time DSA monitoring.	[97]
	Prostate	Dog	N	1, 2, or 4/ 10~15	1000~2000V	1~8 (single) 80 (paired)	100	5~10	H	Voltages lower than 1.5 kV produced little to no contraction in anesthetized animals and paralyzed animals.	[25]
	Intestine	Rat	P	2/1	200V	50	70	4	H	Signs of recovery showed 3 days post-surgery by developing and epithelial layer.	[87]
Implanted Tumor		Mice	P	2/3~5	2000 or 2500	80	100, 800, or 1000	0.03~5 k	H, TR	Up to 92% complete tumor regression (3 weeks).	[22]
		Mice	P	2/4	2500	64	100	1	H, TR	Immune response is not instrumental in IRE efficacy.	[98]
		Mice	P	2/8	1300	8	100	1	US, TR, FI, PO	Rapid decline in perfusion after IRE.	[14]
		Mice	P	2/15~30	2500	8 or 80	100 or 1000	0.03~10	H, E	Increase of σ: 10%~180%.	[99]
		Mice	N	1	1300V	100	100	0.3	H, TR, FI	Threshold 1000V/cm. Lesion size: 5~8mm. 5 in 7 cases complete regression.	[100]
		Mice DSFC	N	1	500V	10~99	10~100	10	H, FI	Threshold: 600~1300V/cm. Lesion size: ~3.5mm radius	[101]

		Rat	N	2/10	2500V	8	100	10	H, MRI, TR	IRE lesion is hypointese under T1-MRI and hyperintense under T2-MRI. 52% decrease in tumor size after 15 days.	[29]
Spontaneous Tumor	***Brain***	Dog	NK	2/5	500V and 625V	40 (500V), 80 (625V)	50	ECG synchr onized	MRI, TR	74.2% average tumor volume reduction with T1-MRI 48hrs after IRE.	[102]
		Dog	NK	2/5	625V and 500V	80	50	~1	MRI, CT	Lesion size: 0.15~0.24cm^3 for 500V and 0.24~0.4cm^3 for 625V.	[103]
	Soft Tissue	Dog	NK	1 or 2/8~15	800V~1500V	90	70 or 100	1.5	H, CT, TR	52% volume reduction with CT 8 days after IRE.	[104]
Cardio-vascular	***Artery***	Rat	C	/0.3	3800	10	100	10	H, VS	VSMC 80% less 28 days after IRE, with no apparent damage to ECM and structure.	[105]
		Rat	Ca	n/a	3300	10	100	10	H	Ave temp increase: 0.6^{o}C.	[106]
		Rat	C	n/s	1750 or 2500	10, 45 or 90	100	1 or 10	H, VS	VSMC 89~94% less 28 days after IRE, with no apparent damage to ECM and structure.	[107]
		Rat	C	/0.4	1700	90	100	1~4	H, VS	VSMC complete ablated after 7 days.	[108]
		Rat	C	/0.4	1750	90	100	4	H, VS	VSMC almost completely ablated after 7 days.	[109]
			Ca	n/a	>1000					Endothelial layer regenerate by 7 days after IRE.	
	Heart	Pig	P	n/s	1500~2000V	8, 16, or 32	total 1s to 4s	5	H	Lesion size: 0.4~1.4cm depth, 3~3.5cm length, 0.5~1.0cm width.	[110]

* P- plate, N- needle, NK- Nanoknife, C- clamp, Ca- catheter
^ Unless otherwise noted

Injury Evaluation
H- Histology
MRI- MRI
U- Ultrasound
EM- Electron microscopy
CT- CT scanning
ECG- ECG monitoring
D- Density score
A- Angiography
E- Electrical properties
TR- Tumor regression
FI- Fluorescent imaging/ bioluminescence
TTC-TTC Staining
PO-Tissue oxygenation
VSMC-Vascular smooth muscle cells count

1.4 Translational Studies of IRE Therapy

Since Davalos et. al. [16] first proposed the use of electroporation as a means of soft tissue destruction, a great number of pre-clinical tests have been undertaken to support this new modality. Among them, *in vivo* testing on animal organs has generated the most abundant data and useful conclusions so far. The goal of this section is to summarize these experimental findings and categorize them in a manner that is readily available for clinicians and researchers relatively new to the field. A complete summary of these *in vivo* studies can be found in Table 1.2 and will be the basis of our discussion in the following sections.

1.4.1 Tissue IRE Probes

There are four major types of IRE probes: plate, needle, clamp, and catheter. Their popularity in usage can be found in Figure 1.7a below. The plate probe design can provide the most homogeneous E-field distribution to the target tissue. The E-field is easy to determine and is relatively well constrained between the two plates. However, plate probes are much more invasive if they need to be placed inside the body. Their usage can also be limited due to the difficulty of placement and having to maintain the relative parallel position between the two plates. Therefore, they are more often considered when the target tissue is more easily accessible (e.g. during an open surgery). The needle design is the most popular selection reviewed (58% of all cases) for tissue destruction. The needle is relatively less invasive, flexible, yet provides easy manipulation for placement. The number of needles can be one, two, or more (Figure 1.7b). However, the E-field generated by needle probe(s) is not homogeneous and needs to be carefully calculated before treatment using advanced simulation software.

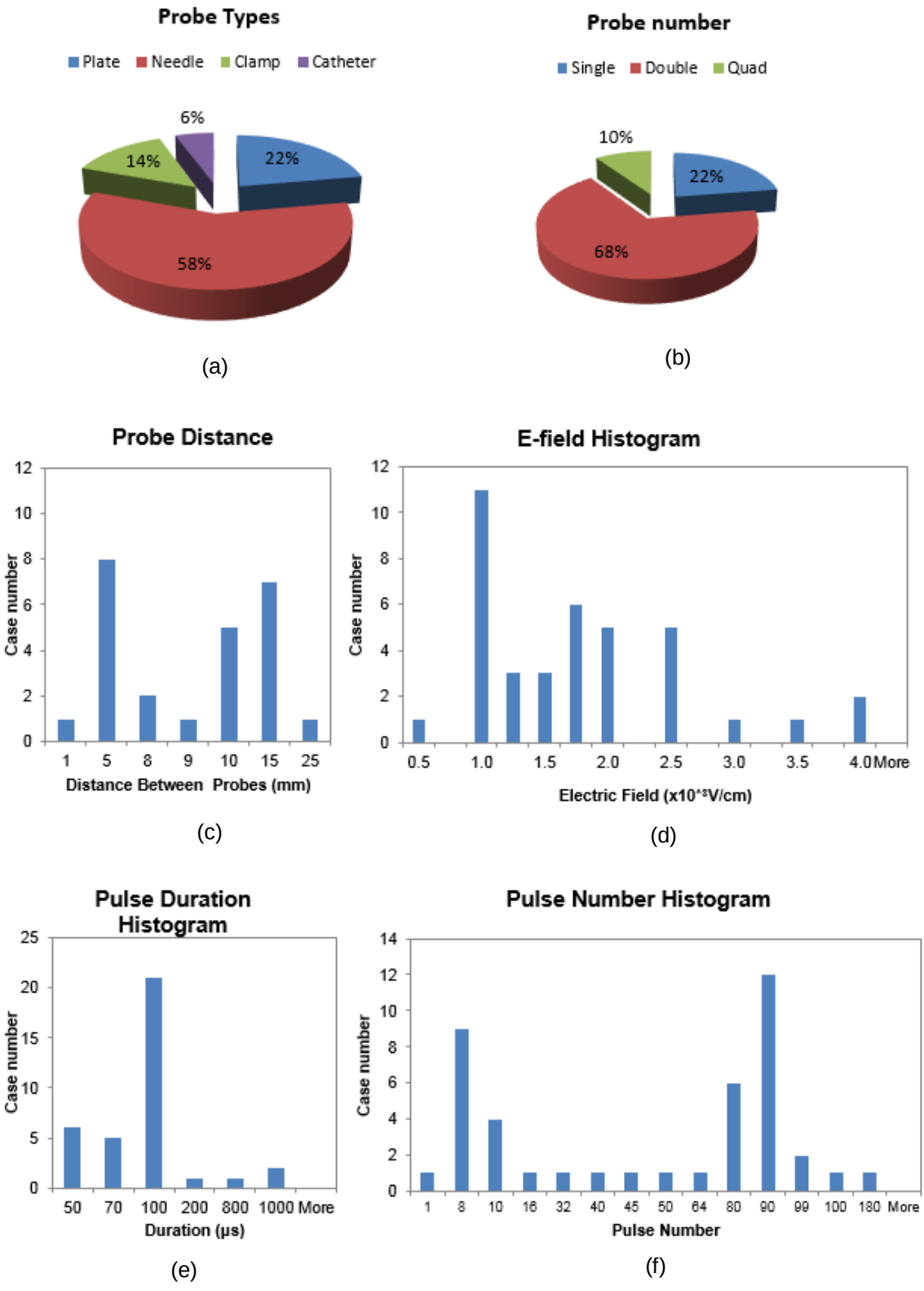

Figure 1.7. *Distribution of IRE probe design and parameter choices from Table 1.2.*

Also due to the uneven distribution of E-field around the needle, effective treatment volume can be small due to the restriction of the highest potential on the probe. Adding probe number and optimizing the probe placement can help increase the effective treatment volume, but that will make the treatment more invasive as well. A clamp probe design can also be more invasive and suffers similar limitations as the plate probe. However, they can provide more secure contact that can work better for specific organs, such as arteries and intestines during open surgery. The catheter probes are also designed for tubular organs. They require more skill to manipulate and navigate to the target site but can be the least invasive compared to other probe designs.

Several researchers have expressed concerns about the impact of probe size to the actual treatment volume. This issue is relevant to the needle probe design. It has been found [91], [111] that the smaller the diameter of the needle electrode, the higher the voltage that has to be applied to obtain the same electric field intensity in the vicinity of the electrode. According to Laplace equation, the E-field drops exponentially with the distance away from the electrode. However, such drop is steeper with a smaller electrode diameter. Therefore, the size of the probe matters for the distribution of the E-field strength and needs to be accounted for in the calculation.

When multiple probes are used, the distance between the probes (Figure 1.7c) also needs to be accounted for in the E-field calculation and treatment planning. Another important safety factor for probe placement is the impact of the distance from the IRE probe to critical organs. As in the case for the heart, Deodhar et. al. [96] has found that within 1.7cm from the heart, fatal events occurred with all unsynchronized IRE in a study

of 11 pigs with lung and myocardium tissue destructions. ECG synchronized IRE delivery could avoid significant cardiac arrhythmias although minor events still present.

1.4.2 IRE Pulse Parameters (E-field applied, pulse duration, and pulse number)

The three most critical parameters affecting outcome of IRE are the E-field strength, pulse duration, and pulse number (Figure 1.7d~1.7f). The E-field used by the studies surveyed in Table 1.2 are summarized and compared below in Figure 1.7d. It can be seen that the majority (89%) of researchers used an E-field above 1000V/cm and below 2500V/cm for tissue destruction. This agrees well with *in vitro* work in Figure 1.6 (1250V/cm threshold for complete cell death). The pulse durations ranged from 50 to 100 µs in 87% of the studies reviewed (Figure 1.7e). And finally, the pulse number ranged between 10 and 90 for most studies (Figure 1.7f). As was discussed in our *in vitro* section, it requires a certain amount of cumulative pulse time to achieve complete cell death even when above threshold E-field level. This can be achieved by either increasing the pulse duration or the total pulse number. However, there are constraints on increasing pulse duration due to Joule heating (i.e. thermal effects), and procedure time is lengthened by increasing pulse number.

1.4.3 Injury Evaluation

The injury evaluation in tissue is more complex than *in vitro* or cell cases. For instance, the injury can be monitored in real time intra-operatively or after a procedure in an acute or chronic manner. The injury can also be screened on live animals, or examined post-mortem. The injury evaluation method used are summarized in Figure 1.8.

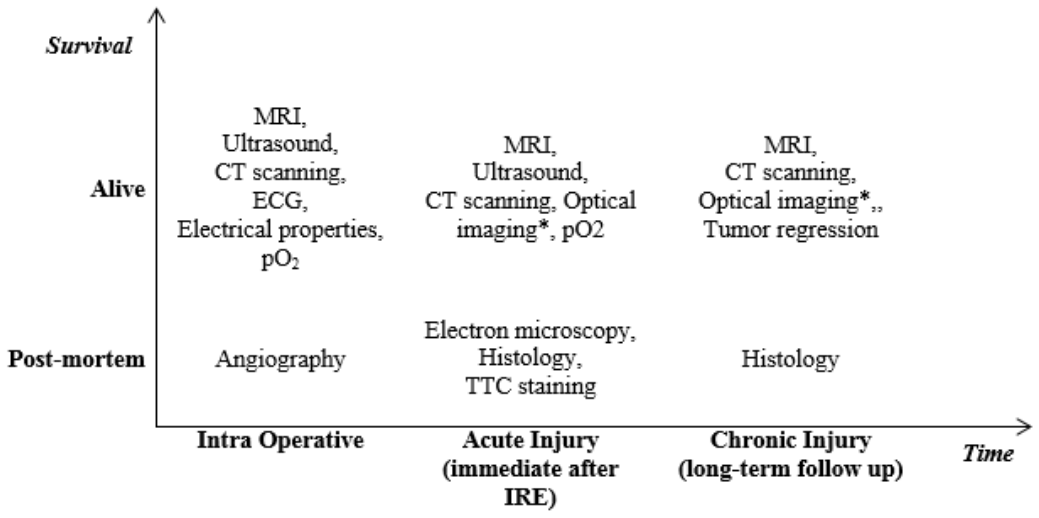

Figure 8. *Choices of injury evaluation method for in vivo IRE studies from Table 2. *Optical imaging methods are limited by penetration depth, and therefore are used predominantly in intravital chamber systems.* [52], [101], [112]

MRI, Ultrasound, and CT scanning are all direct, non-invasive imaging methods for live animals. They can be performed any time before, during, or after the procedure. A good review on imaging methods for IRE tumor treatments are given in [113]. Using these modalities, the IRE lesion is reported to be hypointense under T1-MRI and hyperintense under T2-MRI by Guo et al [29] and hyperintense for both TI and T2 MRI in [23], [95]. Lesions were reported to be hypointense during, and hyperintense 24hrs after IRE from untrasound monitoring [24], [114], [115]. For CT results, both intraoperative and follow up scans found hypodense nonenhancing lesion [27]. Not all studies have reported detailed description of their imaging results, and disagreement can be found in some studies.

Histological assessment of (usually H&E) stained samples is the most used evaluation method for IRE therapy post mortem [24], [58], [90], [91]. The lesion volume measured

from the histology sample can vary greatly depending on the time after IRE treatment, as was described as injury development *in vivo* [24], [105]. In general, follow up to a minimum of 3 days is necessary to evaluate the injury development unless only acute injury is of interest.

TTC, or Triphenyl tetrazolium chloride staining is another evaluation method for IRE injury post mortem. It is similar to the NAD(P)H-based assay for *in vitro* assessment and is used to differentiate metabolically active and inactive tissues. Compared to histology staining, TTC is faster and less expensive. However, the TTC stained samples cannot be stored and used at a later time like the histology samples. Both the start and incubation timing can affect the viability results. Therefore, careful study must be done to get the optimal assessment timing for a specific type of tissue [116], [117].

Optical imaging uses fluorescent dyes in an intravital method (i.e. dorsal skin fold) to examine the perfusion defect in tissue after IRE treatment. It measures the IRE injury at the tissue level. Like the histological assessment, optical imaging results can also change as the injury develops in tissue. However, since the same animal can be imaged respectively over time, optical imaging requires much less animals and money to study the injury development pattern compared to histology [52], [101], [118].

Tumor regression is another method to determine the treatment efficacy of IRE. Although tumor regression results have been reported in some studies [100], [102], [114], large scale, randomized animal studies are still not available on IRE therapy at this time.

Since IRE is still more often used in combination with chemotherapy or other enhancement reagents, the influence of chemo drug (bleomycin or other cytotoxic agents) or adjuvants on the viability results needs to be carefully accounted for. Specifically, it is important not to confuse the combinatorial IRE therapy outcomes with independent IRE monotherapy, as the results of the two are not directly comparable.

1.4.4 Outcomes and Thresholds

The IRE thresholds are mainly determined by overlapping the modeled electric field distribution with the lesion volume measured from viability studies. Most *in vivo* studies have found the threshold to be 500~1000V/cm (Table 1.2), which agrees well with the *in vitro* results we have reviewed in Table 1.1. The lesion size determined by these studies varies greatly due to different viability assays, different evaluation timing (intra-operative, after, etc.) and different tissue/animal subject. But generally, the IRE treatment volume is relatively small in our surveyed studies [26], [29], [57], [110]. Although one could consider the use of high voltages in the living body to be a safety concern, it is important to realize that the energy delivered is extremely low due to the short duration of the pulses. IRE uses was shown to be safe during tissue destruction in the studies surveyed here. Specifically, all animals treated with IRE survived after the treatment and only few cases have reported side effects associated with electrical shocking such as temporal muscle contraction and arrhythmia [24], [96]. More recent studies have adopted ECG synchronized IRE combined with general anesthesia to address the above side effects.

1.5 Clinical Results

IRE has been used clinically for more than fifteen years in combination with chemo therapy, and is on the rise as a monotherapy over the last five years. Internationally,

there are a number of ongoing clinical trials of IRE therapy [119]–[126] also reviewed in Table 1.3. For instance, Gothelf et al., [13] reviewed IRE electrode placement, field strength of pulses, drug delivery, anesthesia, and treatment evaluation for animal & human clinical trials. However, the studies covered in Gothelf's review were based on electrochemotherapy and all results were a combinational result of IRE injury with bleomycin. In 2010, Pech et. al. [120] (U of Magdeburg) reported the first in-man clinical study with IRE treatment on kidney (n=6). The study was for safety verification only. The tumors were surgically resected 5 minutes after IRE, and no treatment protocol was recorded in that paper. In 2011, Thomson et al. [121] published a larger scale of studies on various organs (clinical studies done in Australia). They investigated ECG synchronized IRE in 38 humans with advanced malignancy of liver (n=25), kidney (n=7), and lung (n=3), a total of 69 separate tumors (average=46cm^3). Complete tumor destruction verified by CT was achieved in 66% (46/69) tumors without IRE related adverse event. Complications found in this study include cardiac arrhythmia, temporary plexus injury, partial ureteric obstruction, and short term post procedure pain. In 2013, Cheung et. al. [125] (Australia) reported another IRE study on 11 patients with 18 unresectable hepatocellular carcinoma that were not RF suitable. The mean follow-up time period was 18 months. 13 of the 18 (72%) lesions were completely ablated with 93% success for lesions $\leqslant 3$ cm (13/14). The local recurrence-free period was 18 ± 4 months and the distance recurrence free period was 14 ± 6 months. No serious complications were observed in this study, although minor complications were found such as transient urinary retention, transient local post-procedure pain, and lesions lying adjacent to important structures or organs. In 2014, Neal et. al. [127] (Australia) reported two cases on IRE treatment of prostate cancer 3~4 weeks before surgical resection to evaluate safety and characterize the relevant properties to improve treatment planning

and outcome predictions. IRE has also been investigated for locally advanced pancreatic cancer in a series of studies by Martin et. al. [126], [128] and found to be safe and effective.

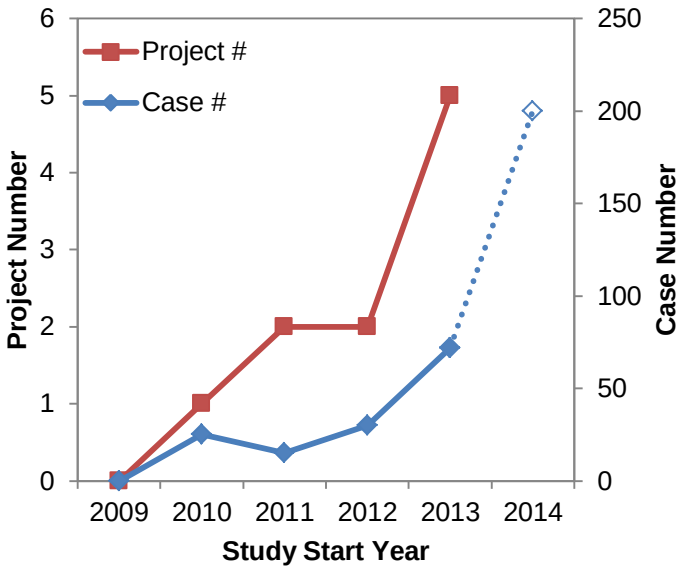

Figure 1.9. *Numbers of IRE clinical trials that are recruiting patients and registered in the United States from Table 1.3.*

A further list of organizations pursuing IRE clinical trials that are recruiting patients and registered in the United States can be found in Table 1.3. From this table, we can see that the number and scale of clinical studies on IRE have greatly increased since 2013 (Figure 1.9). Many of the studies on this list are still ongoing, and published results are not yet available. Hopefully, the published results will yield systematic observations that validate the use of IRE in the clinic.

Table 1.3. *Clinical trials of independent IRE studies registered on clinictrials.gov*

NCT Study #	Start/Finish Time	Patient #	Country	Targets	Endpoint Classification (Phase #)
NCT01078415	Feb 2010, Oct 2011	25	France, Germany, Italy, Spain	Carcinoma, Hepatocellular	S/E
NCT01442324	Feb 2011, Sep 2012	5	Italy	Metastatic Liver Cancer; Cholangiocarcinoma; Neoplasm Metastasis	S/E
NCT01369420	May 2011, Dec 2011	10	Italy	Pancreatic Adenocarcinoma	S (2)
NCT02010801	Apr 2012, Dec 2013	20	Taiwan	Malignant Liver Tumors	n/a
NCT01799044	Nov 2012, Sep 2013	10	Netherlands	Colorectal Liver Metastases; Metastatic Liver Disease	S/E (1)
NCT01790451	Aug 2013, Mar 2014	16	Netherlands	Prostate Cancer	S/E (1)
NCT01939665	Sep 2013, Sep 2014	10	Netherlands	Locally Advanced Pancreatic Carcinoma (LAPC); Non-metastasized Unresectable Pancreatic carcinoma; Pancreatic Cancer	S/E (1,2)
NCT01726894	Oct 2013, Apr 2015	20	UK	Prostate Cancer	n/a
NCT01967407	Oct 2013, Dec 2015	20	Germany	Kidney Tumor; Renal Cell Cancer	E (1,2)
NCT01972867	Nov 2013, July 2014	6	US	Prostate Cancer	S
NCT01835977	Jan 2014, Jan 2018	200	Netherlands	Prostate Cancer	S/E (2)

S-Safety, E-Efficacy

1.6 Limitations and Challenges of IRE

Despite the advantage and progress discussed above, IRE is still not the preferred choice of treatment for most diseases. IRE is usually considered only when other therapies are not applicable or fail to show an improvement. This lack of acceptance of IRE within the medical community is due in part to the status of development of the technology, and to several issues with the outcomes of IRE. Specifically, IRE has shown an inability to destroy large volumes of tissues without repeats or repositioning the

electrodes. This is an important limitation that remains to be fully addressed. For instance, the common lesion sizes reported in literature without repeats or repositioning the electrodes are still relatively small [26], [29], [57], [110]. This is because extremely high electric field needed to created larger lesions (greater than 2500 V/cm) cannot be applied clinically without damage to adjacent nerves and the cardiovascular system [96], [129]. Thus, using multiple probes or repeat treatment with repositioned probes are ways to increase the lesion size. Theoretically, with well-planned probe layouts, a larger and customized lesion could be achieved fitting the exact geometry of the target tumor. However, the addition of multiple probes increases the complexity and difficulty of the procedure, and makes the treatment more invasive to the patient.

A further limitation is the heterogeneity of injury within the target treatment zone. For instance, some studies [29], [101] show that incomplete treatment (live tumor patches in a target treated zone) have been found after IRE. This phenomenon is a real concern for cancer treatments due to the likelihood of recurrence, and if unresolved, represents a threat to the eventual translation of IRE. Importantly, local recurrence after hyperthermia and cryosurgery is significant and reported in the clinical literature [130]–[132]. However, having studied pre-clinical lesions for IRE, heat and cryo in an identical animal model, the appearance of live tumor patches within the treated tumor volume (rather than at the boundary) appears at this stage to be unique for electroporation [101], [133]. It is possible that the live cell patches are a result of local electrical property heterogeneity within the tumor tissue thereby lowering the effective electric field in the target region [134]. Thus, the challenge to improve the reliability of IRE cancer therapy calls for methods of enhancement that can ensure the electric field distribution over the entire target region is above the IRE threshold.

1.7 Potential Enhancement Approaches

1.7.1 Cytotoxic Agents

Perhaps in recognition of the smaller volume or potential for heterogeneous response within the tissue, several groups have already championed a combinatorial approach as mentioned earlier in the review entitled: “electrochemotherapy”. This method uses electroporation to open the membranes to allow chemotherapeutics such as bleomycin which are normally not taken up by cells to more easily internalize and destroy cells [13], [14]. A similar method proposed by Frandsen et. al. [61] uses direct intratumoral calcium injection followed by electroporation, leading to lethal intracellular calcium events. While promising, cytotoxic drug or molecules are still limited by the dose and side effects, thus further methods remain of interest to research and clinical groups.

1.7.2 Use of High-Frequency IRE

High-Frequency IRE (H-FIRE) is also a promising approach that could enhance the treatment outcome of IRE therapy. Unlike conventional IRE, H-FIRE protocols involve the use of microsecond bursts of bipolar pulses on the order of 500ns-5us, delivered at a pulse repetition rate of 1 Hz [94], [135]. The benefit of high-frequency IRE is that it provides the ability to administer IRE therapy without the use of neuroblocking agents to mitigate muscle contractions during the procedure [94]. In addition, high-frequency fields have the potential to overcome impedance barriers posed by low conductivity tissues, which could provide more predictable lesion volumes by mitigating the effects of patient-to-patient tissue variability, conductivity changes due to electroporation, and tissue heterogeneities [135]. H-FIRE is a relatively unexplored area of research at this moment [31] and future work is needed to elucidate the relationship between H-FIRE parameters and treatment volumes.

1.7.3 Membrane Modifications

Another class of studies focuses on enhancing the destructive efficacy of IRE itself without relying on chemotherapeutic drugs or cytotoxic agents to enter and kill the cancer cells. Specifically, approaches that directly modify membrane properties (i.e. line tension and surface tension) with surfactants, impeding the resealing process (big molecules, channel holders, etc), and fine tuning the pulse timing have all been tried and shown effective in enhancing the IRE destructive potential, as was summarized in Table 1.4.

Specifically, a study on IRE enhancement with DMSO has shown that over 60% increase in cell destruction *in vitro* and greater than 136% increase in treatment volume *in vivo* can be achieved by adding 5% volume percentage of DMSO to the cell suspension or perfused into the tissue [52]. Another study on lipid bilayer model has shown that as low as 0.1μM of $C_{12}E_8$ can lower the IRE transmembrane voltage threshold from 450mV to 333mV with their experiment setup [66]. Moreover, studies have shown that the pulse timing method can increase the cell destruction by 67% *in vitro* [136] and tissue destruction volume by 101% in *vivo* [52], respectively. Because the pulse timing approach does not introduce any foreign molecules into the body, it enhances the efficacy of IRE with virtually no additional cost (except for slightly longer procedure time) and can be combined with any existing treatment or enhancement protocols.

The number and variety of studies on IRE enhancement is still limited at this time. However, it is a promising path to follow and can greatly increase the acceptance and capability of IRE tissue destruction for clinical applications.

Table 1.4. *Membrane targeted enhancements for IRE*

	Model	Adjuvant	Dose	Timing	Injury Evaluation	Indications	Ref.
Surfactant addition	Prostate cancer cells	DMSO	1% ~15% v/v	1 min before IRE	PI and Hoechst	>75% increase in cell destruction	[136]
	Mice DSFC tumor	DMSO	5% v/v	6 min before IRE	Histology, intravital imaging	>136% increase in injury volume	[52]
	Lipid bilayer	$C_{12}E_8$	conc. dependent, but worked as low as 0.1uM			Lower threshold voltage	[66]
	Pig skin	SDS (sodium dodecyl sulfate)					[137], [138]
Channel effect	Lipid bilayer	Gramicidin D	conc. >1:500			Increase threshold voltage	[67]
	Lipid bilayer	a-hemolysin					[139]
Pore holder	Pig skin	Heparin					[140]
	Pig skin	Sodium thiosulfate					[141]
Pulse timing	Prostate cancer cells			3 trains with 10s~2mins delays	PI and Hoechst	>67% increase in cell destruction	[136]
	Mice DSFC tumor			3 trains with 30s delays	Histology, intravital imaging	>101% increase in injury volume	[52]

Chapter 2. *Membrane-Targeting Approaches for Enhanced Cancer Cell Destruction with Irreversible Electroporation*

Contributing Authors: Chunlan Jiang, Zhenpeng Qin, and John C. Bischof

The following chapter appeared in publication:

C. Jiang, Z. Qin, and J. C. Bischof, "Membrane-Targeting Approaches for Enhanced Cancer Cell Destruction with Irreversible Electroporation," Ann Biomed Eng, August, 2013.

2.1 Introduction

Electroporation, or electropermeabilization, is a promising technology that induces significant increase in conductivity and permeability of the plasma membrane by exposing the cells to a series of short, high-voltage electric pulses [1]. It has been widely used in molecular biology as a method to introduce foreign molecules, including ions, dyes, antibodies, RNA and DNA fragments, into living cells thereby supporting fields such as drug delivery and gene transfer [6], [7]. Recently, Davalos, Rubinsky, and Mir [16] proposed the use of electroporation as a means of soft tissue destruction, sometimes termed "ablation" in the medical community. Pre-clinical testing *in vitro* [19] and *in vivo* [21], [22], [110] has been undertaken to support this new modality. Unlike traditional electroporation, where cells are only expected to be temporarily permeabilized and recover after the treatment; irreversible, or lethal poration is the goal in cancer therapy applications. Therefore, the term "irreversible electroporation" (IRE) is used to distinguish this approach. The purported benefits of IRE are that it is simpler and faster while maintaining the minimally invasive nature of existing thermal therapies (i.e. RF and

cryosurgery). Electric pulses of IRE are normally delivered by millimeter-sized probes and take only seconds to deliver. In addition, *in vivo* studies have shown that the demarcation between live and treated tissue (usually referred to as the “transition zone”) is sharper compared with thermal therapies [24], [142]. It has also been suggested that IRE could destroy tumor cells while preserving tissue structures such as major ducts and vessels within the target region [24]. Being a non-thermal therapy [143], [144], IRE is free from the heat sink effect of local vascular systems, which helps future clinical planning as it is less dependent on perfusion (currently a limiting issue in thermal therapies [25], [145]), making IRE a superior candidate for tumors that are adjacent to major blood vessels or ducts.

A wide variety of cell [17]–[20], [57], [68], organ [26]–[28], and animal [21], [24], [29] models have been used to characterize IRE in different cancer types. The first in-man phase I clinical trial [120] has also been conducted on patients with renal cell carcinoma. No significant safety issues were noted based on hematological, serum biochemical and ECG recordings of the patients, although long-term effects remain to be studied in larger clinical trials. More recent clinical trials have been reviewed in [30]. However, despite these encouraging results reported, there are several limitations with this emerging technique, which could present hurdles to its clinical translation. Perhaps the most critical one is the inability of IRE to destroy large volumes of tissue under a safe electric field strength level. For instance, the common lesion sizes reported in the literature with double needle probes are currently small [26], [29], [57], [110]. While it is possible to enlarge the treatment volume by increasing the voltage on the central electrode, extremely high electric fields (greater than 2500V/cm) are needed and not appropriate for clinical application as adjacent nerves and the cardiovascular tissue may be

damaged with such high fields [96], [129]. Using multiple probes is another way to increase lesion size. Theoretically, with well-planned probe layouts, a larger and customized lesion could be achieved fitting the exact geometry of the target tumor. However, the addition of multiple probes not only makes the treatment more invasive to the patient, but also increases the complexity of the operation procedure, making IRE a less attractive approach to the surgeon.

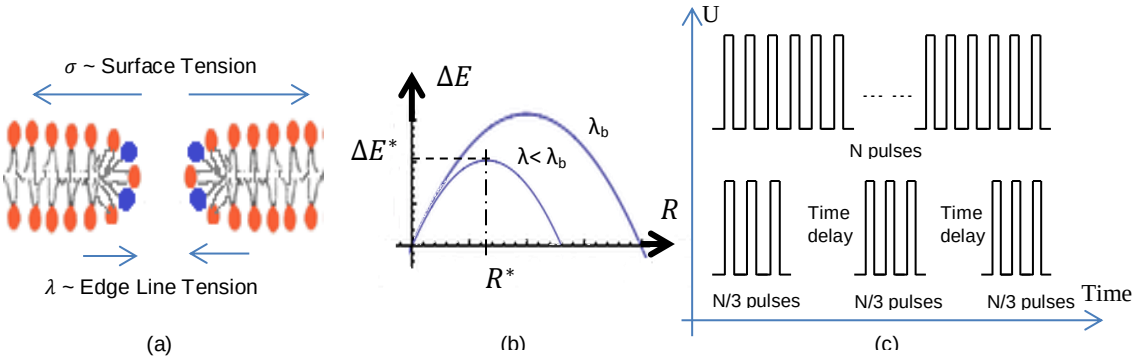

Figure 2.1. *Reported IRE enhancement strategies: (a) competing factors (surface tension and edge line tension) during pore formation, (b) nucleation based energy model and critical pore radius & energy, and (c) illustration of the pulse timing delivery method*

There are several approaches to expand the tissue volume that can be treated by electroporation including the addition of chemotherapeutic or cytotoxic agents, and approaches that increase electropermeabilization of the membrane. Combining chemotherapy with IRE has been championed by several groups and is referred to as “electrochemotherapies” [13], [14]. A similar method was also proposed recently by Frandsen et al. [61] using direct intratumoral calcium injection followed by electroporation, which led to lethal intracellular calcium events. While these studies demonstrated improved cell killing, the focus was on enhancing the ability of

chemotherapeutic drugs or cytotoxic agents to enter and kill the cancer cells rather than enhancing the efficacy of IRE itself. However, the aim of this study is to investigate the ability to increase the destructive ability of IRE without relying on cytotoxic drugs. Specifically, mechanisms that directly modify membrane properties (i.e. line tension and surface tension, See Figure 2.1a) should reduce the voltage threshold for lethal permeabilization and therefore increase the efficacy of cell killing and therefore the volume treated after a given IRE. Two methods to achieve these changes are proposed in this study: 1) addition of surfactant (e.g. Dimethyl sulfoxide, or DMSO) to directly interact with membrane lipids thereby changing membrane line tension and surface tension, Figure 2.1b, and 2) use of pulse timing (i.e. introduction and persistence of defects in the membrane between pulses, Figure 2.1c). Experimental studies were conducted on a human prostate cancer model (LNCaP Pro 5) under both *in vitro* (cell suspension) and *in vivo* (Dorsal Skin Fold Chamber) conditions, both with multiple viability assessment methods to evaluate and compare the injury levels with or without IRE enhancement. Here, we document that both of the two non-toxic approaches we propose (surfactant adjuvant and pulse timing) can be highly effective in enhancing the destructive potential of IRE *in vitro* and *in vivo*. Furthermore, the mechanism of enhancement is shown to be linked to membrane stability thereby allowing a reduction in the energy barrier required for irreversible pore formation.

2.2 Materials and Methods

2.2.1 Tumor Cell Culture

The prostate cancer cell line (LNCaP Pro 5) was cultured as adherent monolayer in Dulbecco's Modified Eagle's Medium (DMEM)/F12 (BD Biosciences, CA) supplemented with 10% fetal bovine serum, 100U/ml of Penicillin/Streptomycin (P4333, Sigma-Aldrich,

MO), and 10^{-9} mol/L dihydrotestosterone (DHT) as previously described [112]. When >85% confluence was reached, the cells were detached by adding 0.05% Trypsin-EDTA (Invitrogen, CA) and then made into a single cell suspension.

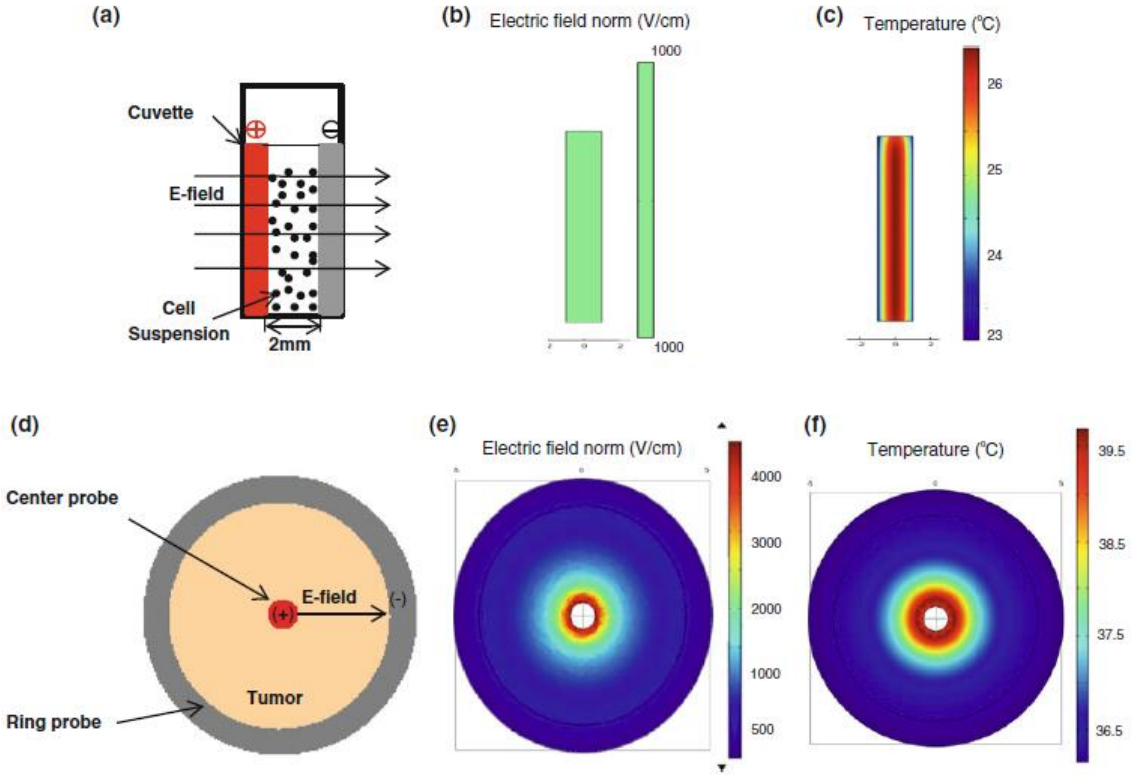

Figure 2.2. *Experiment setup for in vitro IRE system: (a) Schematic graph of the IRE cuvette system, (b) electric field distribution over the cuvette gap with 200V applied across the gap, (c) temperature change after baseline IRE treatment; and in vivo IRE system: (d) Schematic graph of the chamber surface layouts, (e) electric field distribution over the chamber with 500V applied on the center electrode, and (f) temperature change after baseline IRE treatment*

2.2.2 In vitro Electroporation

For each *in vitro* electroporation test, 400 µl of the prepared cell suspension (0.5~0.6 million cells/ml) was pipetted into the electrode gap (2 mm) in an electroporation cuvette

(FB102, Fisher Scientific), which was then placed in an external electric field created by an electric pulse generator (BTX ECM 830, Harvard Apparatus), as is shown in Figure 2.2a. The pulsing frequency is 10Hz unless otherwise specified. The output voltage and current were monitored by an oscilloscope (Tektronix TDS 2002).

2.2.3 Enhancements

DMSO enhancement was achieved by first incubating the cell suspension with DMSO at 1% to 15% volume fraction (v/v) before IRE treatment. This incubation lasted for 1 minute to allow sufficient diffusion of DMSO molecules into the cell membrane while showing minimal toxicity to cells as compared to controls (supplementary information, S2.1). To reduce the impact of DMSO on extracellular electrical conductivity during IRE or toxicity after, the cell suspension was diluted below 1% v/v immediately before the IRE procedure. All groups in Figure 2.5 were exposed to one train of 50 pulses (200V, 50μs per pulse).

With pulse timing, the total energy delivered (51[1] pulses, 200V, and 50μs per pulse) was the same throughout the experiment groups. However, the 51 pulses were divided into 3 trains of 17 pulses with varied delays in between trains (10s, 30s, 1min, and 2 min). The pulse timing delivery method is illustrated in Figure 2.1c.

2.2.4 In vitro Viability Assay

In vitro cell viability for experimental and control groups were evaluated using a Tetrazolium-based CCK-8 assay (Dojindo Molecular Technologies, Inc) that measures the dehydrogenase enzymatic activity associated with metabolic processes in live cells.

[1] We chose to use 51 pulses in the pulse timing method so that the same number of pulses (17) can be delivered in each train. The dose difference between 51 and 50 pulses in our baseline groups is marginal.

The cell suspensions were electroporated as described above. After IRE, 100 µl aliquots of the cell suspensions were mixed with 10 µl of CCK-8 reagent in a 96 well plate and incubated for 4 hours at 37 degrees Celsius in the incubator with 5% CO2. The optical absorption of the sample (Figure 2.3a) was then read in a spectrophotometer (Synergy, BioTek Inc., VT) at a wavelength of 450 nm to determine the viability according to a standard protocol as outlined in the manufacturer's manual. The viability results were presented as a standardized (or normalized) percentage value with respect to the controls. By membrane dye (Hoechst, PI), the viability of controls was consistently 96±3 %.

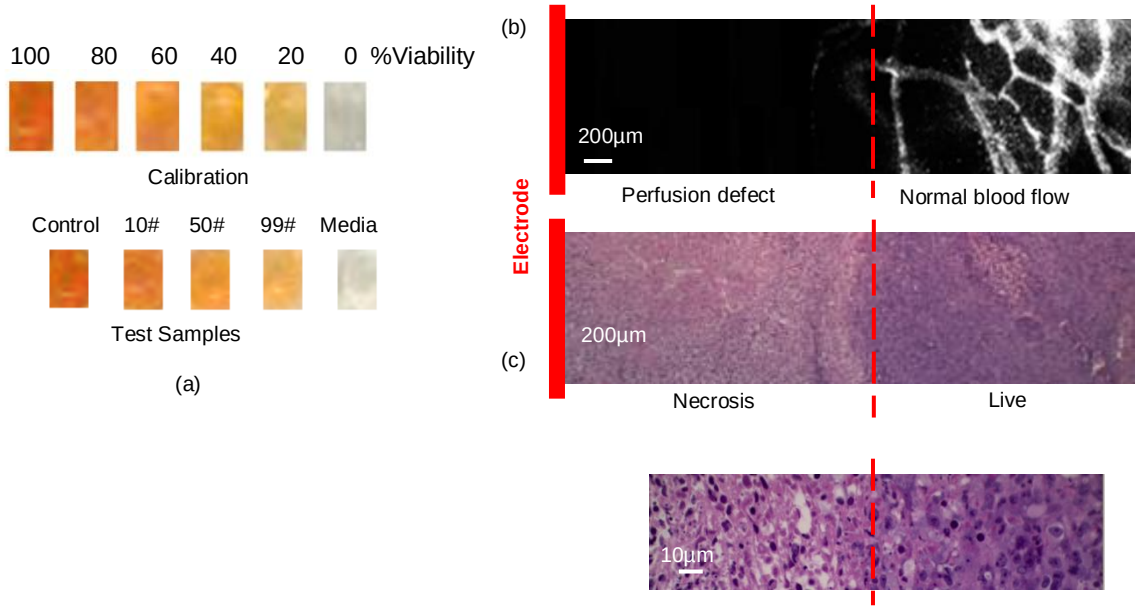

Figure 2.3. *Injury assessment for the in vitro IRE system with the CCK-8 cell viability assay (a); and for the in vivo IRE system injury evaluation by perfusion defect characterization from the intravital microscopy (b), and necrosis characterization from the histological image (c)*

2.2.5 In Vivo Tumor Cell Seeding and Growth

The DSFC tumor system is a two dimensional, controlled environment in which tumor growth is restricted between two anodized aluminum frames, separated by a small

distance of 0.5 mm maintained by spacers on the screws [133]. The frames with a 10 mm diameter viewing window are implanted on the dorsal skin of the animal. The DSFC chambers were implanted in nude mice (Jackson Laboratory, Bar Harbor, ME) as previously described in [133]. In brief, the skin on the back of the mouse was sandwiched between the chambers. The skin on the viewing side was removed to expose the dermis with microvasculature on the opposite side. For clear visualization, excess fascia on the dermis was removed. A quartz glass microslide was used to cover the viewing side of the window to reduce evaporation and keep the tissue sterile during the experiment. All animal usage and experimental procedure protocols were approved by the Institutional Animal Care and Use Committee of the University of Minnesota.

2.2.6 In Vivo Electroporation

For *in vivo* electroporation, a needle electrode (d=1mm) was inserted through the tumor and skin in the center of the DSFC window and a ring electrode connected to the edge of the chamber (thickness = 1mm and height = 2.5mm), as is shown in Figure 2.2d and previously reported by Qin [101]. An insulating layer was placed around the ring electrode to avoid arc formation. The applied voltage and current were monitored by oscilloscope (Tektronix TDS 2002). The pulsing frequency is 10Hz unless otherwise specified. An infra-red (IR) camera was also used to record the temperature from the top surface of the tumor.

2.2.7 Enhancements

For DMSO enhancement, 20 µl of DMSO dilution (5% v/v) in 0.9% saline was applied topically over the DSFC tumor surface. This concentration was determined based on our best results from the *in vitro* experiments (Figure 2.5). The dilution was left on the

window for 6 minutes (see supplementary information, S2.2 for calculation of diffusion time) to allow for diffusion within the tumor volume before electroporation. Electroporation was performed in one train of 50 pulses (500V, 50μs per pulse).

To assess the impact of pulse timing, 51 total IRE pulses (500V, 50μs per pulse) were divided into 3 trains of 17 pulses with delays of 30 seconds in between trains. This delivery pattern was determined based on our best results from the *in vitro* experiments suggesting no further benefit to longer pulse delays (Figure 2.5b).

2.2.8 In Vivo Viability Assessments

The perfusion defect after either DMSO or pulse timing enhancement was visualized by intravital fluorescent microscopy and recorded before treatments, and immediately, 1 day and 3 days after the treatments. The animals were sacrificed on day 3, and tumors were taken for histological staining and evaluation. Perfusion defect (or vascular stasis) can be measured by the lack of fluorescence within a vessel after intravenous injection of a fluorescent dye [101]. The perfusion defect of the electroporated (or control) tumor microvasculature was visualized after 10mg/ml 70-kDa FITC–labeled dextran was administered by tail vein injection. The anesthetized animals were fixed on a specially designed mouse stage which was mounted to an inverted fluorescence microscope (Figure 2.3b). The DSFC is traversed radially in four perpendicular directions (north, south, east, and west) while radial locations of stasis were noted using a micrometer scale fixed on the stage with the chamber center as the origin. This technique has been used extensively by our group [101], [112]. The animals were sacrificed 3 days after IRE (or IRE plus enhancement) treatment and the tumors were removed and fixed in 10% buffered formalin for 48 hours. The tumor samples were then embedded in paraffin,

sectioned at 5µm, and stained with Hematoxylin-Eosin (H&E) dye. The whole tumor section was imaged under a stereomicroscope with a large field of view (Leica MZ FL III fluorescence stereomicroscope) to examine the entire tumor area. Images were taken and then processed using Image J to trace the region of necrosis demonstrating destruction (Figure 2.3c).

2.2.9 Data Analysis and Statistics

Group numbers of n≥4 and n≥8 were achieved for all of our *in vitro* and *in vivo* experiments, respectively. The results are presented as average values ± standard deviations. The student t-test was performed between experimental and control groups where P value ≤ 0.01 was taken to delineate statistical significance between groups. The IRE parameters used in the above experimental models and conditions are summarized in Table 2.1.

Table 2.1. *Summary of experiment conditions and enhancement outcomes*

	IRE pulse parameters					Outcome
In vitro	Volt. (V)	E-field (V/cm)	Duration (µs)	Number	Freq. (Hz)	Enhancement (cell viability)
Baseline	200	1000	50	50	10	(~50%)
DMSO	200	1000	50	50	10	75% increase (~10.42%)
Timing	200	1000	50	3 × 17	10	67% increase (~13.48%)

	IRE pulse parameters					Outcome	
In vivo	Volt. (V)	E-field (V/cm)	Duration (µs)	Number	Freq. (Hz)	Enhancement (necrosis volume on day 3, mm^3)	Enhancement (perfusion defect volume on day 3, mm^3)
Baseline	500	50–4000	50	50	10	(10.3)	(9.0)
DMSO	500	50–4000	50	50	10	136% increase (24.3)	120% increase (19.9)
Timing	500	50–4000	50	3 × 17	10	101% increase (20.9)	107% increase (18.7)

2.3 Modeling

2.3.1 Membrane Poration Model

Arguably, the most critical cellular response to IRE is the permeabilization of the cell membrane during electric pulsing as shown in Figure 2.1. Previous studies have shown that the likelihood of membrane rupture during electroporation is closely associated with the energy dynamics under an external electric field [54]. The free energy ($\Delta \mathrm{E}$) associated with pore formation on the cell membrane can be modeled with a modified nucleation model [33] as described in Eqn (2.1):

$$\Delta E(R,\, U) = 2\pi R \cdot \lambda \, - \, \pi R^2 \cdot (\sigma + aU^2) \tag{2.1}$$

The creation of membrane pores during IRE depends on the free energy *(ΔE)* of pore formation on the cell membrane (See Eqn 2.1). When the pore exceeds a critical radius (R^*), the free energy decreases as the pore expands, which further induces membrane rupture and leads to cell death. In other words, ΔE works as an energy barrier for the pore formation. When an external electric field is applied across the cell membrane (U >0), the energy barrier for such a critical pore to develop is decreased, which explains why electroporation can greatly increase the permeability of the cell membrane.

However, the increase of transmembrane voltage is not the only approach to reduce the energy barrier in this model. As shown in Eqn 2.1, decreasing the edge line tension λ can also alter the free energy of pore formation (ΔE) and thus greatly impact the pore formation process. According to the membrane elastic model by Karatekin [146], the membrane edge line tension λ is influenced by its bending modulus κ, the membrane thickness h, the inclusion fraction θ of foreign molecules, and the spontaneous curvature C_0 of the included molecules, as in Eqn (2.2):

$$\lambda = \pi \cdot \kappa \cdot \left(\frac{1}{h} - \theta \cdot C_0\right) \tag{2.2}$$

Interestingly, earlier studies have shown that the addition of certain surfactants and peptides can reduce the threshold of electroporation in artificial membrane systems [66], [67], [147]. An example of this surfactant group is DMSO. When absorbed in the head regions of the lipid bilayer, they can help lower the edge line tension (λ) by decreasing the bending modulus (k) and introducing positive curvature ($\theta * C_0$) groups. Molecular dynamics simulation in [148] has demonstrated that 11.3 mol % DMSO leads to over 90% decrease in line tension on modeled lipid bilayer membrane, which may cause a significant reduction of IRE threshold (Figure 2.1b).

2.3.2 Electrical and Thermal Models

The electric field distributions in our *in vitro* and *in vivo* systems were modeled using COMSOL Multiphysics software. For the electroporation cuvette, the electric field is considered homogeneous across the 2 mm gap and generates 1000V/cm E- field with the 200V pulses as shown in Figure 2.2b. The E-field distribution in the DSFC is determined by Laplace equation (Eqn (2.3)):

$$\nabla \cdot (\Omega \cdot \nabla \varphi) = 0 \tag{2.3}$$

where Ω is the electrical conductivity of tumor, φ is the electric potential. For homogeneous tissue, the electric field calculated from Eqn (2.3) shown in Figure 2.2e.

When neglecting heat losses, the energy from electric current all goes to tissue heating, which is illustrated by:

$$SAR = \Omega \cdot |\nabla \varphi|^2 \tag{2.4}$$

Using the bioheat equation implemented in COMSOL by adding a heating term (SAR in Eqn (2.4)) from the electric pulsing:

$$\rho c_p \frac{\partial T}{\partial t} = \nabla \cdot (k \nabla T) + \rho_b \omega_b c_b \cdot (T_b - T) + q''' + SAR \tag{2.5}$$

where ρ, c_p, and T are density, heat capacity and temperature of the tissue, ρ_b, ω_b c_b, and T_b are density, flow rate, heat capacity and temperature of the blood, and q''' is metabolic heat. In the *in vitro* case, the blood flow and metabolic heat terms were set zero. The parameters used in our models are summarized in Table 2.2. This model allows the temperature rise after IRE pulsing to be captured as shown in Figure 2.2c and 2.2f. It is worth noting that the conductivity of tissue will increase during IRE due to electroporation's permeabilization effect which has been noted in previous work from our lab [101]. We have elected not to pursue this here in order to focus solely on the impact of DMSO and pulse timing without the confounding effects of conductivity change. Certainly more careful study is warranted in the future.

Table 2.2. *Summary of parameters used in our models*

Quantity	Symbol	Units	Value
Tissue electrical conductivity	Ω	S/m	0.286
Tissue thermal conductivity	K	W/(m K)	0.5
Tissue heat capacity	c_p	J/(kg K)	3750
Tissue density	A	kg/m^3	1000
Blood temperature	T_b	C	37
Blood density	ρ_b	kg/m^3	1000
Blood heat capacity	c_b	J/(kg K)	3640
Blood perfusion rate	ω_b	kg/(m^3 s)	0.5
Metabolic heat	q'''	W/m^3	16,900
Heat transfer coefficient	h	W/(m^2 K)	50
Initial tumor temperature	T_0	C	37
Room temperature	T_r	C	25
IRE electric potential	φ	volt	200 or 500
IRE pulse duration	td	μs	50
IRE total pulse number	N	n/a	50
IRE frequency	f	Hz	10
Free energy with pore formation	ΔE	J	
Pore radius	R	m	
Transmembrane voltage	U	volt	
Membrane line tension	λ	J/m	$1–6 \times 10^{-11}$
Membrane surface tension	σ	J/m^2	$0.5–2 \times 10^{-3}$
Lipid–water dielectric coefficient	a	n/a	0.043
Membrane bending modulus	κ	J	2.7×10^{-20}
Membrane thickness	h	m	10×10^{-9}
Inclusion fraction of foreign molecules	θ	n/a	
Spontaneous curvature of the included molecules	C_0	1/m	
Boltzmann's constant	k	m^2 kg/s^2/K	1.38×10^{-23}
Absolute temperature	T_a	K	298
Avogadro's number	N_A	n/a	6.022×10^{23}
Radius of water molecule	r_w	m	0.957×10^{-10}
Viscosity of the suspending solution	η	P	0.9×10^{-3}
Molar volume of water	v	m^3/mol	18×10^{-6}
Membrane surface area	A_m	m^2	2×10^{-6}

2.4 Results

2.4.1 In vitro Enhancement

The results obtained with proposed enhancement strategies will be compared with a "baseline electroporation". Specifically, a baseline dose was established which achieved close to 50% cell death after IRE. Here we based the dose on the pulse number while holding other parameters fixed. For instance, the electric voltage, pulse duration, and frequency were fixed at 200V (over the 2 mm cuvette gap), 50 µs, and 10Hz and then the pulse number was increased from 10 to 99 times. This showed a dose-dependent decrease in cell viability after electroporation (Figure 2.4). Based on this data we chose 50 pulses as our baseline dose (i.e. 50% cell destruction) after IRE.

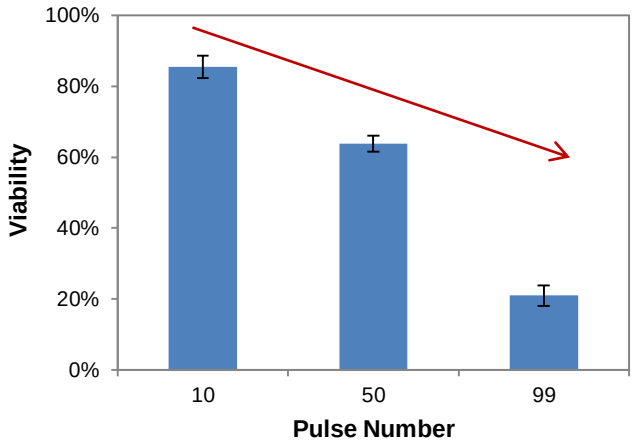

Figure 2.4. *. Baseline viability results after IRE treatment in vitro. Each data point represents the average of n=4 measurements ± SD*

The change of cell viability with the addition of DMSO alone was negligible when concentrations were under 5% v/v (supplementary information, S1). However, when combined with IRE pulsing, the cell viabilities dropped significantly as DMSO concentration was increased (Figure 2.5). A significant enhancement of 75% more cell killing based on cell viability before and after IRE pulsing was found with addition of 5% v/v DMSO in our experimental sets (Figure 2.5, n=4, student t-test, p=0.01).

With pulse timing, the IRE dose, or total energy delivered was similar (51 pulses, 200V, and 50μs per pulse), however the total pulses were spread out. Figure 2.5b demonstrates that this pulse timing has a dramatic impact and an enhancement of 67% in cell killing was achieved. Interestingly, the introduction of time delays also increased the time for heat to diffuse, therefore reducing the maximum temperature rise (ΔT_{max}) from 2.7 degrees to less than 1 degree. The time delays were varied for 10s, 30s, 1 min and 2 mins, and yielded consistent enhancement results between the baseline IRE and

the timing method (student t-test, p=0.008), although no significant difference was observed among the different delay times. After demonstrating that DMSO and delayed pulse timing were capable of significant enhancement *in vitro*, these effects were also tested *in vivo* with a tumor model.

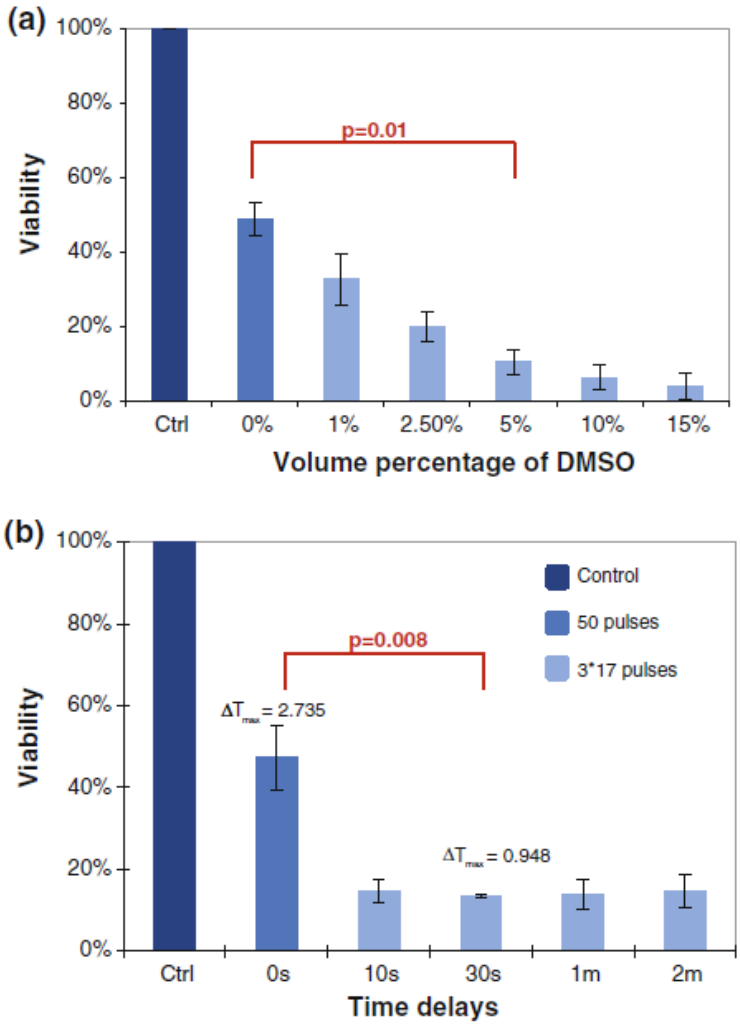

Figure 2.5. *. In vitro IRE with varied concentrations of DMSO (a) and pulse timing (b). Each data point represents the average of n=4 measurements ± SD*

2.4.2 In Vivo Enhancement:

In order to demonstrate enhancement *in vivo* it was again necessary to establish a baseline electroporation dose in the DSFC tumor model. This was chosen based on a previous IRE study conducted in our lab [101] with the same experimental system. Specifically, we chose 50 pulses (500V, 50μs per pulse) as our baseline treatment dose as it gives a moderate level of injury of nearly ½ the chamber radius after IRE (10.3 mm^3 by histology and 8.7 mm^3 by perfusion defect).

The enhancement results by histology are presented in Figure 2.6, for both DMSO treatment and pulse timing. Specifically, Figure 2.6a shows that the tumors treated with 5% v/v DMSO developed a 24.3 mm^3 necrotic lesion compared with the baseline level (10.3 mm^3) demonstrating a 136% augmentation of volume ($p=0.001$ from the student t-test). Similarly, in Figure 2.6c, pulse timing lead to a 20.9 mm^3 of necrosis corresponding to a 101% increase in volume over baseline ($p=0.003$ from the student t-test).

No perfusion defect was observed in tumors via intravital imaging before the IRE treatment, with or without application of DMSO. Immediately after IRE treatment, the blood perfusion was blocked almost across the entire chamber, with or without enhancement (Figure 2.6b and 2.6d). This effect has been reported before in [96] and is believed to be related to electrical stimulation on the smooth muscle cells, also known as the “SMC effect”. In our study, this acute perfusion block is temporal and reversible, as revealed by the rapid recovery of perfusion defect by day 1 in all experimental groups.

At day 1, the perfusion defect stabilized and could be measured. The enhancement measured by perfusion defect was similar with that measured by histology. For instance, with DMSO addition, the perfusion defect volume was 139% greater than baseline on

day 1 and 120% greater on day 3. For the pulse timing method, the perfusion defect volume was 111% greater than baseline on day 1 and 109% greater on day 3. The perfusion defect radius slightly increases from day 1 to day 3, however, the difference is not significant (p>0.15 by student t-test).

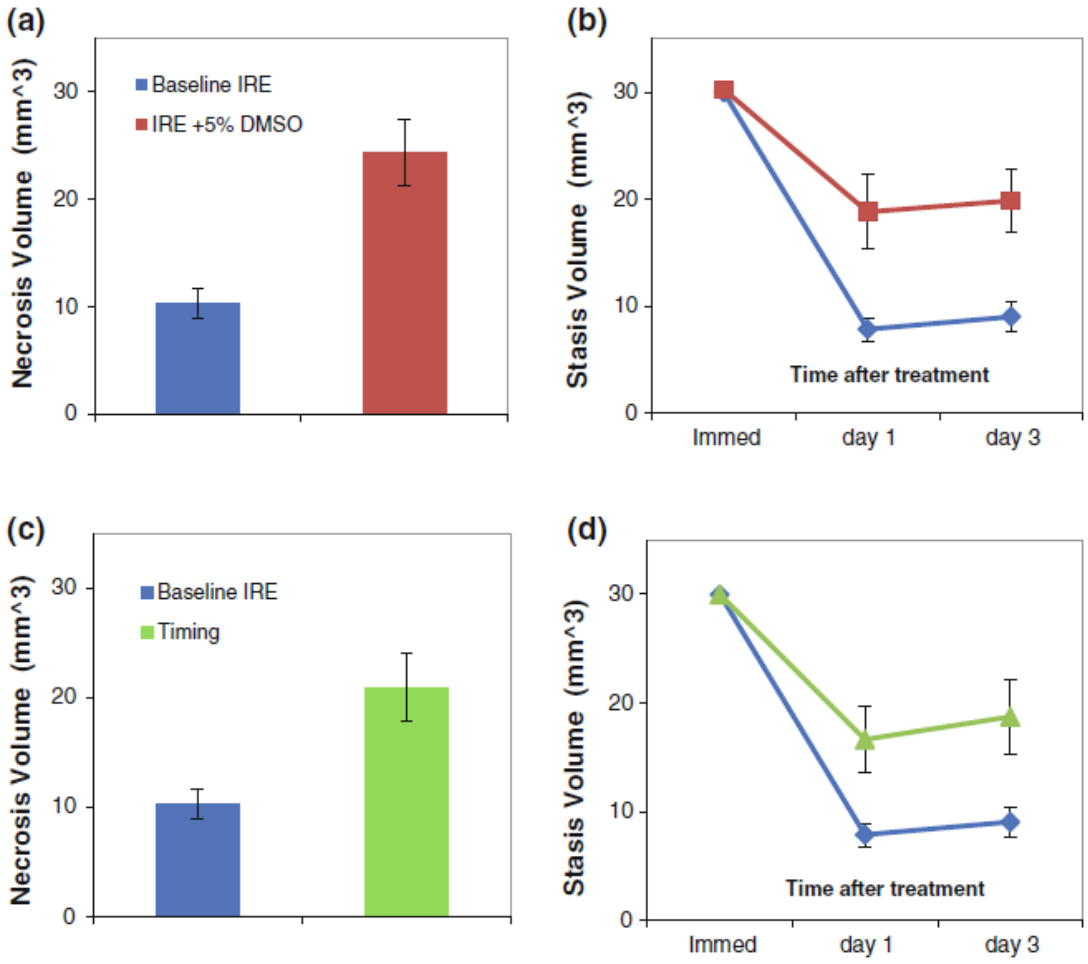

Figure 2.6. *In vivo IRE results with: 5% v/v of DMSO (a) and (b), and pulse timing enhancement (c) and (d). Each data point represents the average of n=8 measurements ± SE*

2.5 Discussion

A noted limitation of IRE is insufficient treatment volume in tumors. In this work, we applied membrane-targeting approaches to increase the treatment volume under similar IRE dose (pulse voltage, duration, and number). Specifically, we demonstrated that direct application of DMSO at non-toxic concentrations and introducing time delays between pulse trains could both increase the destructive potential of IRE. *In vitro* results show 67%~ 75% enhancements in cell killing. Further, *in vivo* study reproducibly shows more than 100% enhancement in the treatment volume by two independent methods ($p \leq 0.001$ from student t-test). Importantly, we believe that the common mechanism of our proposed approaches (DMSO and pulse timing enhancement) is linked to change of line tension in the membrane rather than cytotoxicity. This can be argued theoretically below for both DMSO and pulse timing.

To demonstrate the impact of decreased line tension on reducing IRE threshold, we implemented the nucleation model in [33], [54] with the rate of critical pore formation determined by Eqn (2.6):

$$I(\Delta E^*) = 4kT_a N_A r_w \cdot \left(\frac{\Delta E^*}{kT_a}\right)^{\frac{1}{2}} \cdot \exp(-\frac{\Delta E^*}{kT_a})/\left(3 \cdot \sqrt{\pi}\eta v h^3\right) \tag{2.6}$$

where critical pore energy $\Delta E^*$is given in Eqn (2.7).

$$\Delta E^*(R^*, U) = \frac{\pi\lambda^2}{(\sigma + aU^2)} \tag{2.7}$$

The parameters used in our model are summarized in Table 2.2. When a large population of cells is exposed to electroporation, the occurrence of irreversible membrane breakdown as a result of random fluctuations of pores can be assumed to be a stochastic process, with the probability

$$P(U,t) = 1 - \exp(-\int_0^t I(U)A_m\, dt) \tag{2.8}$$

We first define U_{th} as the threshold of transmembrane voltage which accounts for complete membrane breakdown (P>0.99), the impact of line tension λ on U_{th} can be calculated from the above equations. The values of membrane line tension reported in literature are $1*10^{-11}$ ~$6*10^{-11}$ J/m [53]. From Figure 2.7a, we can see the reduction of membrane line tension has a dramatic impact on IRE threshold. Over one order of magnitude of drop in U_{th} can be achieved by reducing λ from $5*10^{-11}$ to $1*10^{-11}$ J/m. In our case, the inclusion of 5% v/v DMSO can lower the line tension by at least 20% [149]. Therefore, our proposed explanation for DMSO enhancement is that the inclusion of DMSO molecules in the cell membrane can lower the edge line tension thus decreasing the energy barrier for pore growth, leading to enhanced membrane rupture and cell injury after IRE.

Notably the introduction of DMSO also reduces the surface tension of the membrane. However, the impact of surface tension on U_{th} is marginal compared with line tension as shown in the sensitivity curve of $U_{th}$to the membrane surface tension σ (Figure 2.7b). Specifically, less than 1% drop of $U_{th}$was induced when increase σ for one order of magnitude ($0.1*10^{-3}$ to $1*10^{-3}$ J/m^2), compared to more than one order of magnitude of

drop achieved by reducing λ for one magnitude. Therefore, the changes of surface tension are neglected in our modeling.

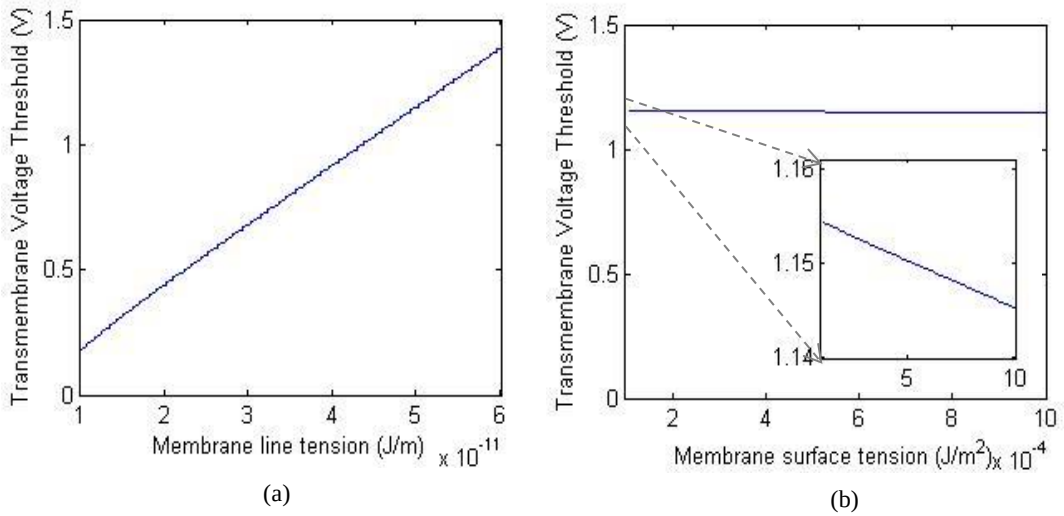

(a) (b)

Figure 2.7. *Impact of membrane (a) line tension and (b) surface tension on IRE transmembrane threshold.*

Similar to DMSO, pulse timing can also be used to directly impact membrane poration by reducing line tension in recovering pores. For instance, experimental measurements and theoretical estimations of electroporation [46] reveals that under intense electric pulsing, membrane defects originates within μs, and can last through the entire time the external field is applied (several μs to hundreds of ms). However, the membrane defect recovery timing is much slower once the pulsing is finished, generally longer than 1s and can take up to minutes [77]. The difference in the two time scales makes it possible to enhance the IRE killing effect by fine tuning the pulse timing to leverage these half recovered pores.

At least two contribution factors can explain the enhancement effect of pulse timing. First, earlier pulses can lead to formation of both reversible and irreversible pores on the membrane. Since complete resealing of the membrane can take up to minutes, the cell membrane will remain more susceptible to further pulsing due to both reduced membrane thickness from recovering pores and reduced line tension [146] during this recovery period. Although qualitative calculation is not given here, the dramatic impact of reduced line tension has been demonstrated in Eqn (2.6~2.8) and Figure 2.1 and 2.7 and can help explain the significant enhancement effect from pulse timing. Second, extended pore opening time can also increase cell injury and death due to loss of critical ions, proteins, and even cell components. When the pulses are delivered in one train, only one recovery period is presented after the pulsing. However, when the pulses are delivered in several trains with seconds of delays in between, the total pore exposure time is the sum of all delays and the final recovery period. Therefore, more secondary injury could be caused due to this extended pore opening time.

Importantly, there is the potential for non-uniform DMSO distribution in tissue to affect IRE enhancement. In our DSFC model, the local tissue conductivity is assumed to be elevated homogeneously as the fluid (saline + DMSO) is added topically and allowed to diffuse throughout. We can then argue that the distribution of electric field within the tumor should remain relatively constant. It is however, possible that if the solution were injected locally into the tissue, as in a solid tumor case, there could be conductivity variations which would change the overall electric field. In addition, testing and optimization of the pulse frequency, delay times between pulses, and numbers of pulse groups in our pulse timing method are worthy of further study in the future.

2.6 Summary

In this study, two membrane-targeting approaches were shown to increase the treatment volume of IRE for local malignant tumors. Specifically, the use of either surfactants (i.e. DMSO) or pulse timing to modify membrane properties can greatly enhance IRE treatment efficacy. Using the above methods, 67~75% more cell killing *in vitro* and more than 100% increase in treatment volume *in vivo* have been achieved without relying on any cytotoxic drugs or agents. Because DMSO is commercially available and regularly used at low concentrations (<10% v/v), this approach could easily be integrated into current IRE procedures to increase the treatment efficacy. In addition, introducing pulse timing delays in IRE also increases the destructive potential of IRE without the introduction of any foreign agents into the body. Clearly further tests in advanced tumor systems (e.g. spontaneous or implanted solid tumors) are needed to more fully evaluate the efficacy of our proposed approaches. Nevertheless, we suggest that the simple and safe nature of these enhancement approaches compared with cytotoxic drugs may help in the refinement of electroporation procedures for cancer.

Supplementary Information

S2.1 DMSO Toxicity Test

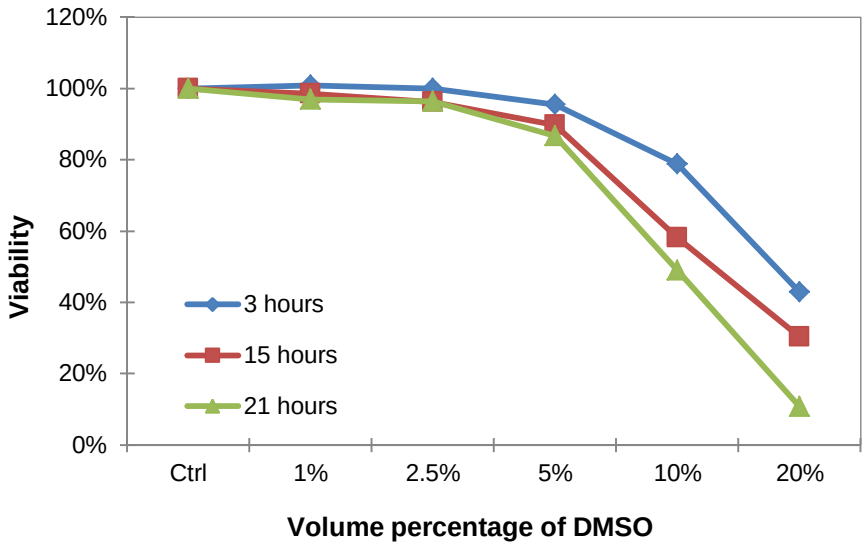

Figure S2.1. *Toxicity of DMSO on LNCaP cell suspension over time at different concentrations.*

S2.2 Calculation of DMSO Diffusion Time in Vivo

Using unsteady diffusion model in a finite medium: in order to reach a concentration 63.2% of the topical applied reagents, the diffusion time $t \approx L^2/2\mathrm{D}$ ≈6 minutes. L is the depth of the point of interest, which is 0.5 mm (the thickness of the DMSO tumor) in our case. D is the diffusivity of DMSO in tissue, which is $3*10^{-6}$ cm^2/s at 23 °C according to [150].

Chapter 3. *Pulse Timing During Irreversible Electroporation Achieves Enhanced Destruction in a Hindlimb Model of Cancer*

Contributing Authors: Chunlan Jiang, Qi Shao, and John C. Bischof

The following chapter is in preparation for publication:

C. Jiang, Q. Shao, and J. C. Bischof, "Pulse Timing During Irreversible Electroporation Achieves Enhanced Destruction in a Hindlimb Cancer Model," Ann Biomed Eng, 2014.

3.1 Introduction

Irreversible Electroporation (IRE) is an emerging technology that has drawn considerable interest in the cancer treatment field. Unlike traditional electroporation, where cells are only expected to be temporarily permeabilized and recover after the treatment; irreversible, or lethal poration is the goal in cancer therapy applications. Although the concept of using IRE as a means of soft tissue destruction was only introduced a decade ago [143], abundant pre-clinical testing *in vitro* [19] and *in vivo* [21], [22], [110] has been undertaken to support this new modality. The purported benefits of IRE are that it is simpler and faster while maintaining the minimally invasive nature of existing thermal therapies (i.e. RF and cryosurgery) [24]. In addition, it has been suggested that IRE could destroy tumor cells while preserving tissue structures such as major ducts and vessels within the target region [24]. Being a non-thermal therapy [143], [144], IRE is free from the heat sink effect of local vascular system, which helps future clinical planning as it is less dependent on perfusion (currently a limiting issue in thermal therapies [25], [145]), making IRE a superior candidate for tumors that are adjacent to major blood vessels or ducts. A first in-man phase I clinical trial [120] has been

conducted on patients with renal cell carcinoma. No significant safety issues were noted based on hematological, serum biochemical and ECG recordings of the patients, although long-term effects remain to be studied in larger clinical trials. More recent clinical trials have been reviewed in [30].

However, despite these encouraging results, there are several limitations with this emerging technique, which could present hurdles to its clinical translation. Perhaps the most critical one is the inability of IRE to destroy large volumes of tissue under safe electric field strengths without repositioning of the probes or repeating treatments. For instance, the common lesion sizes reported in the literature with double needle probes are currently still small [26], [29], [57], [110].

There are several approaches to expand the tissue volume treated by IRE including the addition of chemotherapeutic or cytotoxic agents, and approaches that increase electropermeabilization of the membrane. Combining chemotherapy with IRE has been championed by several groups and is referred to as “electrochemotherapy” [13], [14]. A similar method was also proposed recently by Frandsen et al. [61] using direct intratumoral calcium injection followed by electroporation, which led to lethal intracellular calcium events. While these studies demonstrated improved cell destruction, the focus was on enhancing the ability of chemotherapeutic drugs or cytotoxic agents to enter and kill the cancer cells rather than enhancing the efficacy of IRE itself. More recently, our group has proposed approaches that enhanced the destructive efficacy of IRE itself without relying on chemotherapeutic drugs or cytotoxic agents to enter and kill the cancer cells [52]. Specifically, mechanisms that directly modify membrane properties (i.e. line tension and surface tension, etc.) and improve the impact of pulse timing (which

we hypothesize as affecting membrane properties) have been tested and shown effective in enhancing the IRE destructive potential. More than 60% increase in cell destruction in vitro and greater than 100% increase in treatment volume in a dorsal skin fold model have been achieved [52]. However, advanced tumor models (i.e. 3D solid tumors) were not used in the previous study.

Therefore, the aim of the present study is to verify that pulse timing enhancement works in a 3D tumor model without relying on cytotoxic drugs. For simplicity, enhancement protocols with pulse timing were assessed in a human prostate cancer model (LNCaP Pro 5) *in vivo* (hindlimb tumor) on nude mice. The outcome was assessed by relative tumor volume reduction and tumor growth delay with or without IRE enhancement. Here, we document that the pulse timing approach we propose can be highly effective in enhancing the destructive potential of IRE *in vivo.* We speculate that the mechanism of enhancement is linked to reduced membrane stability and extended comprised membrane time.

3.2 Materials and Methods

3.2.1 Tumor Cell Culture and Preparation

The prostate cancer cell line (LNCaP Pro 5) was cultured as adherent monolayer in Dulbecco's Modified Eagle's Medium (DMEM)/F12 (BD Biosciences, CA) supplemented with 10% fetal bovine serum, 100U/ml of Penicillin/Streptomycin (P4333, Sigma-Aldrich, MO), and 10^{-9} mol/L dihydrotestosterone (DHT) as previously described [52]. When >85% confluence was reached, the cells were detached by adding 0.05% Trypsin-EDTA (Invitrogen, CA) and then washed twice with serum-free DMEM/F12. Approximately 1-2 million of the above prepared LNCaP Pro 5 cells were suspended in 100 µL of Matrigel

mix (Matrigel, BD Biosciences, San Jose, CA diluted 1:1 in serum-free DMEM/F12 medium) for one tumor seeding injection.

3.2.2 Animals and Hindlimb Tumor Seeding

All animal usage and experimental procedure protocols were reviewed and approved by the Institutional Animal Care and Use Committee of the University of Minnesota. 6-8 weeks old nude mice NU/J were obtained from the Jackson Laboratory (Bar Harbor, ME). 100 μL of the above prepared Matrigel-cell suspension were injected subcutaneously into the hindlimbs of mice under general anesthesia. Experiments were performed 4 to 6 weeks after tumor seeding when a tumor diameter of 6 to 8 mm was obtained. Animals were randomized into the various groups for experiments.

3.2.3 IRE Setup for Hindlimb Tumor

The IRE treatment was delivered by a pair of customized needle probes (Figure 3.1) connected to an electrical pulse generator (BTX ECM 830, Harvard Apparatus). The needles (OD=0.7mm) were fixed on a plastic block with a center to center distance of 4mm. An insulating layer was coated outside each needle leaving a 3mm tip for treatment. For hindlimb tumor treatment, the needle probes were inserted symmetrically to the center of the tumor through the skin. In cases when the tumor is not perfectly round, the needle plane was aligned with the major axis of the ellipse. Effective treatment depth is determined by the exposed needle length (3mm).

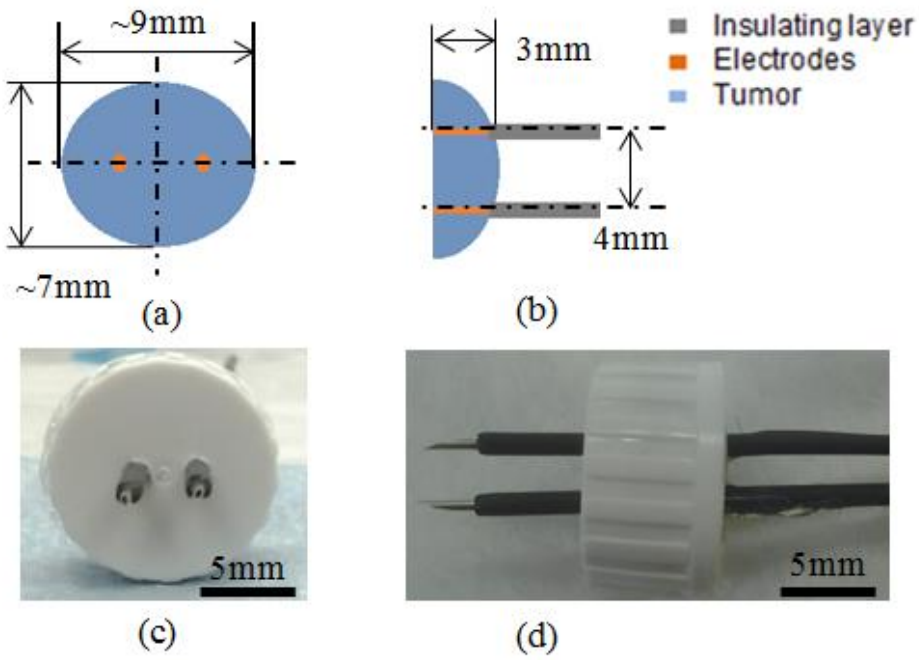

Figure 3.1. *IRE treatment setup and probe design. Bottom (a) and side view (b) of the IRE needle probe positioned in the hindlimb tumor. (c) and (d) Photos of the actual IRE probe used.*

3.2.4 IRE Treatments

The IRE and enhancement protocols were designed based on our previous study on the enhancement of IRE with pulse timing on cell suspension (*in vitro*) and dorsal skin fold chamber (*in vivo*) models [52]. IRE parameters and animal grouping can be found in Table 3.1. Specifically, 27 tumors were randomly divided into three groups (n=9 each). Both baseline and pulse timing groups were given 51 IRE pulses at pulse strengths of 600 Volts (potential between two probes), durations of 50µs, and frequencies of 10Hz. However, for the pulse timing group, the 51 pulses were delivered in 3 trains of 17 pulses with delays of 30 seconds in between trains. This delivery pattern was determined based on our best results from the *in vitro* experiments suggesting no further benefit of longer pulse delays [52]. In addition, the pulse strength (600V) was chosen so that the estimate treatment volume is roughly 60% of the total tumor volume (see

"Treatment Planning Models" section below), leaving space for the enhancement effect to show up. The sham group also received needle penetration with the same set of IRE probes, although no IRE or other treatment was delivered.

Table 3.1. *IRE parameters and animal grouping*

	N	Pulse strength (Volts)	Pulse duration (μs)	Pulse number	Freq. (Hz)
Sham	9	n/a	n/a	0	n/a
IRE	9	600	50	51	10
Enhancement	9	600	50	51 (3*17 with 30s delays)	10

3.2.5 Tumor Growth Delay Assessments

After IRE treatment, the mice were returned to their cages and monitored for any complications. Tumor growth measurements were taken twice a week using a caliper. The sizes of the major axis (L), minor axis (S), and the thickness (H) of the tumors were measured three times and the averaged values were recorded and used to calculate tumor volumes (V) with Eqn (3.1). All the tumors were monitored for at least 28 days after the IRE treatment.

$$V = \frac{1}{6}\pi \cdot L \cdot S \cdot H \tag{3.1}$$

3.2.6 Data Analysis and Statistics

Group numbers of n≥9 was achieved for the tumor growth delay. The tumor growth delay results are presented as average values ± standard deviations. Single factor ANOVA tests were performed among the sham and two experimental groups where P value ≤ 0.01 was taken to delineate statistical significance among groups.

3.3 Treatment Planning Models

The IRE E-field distributions in the hindlimb tumor were modeled using COMSOL Multiphysics software. For our delivery setup shown in Figure 3.1a and 3.1b with 600 Volts across the two electrodes, the E-field distribution in the hindlimb tumor is determined by Laplace equation (Eqn (3.2)):

$$\nabla \cdot (\Omega \cdot \nabla \varphi) = 0 \tag{3.2}$$

where Ω is the electrical conductivity of tumor, φ is the electric potential. For homogeneous tissue, the electric field calculated from Eqn (3.2) shown in Figure 3.2a. The threshold of IRE injury has been experimentally found to be between 400~1000V/cm [23], [24], [27], [91], [92], [100], depending on the tissue type and evaluation method. If we use 600V/cm as a threshold (obtained from our previous study using the dorsal skin fold tumor system [101]), the estimated injury region is roughly a circle with a radius of 3mm, which corresponds to about 60% of the entire tumor.

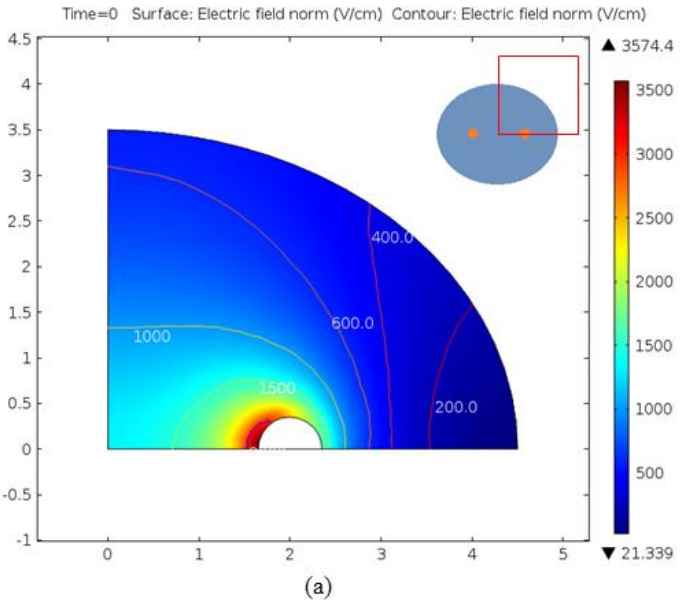

(a)

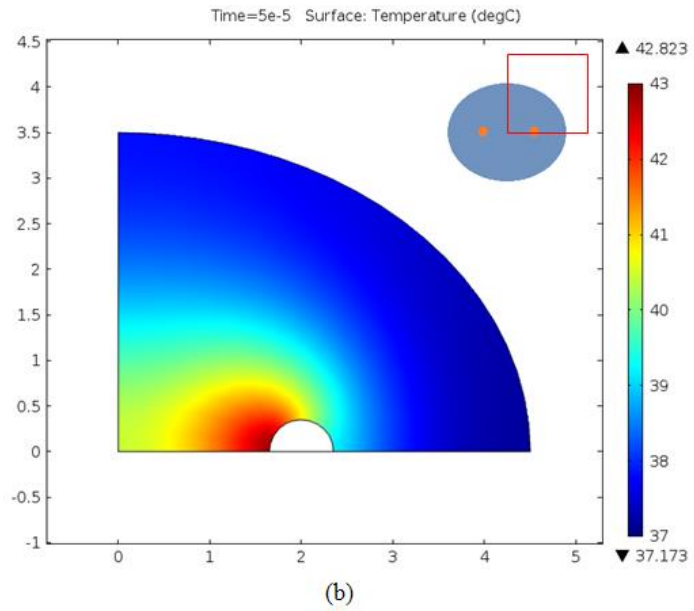

Figure 3.2. *Modeling of IRE in hindlimb tumor: (a) E-field distribution with 600 Volts across the two electrodes and (b) end temperature after baseline IRE treatment (51# of 600V, 50µs pulses at 10Hz), and (c) end temperature after pulse timing enhancement IRE treatment (3 trains of 17# of 600V, 50µs pulses at 10Hz). All figures show the first quadrant of the tumor's cross section*

Table 3.2. *Summary of parameters used* [52], [78], [143]

Quantity	Symbol	Unit	Value
Tissue electrical conductivity	Ω	S/m	0.286
Tissue thermal conductivity	K	W/(m*K)	0.5
Tissue heat capacity	c_p	J/(kg*K)	3750
Tissue density	ρ	kg/m^3	1000
Blood temperature	Tb	C	37
Blood density	ρ_b	kg/m^3	1000
Blood heat capacity	c_b	J/(kg*K)	3640
Blood perfusion rate	ω_b	$kg/(m^3*s)$	0.5
Metabolic heat	q'''	W/m^3	16900
Heat transfer coefficient	h	$W/(m^2*K)$	50
Initial tumor temperature	T0	C	37
Room temperature	Tr	C	25
IRE electric potential	φ	volt	600
IRE pulse duration	td	us	50
IRE total pulse number	N	n/a	50
IRE frequency	f	Hz	10
Free energy with pore formation	ΔE	J	
Pore radius	R	m	
Transmembrane voltage	U	Volt	
Membrane line tension	λ	J/m	$1\sim6*10^{-11}$
Membrane surface tension	σ	J/m^2	$0.5\sim2*10^{-3}$
Lipid-water dielectric coefficient	a	n/a	0.043
Charging time constant	τ_c	1/s	
Membrane thickness	h	m	$10*10^{-9}$
Specific membrane capacitance	C_m	$\mu F/cm^2$	0.95
Specific intracellular conductivities	σ_i	mS/cm	4.55
Specific extracellular conductivities	σ_e	mS/cm	50

When neglecting heat losses, the energy from electric current all goes to tissue heating, which is illustrated by:

$$SAR = \Omega \cdot |\nabla \varphi|^2 \tag{3.3}$$

Using the bioheat equation implemented in COMSOL by adding a heating term (SAR in Eqn (3.4)) from the electric pulsing:

$$\rho c_p \frac{\partial T}{\partial t} = \nabla \cdot (k \nabla T) + \rho_b \omega_b c_b \cdot (T_b - T) + q''' + SAR \tag{3.4}$$

where ρ, c_p, and T are density, heat capacity and temperature of the tissue, ρ_b, ω_b c_b, and T_b are density, flow rate, heat capacity and temperature of the blood, and q''' is metabolic heat. The parameters used in our models are summarized in Table 3.2. This model allows the temperature rise after IRE pulsing to be captured as shown in Figure 3.2b and 3.2c. Based on our simulation results, the maximum temperature rise is found next to the inner side of the electrodes, and is less than 43 degrees Celsius (Figure 3.2b) for a continuous delivery of 51 pulses for parameters shown in Table 3.1. Even for the worst case scenario case in which the tissue is kept at 43 degrees Celsius for the entire treatment period (5 seconds), the thermal dose is still far too low to cause thermal injury according to the CEM_{43} (cumulative equivalent minutes at 43 degrees Celsius) method [151]. For the enhancement method (see pulse timing in Table 3.1), the temperature rise is even less (about 41 degrees Celsius, Figure 3.2c) because more heat has dissipated during the two delay periods. It is worth noting that the conductivity of tissue will increase during IRE due to electroporation's permeabilization effect which

has been noted in previous work from our lab [101] and others [85], [99]. We have elected not to pursue this here in order to focus solely on the impact of pulse timing without the confounding effects of conductivity change. Certainly more careful study is warranted in the future.

3.4 Results

3.4.1 Animal Response

All the animals in the treated groups (with or without enhancement) survived the procedure. Upon application of the IRE pulses, a mild to moderate level of generalized muscle contraction occurred in each animal. This effect has been noticed and reported in many *in vivo* studies [24], [25]. It has been reported that when Pancuronium is administered to the animals the contractions are manageable even when a maximal voltage of 3kV was applied [24], although this was not used in this study. A mild swelling was also observed on each IRE treated tumor (with or without enhancement) for about 24 hours after treatment, but not on sham tumors. By 48 hours after IRE, all the swelling conditions were gone and the needle penetration sites were hardly noticeable. No other complications were observed in our experiments.

3.4.2 Tumor Growth Evaluation

The average tumor size before IRE treatment in our experiments was $96mm^3$ from Eqn (3.1), with L=8.89±0.22mm, S=6.99±0.11mm, and H=2.97±0.09mm. After treatment, each tumor's volume was monitored for 30 days and compared to the initial volume. The relative growth delays are shown in Figure 3.3 and Table 3.3. Specifically, tumors treated with either baseline IRE or pulse timing enhanced IRE exhibited reductions in tumor volumes compared to the shams. Baseline IRE treatment lead to a 26% to 30%

tumor destruction compared to sham over the course of study. This contrasts with the pulse timing enhancement group, which showed 54% to 62% tumor destruction compared to sham. This suggests that a consistent enhancement of more than 33% over baseline IRE up to the 28 days in our study. Furthermore, it took 1 week for the baseline IRE treated tumors to grow back to their original sizes, compared to 3 weeks for the pulse timing enhancement group. In other words, the pulse timing enhancement approach demonstrated 2 additional weeks of tumor growth delay compared to the baseline IRE. Also, only pulse timing enhanced IRE was able to achieve complete tumor regression with our experiment setup and chosen parameters.

Using single factor ANOVA test, the above differences in tumor volume measurements are statistically significant, with a p value of 0.0065.

Table 3.3. *Relative tumor volume reduction with various treatments*

	Day	**0**	**7**	**14**	**21**	**28**
Sham	Relative size	1	1.269	1.835	2.393	2.829
IRE	Relative size	1	0.898	1.358	1.764	1.965
	Reduction compared to Sham		29.19%	26.01%	26.28%	30.54%
Enhancement	Relative size	1	0.553	0.706	1.046	1.302
	Reduction compared to Sham		56.44%	61.52%	56.27%	53.99%
	Reduction compared to IRE		38.48%	47.99%	40.67%	33.76%

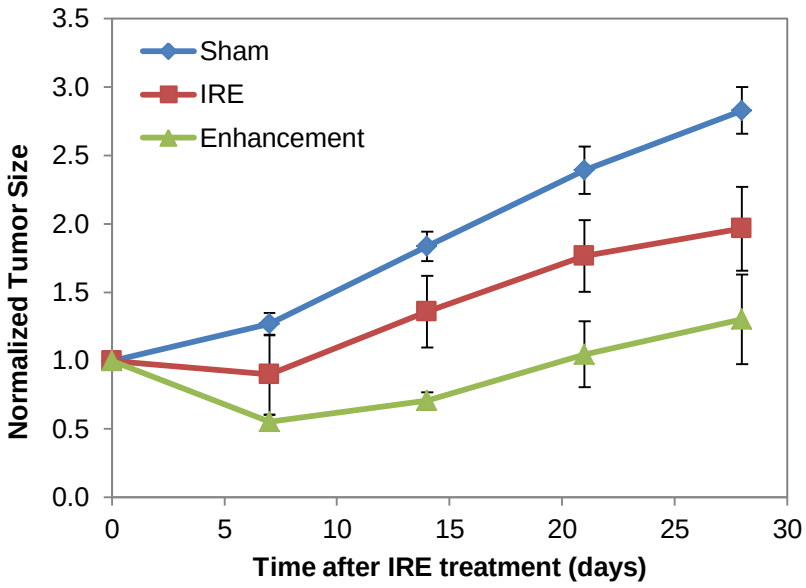

(a)

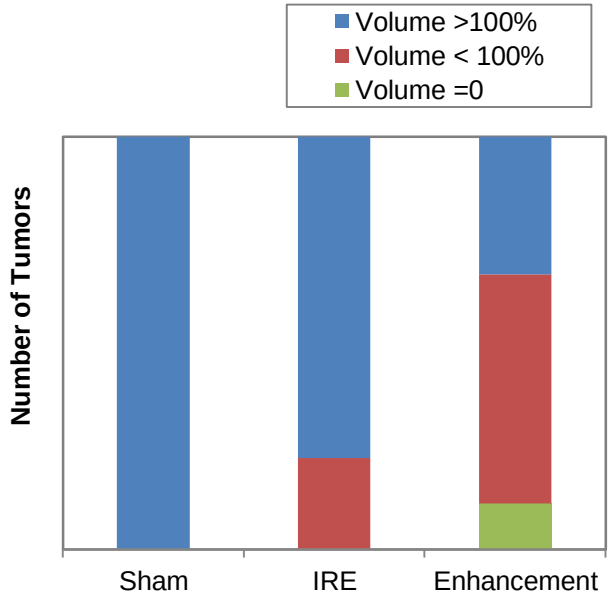

(b)

Figure 3.3. *Injury response of pulse timing enhanced IRE treatment in the LNCaP hindlimb tumor model. (a) Normalized tumor sizes over 28 days after IRE treatment. Each data point represents the average of n=9 measurements ± SE. (b) Tumor response at day 28 after IRE for various treatments. Volume=0 represents no palpable tumor on the overlying skin*

3.5 Discussion

This work is an extension of our previous study on membrane targeting approaches to enhance IRE. Specifically, in the previous study we demonstrated significant enhancement (67–75% more cell destruction *in vitro* and >100% increase in treatment volume in an intravital dorsal skin fold chamber tumor model) can be achieved with direct application of DMSO at non-toxic concentrations and through pulse timing (i.e. introducing time delays between pulse trains) [52]. In the current study, we are able to verify the enhancement effect of the pulse timing approach in an solid 3D tumor model *in vivo*, and demonstrated 2 weeks longer of tumor growth delay compared to baseline IRE treatment. The results from our different models are compared and summarized in Table 3.4.

Table 3.4. *Summary of IRE enhancement results*

Model	Approach	Outcome	Ref.
In Vitro **(Cell suspension)**	Baseline IRE	Baseline cell destruction (~50%)	[52]
	DMSO	**75%** increase over baseline	
	Timing	**67%** increase over baseline	
In Vivo **2D Tumor (DSFC)**	Baseline IRE	Baseline histological destruction (10.3mm^3)	[52]
	DMSO	**136%** increase over baseline	
	Timing	**101%** increase over baseline	
In Vivo **3D Tumor (Hindlimb)**	Baseline IRE	Baseline tumor growth delay (1 week)	This study
	Timing	**200%** increase over baseline	

In addition to experimental verifications, we would like to further explore the possible mechanisms of the pulse timing enhancement approach. The energy based nucleation model and influences of modifying the membrane properties (i.e. line tension and surface tension) on the outcome of IRE treatment have been discussed in our previous

study [52]. Our proposed explanation for DMSO enhancement is that the inclusion of DMSO molecules in the cell membrane can lower the edge line tension thus decreasing the energy barrier for pore growth, leading to enhanced membrane rupture and cell injury after IRE. To understand the mechanism of pulse timing enhancement, it is worth discussing the time frames of IRE (Figure 3.4). The generation of transmembrane potential around the cells depends on ion concentration of the surrounding medium, but is in the range of micro-seconds [31], [56], [77], [78] from modeling. Take a single cell (r =50μs) as an example, the membrane charging time constant (τ_c) can be determined by Eqn(3.5) [34], [46]:

$$\tau_c = r \cdot C_m \cdot (\frac{1}{\sigma_i} + \frac{1}{2\sigma_e}) \tag{3.5}$$

in which C_m is the specific membrane capacitance, σ_i and σ_e are intracellular and extracellular specific conductivities. With the typical values used in Table 3.2, the charging time is estimated to be 1.1 μs. Compared to the pulse duration (50 μs), intervals (100ms), and time delay between pulse trains (30s) (Figure 3.4), this charging time can be neglected. Membrane defects usually originates within μs, and can last through the entire time the external field is applied (several μs to hundreds of ms) [82], [86]. However, the membrane defect recovery timing (if reversible) is much slower once the pulsing is finished, generally longer than 1s and can take up to minutes. The difference in the two time scales makes it possible to enhance the IRE killing effect by fine tuning the pulse timing to leverage these half recovered pores.

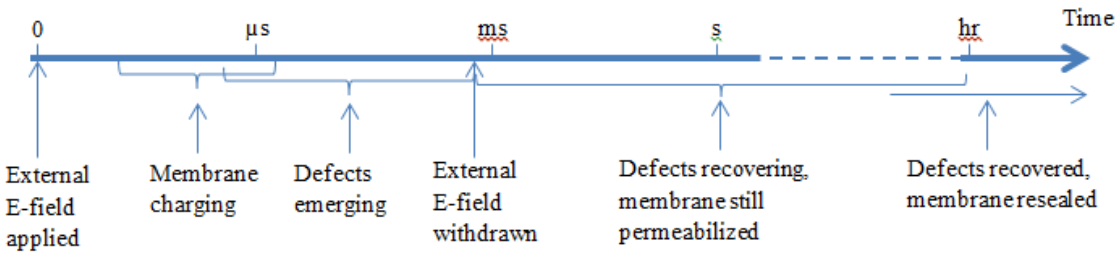

Figure 3.4. *Illustration of the time frames of reversible membrane defects created by IRE pulses.*

At least two contributing factors can explain the enhancement effect of pulse timing. First, similar to DMSO, pulse timing can also directly impact membrane poration by reducing line tension in recovering pores. Earlier pulses can lead to formation of both reversible and irreversible pores on the membrane. Since complete resealing of the membrane can take up to minutes, the cell membrane will remain more susceptible to further pulsing due to both reduced membrane thickness from recovering pores and reduced line tension [146] during this recovery period. Although qualitative calculation is not given here, the dramatic impact of reduced line tension has been demonstrated in [52] and can help explain the significant enhancement effect from pulse timing. Second, extended pore opening time can also increase cell injury and death due to loss of critical ions, proteins, and even cell components. When the pulses are delivered in one train, only one recovery period is presented after the pulsing. However, when the pulses are delivered in several trains with seconds of delays in between, the total pore exposure time is the sum of all delays and the final recovery period. Therefore, more secondary injury could be caused due to this extended pore opening time.

Lastly, it is of great interest to explore what other pulse timing delivery patterns can provide enhancement to IRE, and whether there is an optimum delivery pattern. The 30 seconds delay in our proposed approach was selected based on our previous study

[136] which showed that other delay periods (10s, 1min, and 2mins) yield equivalent or less benefit in our experiment setup. However, the range we studied was limited and further testing on other delay period selections are still needed to fully characterize the potential of the pulse timing approach. Similarly, in our study the pulses were divided into three trains, but other or better possibilities may exist. It may also be helpful to develop a model to characterize the effect of pulse timing. To achieve that, a better understanding of the pore recovery time frame and IRE injury mechanism is highly needed. Finally, it should be noted that these enhancement results were generated on one cell and tissue system (LNCaP Pro 5 prostate cancer). While we believe that the enhancement mechanisms will hold in other systems, the precise parameters leading to this enhancement are expected to be system (i.e. particularly membrane) specific.

3.6 Summary

In this study, a pulse timing approach has been used to increase tumor destruction of IRE treatment and thereby delay tumor growth for local hindlimb tumors in mice. Using our experiment setup, more than 33% additional tumor destruction and 2 weeks longer tumor growth delay have been achieved compared to baseline IRE treatment without relying on any cytotoxic drugs or agents. Because the pulse timing approach does not introduce any foreign agents into the body, it could easily be integrated into current IRE procedures to increase the treatment efficacy. Further opportunities exist in optimizing the pulse timing delivery approach and understanding the fundamental mechanisms. Nevertheless, we suggest that the simple and safe nature of the pulse timing approach compared with cytotoxic drugs may help to translate this approach into the clinic.

Chapter 4. *Irreversible Electroporation for Non-Cancer Targets*

Contributing Authors: Chunlan Jiang, Ryan Goff, Pong Patana-anake, Paul A. Iaizzo, and John C. Bischof

The following chapter appeared in publications:

C. Jiang, R. Goff, P. Patana, P. A. Iaizzo, and J. C. Bischof, "Irreversible electroporation of cardiovascular cells and tissues," J. Med. Devices., 7(3), 2013.

C. Jiang, P. Patana, and J. C. Bischof, "Neural Cells Show Higher Sensitivity to Irreversible Electroporation Compared to Cancer and Cardiovascular Cells", presented at the ASME Design of Medical Device Conference, April, 2014.

4.1 Introduction

Since Davalos, Rubinsky, and Mir [16] proposed the use of electroporation as a means of soft tissue destruction, numerous pre-clinical *in vitro* [19] and *in vivo* [21], [22], [110] testing have been undertaken to investigate its therapeutic values in cancer treatment, but far less effort has been given to other disease targets. For example, a wide variety of cell [17]–[20], [57], [68], organ [26]–[28], and animal [21], [24], [29] models have been used to characterize IRE in different cancer types, as reviewed in Table 1.2. A first in-man phase I clinical trial [120] has also been conducted on patients with renal cell carcinoma in 2010, only 7 years after the concept of IRE therapy was first introduced. Currently, large scale, multi-center clinical trials are being carried out around the world on IRE cancer therapy (Table 1.3, Figure 1.9). However, compared to the rapid development of IRE application on treating cancers, much less progress has been made

on other disease types, such as cardiovascular diseases [105], [107] and neural disorders [62], [152], [153]. Therefore, this chapter is dedicated to explore the potential applications of IRE therapy for cardiovascular, neural, and other non-cancer targets.

4.2 IRE of Cardiovascular Cells and Tissues

4.2.1 Background

Cardiovascular disease remains the number one cause of death in the United States and in 2010 was responsible for 17% of the US health expenditures ($272.5 billion) [154]. Many acquired cardiovascular diseases are associated with abnormal proliferation of vascular smooth muscle cells (e.g. heart attack) or irregular electrical pathways (e.g. arrhythmia). Of the various methods applied to manage cardiovascular diseases, using energy-based technologies to create myocardial lesions (i.e. “ablation”) has gained increasing popularities due to their effectiveness, short treatment times, and minimal surgical damages.

Radiofrequency (RF) energy was one of the earliest technologies used for catheter ablation and currently has the greatest patient-year experience [155]. It should be noted that several other thermal technologies, such as high-intensity focused ultrasound (HIFU), catheter-based cryo, focused laser, and microwaves, have also been proposed as potential sources for cardiovascular ablation. However, to date, each of these sources relies on direct diffusion of energy, which can take significant time and increase risks for collateral damage to surrounding structures.

Irreversible Electroporation (IRE), on the other hand, is an emerging technology that may also provide new opportunities for treatments of cardiovascular diseases. Unlike

thermal technologies, IRE is based on the electrical field distribution rather than diffusion, and induces cell death by increasing permeabilities, thus leaving long-term defects within cell membranes [1]. Because IRE does not rely on heating or cooling to create lesions, it also benefits from reduced interaction with blood flow: a distinct disadvantage of thermal ablative techniques within the heart or near large vessels.

In this report, we evaluated the abilities of IRE to destroy both cardiovascular cells and tissues, as a first step to better understand threshold and use in his new area. To do so, we use a cardiac muscle cell line (HL-1[156]) in order to characterize the biophysical effects and thresholds of IRE on cardiovascular cells. Next, we applied direct IRE therapy on isolated pulmonary vein tissues: i.e., to investigate treatment efficacies *in vitro*. Specific influences of IRE applied therapeutic variables (E-field, pulse duration and number) were studied and compared based on the elicitation of injury (i.e., cell membrane integrity and cellular dehydrogenase activity). These results may aid in designing more effective approaches to treat cardiovascular diseases using IRE.

4.2.2 Materials and Methods

4.2.2.1 Cardiac muscle cell cultures

A HL-1 cell line was cultured as adherent monolayers [156]. More specifically, cells were grown in T-75 flasks with Claycomb medium (51800C, Sigma-Aldrich, St. Louis, MO) supplemented with 10% fetal bovine serum, 2mM L-Glutamine, 100U/ml of Penicillin/Streptomycin, and 0.1mM Norepinephrine. When 90% confluence was reached and spontaneous beating was elicited (observed under the microscope), the cells were detached by adding 0.05% Trypsin-EDTA (Invitrogen, CA) and then formed into a single cell suspension.

4.2.2.2 Electroporation and viability assays of HL-1 cell line

400µl volumes of the prepared HL-1 suspensions (0.5~0.6 million cells/ml) were pipetted into electroporation cuvettes (Fisher Scientific), which were then placed in an external electrical field created by an electrical pulse generator (BTX ECM 830, Harvard Apparatus) as shown in Figure 4.1a. The output voltages and currents were monitored by an oscilloscope (Tektronix TDS 2002). After electroporation, 100µl aliquots of treated cell suspensions were transferred from the cuvette to micro centrifuge tubes and incubated with Hoechst 33342 (10µM) and Propidium iodide (PI) dyes (7.5µM) for 15mins. These samples were then observed under a fluorescent microscope and photos were taken to calculate relative cell viabilities.

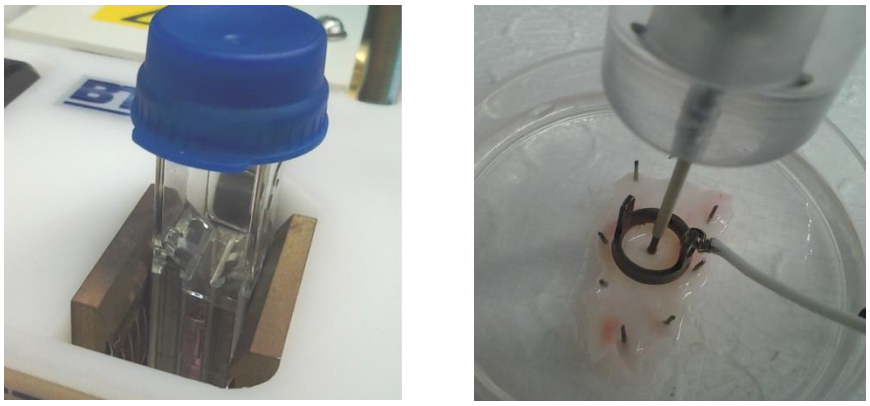

(a) (b)

Figure 4.1. *Electroporation experiment setups for cardiovascular cells and PV tissue: (a) cell suspensions within a cuvette placed in an external electrical field, and (b) treatment of a vascular tissue with ring-needle electrode configuration*

Porcine pulmonary vein tissue preparations: Lungs were harvested immediately post-mortem from Yorkshire-cross swine: those being used for other IACUC approved

studies. The pulmonary veins (PV) distal to the heart were identified and dissected from the lung using blunt dissection techniques. The PVs were washed in Krebs-Henseleit buffer and cut along an axial direction. The PV biopsies were then laid flat in a 5cm petri dish with the endothelial surfaces facing upward. The elastomer formed bottoms of the petri dishes facilitate fixation of the tissue and proper electrode positioning (see Figure 4.1b).

4.2.2.3 Electroporation and injury characterization of the pulmonary tissues

After removal of the Krebs-Henseleit buffer, a ring electrode (cathode) was placed on the tissue surface with a needle electrode (anode) inserted from the center of the ring. The diameters of the ring (inner) and needle electrode were 8mm and 1mm, respectively. After the applied electroporation, each sample was again immersed with the Krebs-Henseleit buffer and incubated for 3 hours followed by staining with 1% Triphenyl tetrazolium chloride (TTC assay) in Trizma buffer (Sigma-Aldrich, St. Louis, MO) for 1 hour. Photos were taken on the stained samples so to measure the relative necrosis areas.

4.2.3 Results

4.2.3.1 Cardiac muscle cell model

The initial electroporation parameters were chosen based on our previous experience with a cell line [52]. We fixed the applied pulses at a voltage of 200V (inducing an external electrical filed of 1000V/cm over the 2mm cuvette gap), and tested electroporation treatments consisting of 10, 50, and 99 pulses with 50μs pulse duration and 10Hz frequency. The cell viability after electroporation was evaluated using the dye-staining assay and obtained results are shown in Figure 4.2.

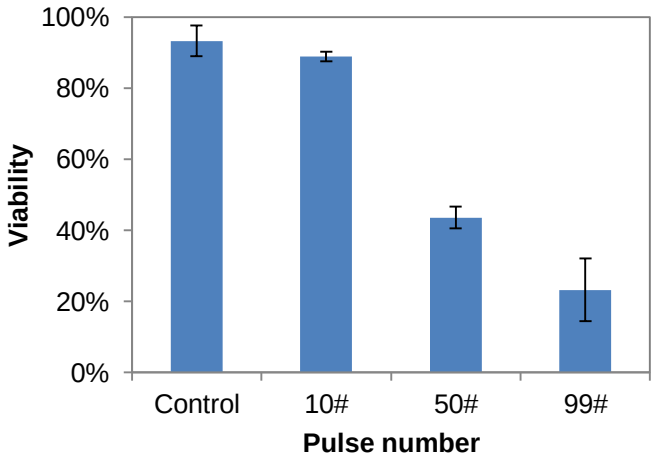

Figure 4.2. *Viability results of the HL-1 cell line after electroporation with 200V, 50μs, 10Hz, and varied number of pulses. (N=4, error bars represent standard deviations.)*

The resultant viability data (Figure 4.2) indicated that IRE can indeed cause damage of cardiac muscle cells within our experimental setup. The moderate injury level (i.e. viability) was induced with a set of 50 pulses of 200V, 50μs durations at 10Hz: i.e., of approximately 43%. As the treatment doses increased (pulse number in this case), the injury level increased accordingly. When compared with results from cancer cell line [52], the injury levels of HL-1 were higher under the same treatment conditions, which may indicate that the HL-1 cells are more susceptible to IRE injury.

4.2.3.2. Pulmonary vein tissue model

For the PV ablation, we applied 500V on the center electrode and grounded the ring electrode, which creates an attenuating electrical field over a radial direction within the ring area (Figure 4.4). The creation of such electrical fields helped identify treatment thresholds: i.e., when comparing the electrical field distributions with resultant lesion sizes. A total of 50 pulses with 50μs duration and 10Hz frequency were delivered for

these treatments. A set of photos demonstrating the staining effect of control and treated samples are shown below in Figure 4.3.

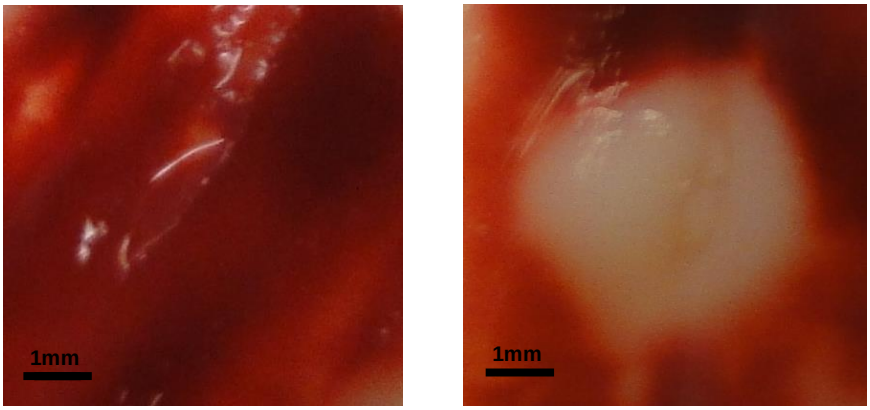

(a) (b)

Figure 4.3. *Relative injuries of PV tissues as determined by TTC staining: (a) control and (b) after IRE treatment*

For the PV ablation system, the electric field distribution within the ring electrode can be calculated from the Laplace equation (Eqn 4.1), as was demonstrated in Figure 4.4.

$$\nabla \cdot (\Omega \cdot \nabla \varphi) = 0 \tag{4.1}$$

The lesion size (measured as radius from the center electrode to the edge of lesion) induced by such therapy was 1.95 mm (n=3, with a standard deviation of 0.07 mm), which corresponds to an electric field strength of 1200V/cm.

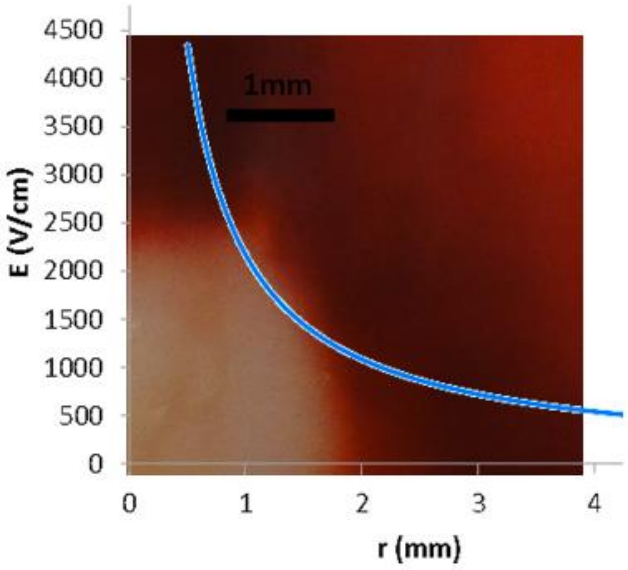

Figure 4.4. *Relative electrical field distributions as a function of radial distances from the center electrode versus the effects on the IRE treated PV samples*

4.2.4 Summary

This preliminary work supports the idea that IRE can be used for creating lesions in patients with cardiovascular diseases. For example, effective injury was achieved with electric field strength of 1000V/cm for isolated cardiac muscle cells, and 1200V/cm for PVs.

4.3 Irreversible Electroporation of Neural Cells

4.3.1 Background

In 2012, around one billion people worldwide were suffering from neurological disorders such as epilepsy, incontinence, chronic and arthritis pain, which significantly affect the patient's quality of life. These disorders are associated with biochemical or electrical abnormalities of the central and peripheral nervous system (brain, spinal cord,

autonomous nervous system, etc.). Although many of these disorders can be controlled or mitigated by drugs, the efficacy and long term side effects of drugs are limiting their acceptance. More recently, energy-based focal therapies (e.g. Radiofrequency) have been used for neural ablation. For instance, studies have shown that ablation can effectively help treat chronic pain (joint [157], back, sciatica [158], etc). Radiofrequency ablation applied to renal arteries resulted in a substantial and sustained reduction in blood pressure without apparent procedural or subsequent biochemical complications [157], [159]. In addition, research on using cryoablation on the pulmonary vein to manage atrial fibrillation is also underway [160], [161].

Irreversible Electroporation (IRE), an emerging technology that has attracted much interest and lead to numerous studies in cancer therapy, may also provide new opportunities for treatment of neural disorders. Unlike thermal technologies, IRE is based on the electric field (E-field) distribution rather than heat diffusion, and induces cell death by increasing permeability [1]. Because IRE does not rely on heating or cooling to create lesions, it also benefits from increased speed and reduced interaction with blood flow: a distinct disadvantage of thermal ablative techniques in and around large blood vessels.

In this report, we evaluated the ability of IRE to destroy neural cells to understand potential therapeutic value in treating neural disorders. To do so, we used an adult male mouse hypothalamic cell line (CLU-172 [162]) to characterize the biophysical effects and injury thresholds of IRE on neural cells. Specific influences of IRE therapeutic variables (E-field, pulse number and duration) were studied and compared based on the elicitation of injury (i.e., dehydrogenase activity). Further, a direct comparison of these results with

those from cancer (LNCaP Pro5) and cardiovascular (HL-1) cell lines demonstrates a higher sensitivity of neural cells to IRE than other cell types. These results will aid in exploring the potential of IRE to treat neural disorders and selection of appropriate IRE therapeutic variables.

4.3.2 Materials and Methods

4.3.2.1 Neural cell culture

The CLU-172 cell line was cultured as adherent monolayers as described in [162]. More specifically, cells were grown in T-75 flasks with high glucose DMEM medium (D5796, Sigma-Aldrich, MO) supplemented with 10% fetal bovine serum, 100U/ml of Penicillin/Streptomycin/Neomycin (15070-063, Invitrogen, CA). When 90% confluence was reached, the cells were detached by adding 0.05% Trypsin-EDTA (Invitrogen, CA) and then formed into a single cell suspension.

4.3.2.2 Cardiac muscle cell cultures

The cell culture procedure of the HL-1 cell line is similar to above with slight changes: the cells culture medium was made with Claycomb medium (51800C, Sigma-Aldrich, MO) supplemented with 10% fetal bovine serum, 2mM L-Glutamine, 100U/ml of Pen/Strep, and 0.1mM Norepinephrine.

4.3.2.3 Cancer cell culture

The culture procedure of the LNCaP Pro 5 cell line has been detailed in [52].

4.3.2.4 Electroporation Treatment

400µl volumes of the prepared cell suspensions (0.5~0.6 million cells/ml) were pipetted into electroporation cuvettes (Fisher Scientific) which were then placed in an homogeneous external electrical field created by an electrical pulse generator (BTX ECM 830, Harvard Apparatus). The output voltages and currents were monitored by an oscilloscope (Tektronix TDS 2002).

4.3.2.5 Injury Evaluations

The viability of neural and cancer cell lines were evaluated using a Tetrazolium-based CCK-8 assay (Dojindo Molecular Technologies, Inc) that measures the dehydrogenase enzymatic activity associated with metabolic processes in live cells. After IRE, 100 µl aliquots of the cell suspensions were mixed with 10 µl of CCK-8 reagent in a 96 well plate then incubated for 4 hours at 37 ^{o}C with 5% CO2. The optical absorption of the sample was then read in a spectrophotometer (Synergy, BioTek Inc.) at a wavelength of 450 nm to determine the viability according to a standard protocol in the manufacturer's manual. The viability results of the HL-1 cell line were evaluated using membrane dye assay because of the interference of the HL-1 cell culture medium with the CCK-8 reagent. After electroporation, 100µl aliquots of treated cell suspensions were transferred from the cuvette to micro centrifuge tubes and incubated with Hoechst 33342 (10µM) and Propidium iodide (PI) dyes (7.5µM) for 15 minutes. These samples were then examined under a fluorescent microscope and photos were taken to calculate relative cell viabilities.

4.3.3 Results

All three IRE therapeutic variables (E-field, pulse number and duration) studied in our experiments were influential on the outcome of neural cell destruction, although we

found E-field to be the most critical factor (Figure 4.5). Specifically, for IRE to induce initial cell injury (more than 5% cell death), the E-field needs to be greater than 750V/cm, while to achieve complete cell destruction (more than 95% cell death), the E-field required in our experiment setup is 1000V/cm with 99 of 50μs long pulses.

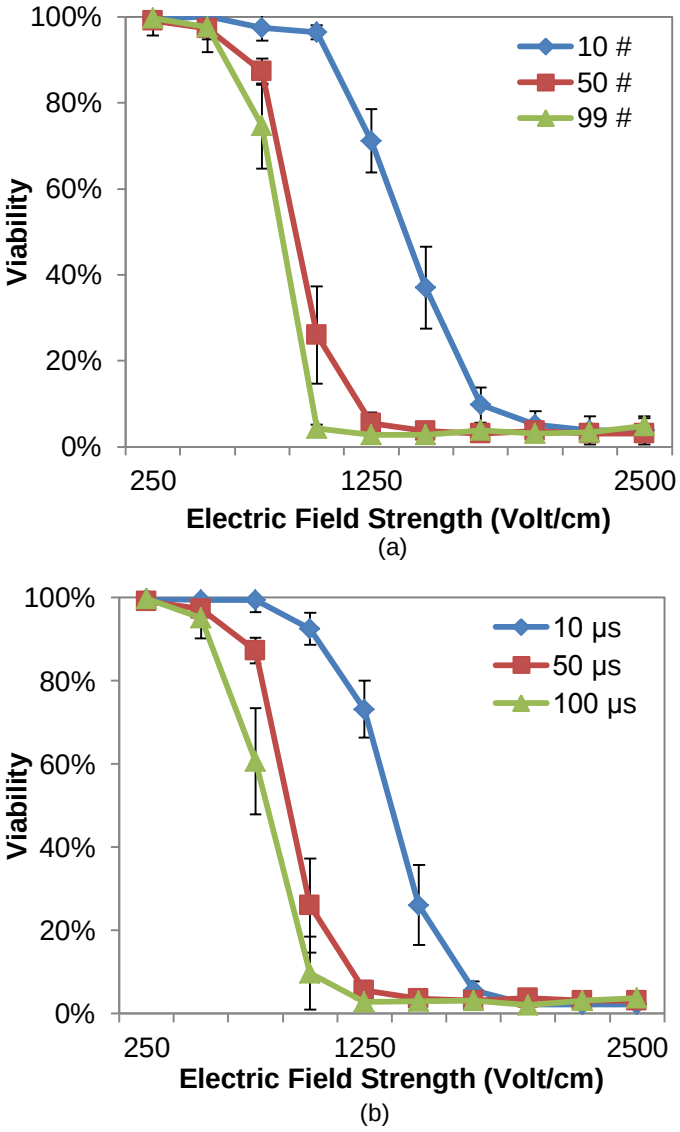

Figure 4.5. *In vitro IRE treatment on CLU-172 cells with various E-field strengths and (a) 10, 50, and 99 pulse number with 50μs duration or (b) 10 μs, 50μs, or 100 μs duration with 50 pulse number. Pulse frequency is 10Hz for each case. N=3, error bars represent standard deviations*

Both pulse number and pulse duration have significant impact on E-field thresholds. With 50μs long pulses (figure 4.5a), the E-field threshold for complete cell destruction increased to 1250V/cm for 50 pulses and to 2000V/cm for 10 pulses. With 50 pulses (figure 4.5b), the E-field thresholds for complete cell destruction are 1250V/cm, 1250V/cm, and 1750V/cm for 10 μs, 50 μs, and 100 μs long pulses, respectively.

The resultant viability data (Figure 4.5) indicated that IRE can indeed cause various levels of damage of the neural cells within our experimental design. The fact that increasing pulse number or duration can lower the E-field threshold is strongly suggesting a “treatment dosage” role of the pulse number and duration in IRE.

It is also interesting to compare the outcome of IRE therapy on neural cells with that of the cardiovascular and cancer cell lines from the same experiment model (Figure 4.6). The initial injury thresholds for all three cell lines are similar (around 750V/cm). However, the E-field threshold for complete cell destruction is the lowest for neural cells and highest for cancer cells. This observation suggests that neural cells are more sensitive to injurious IRE pulses, and have a narrower transition zone from complete live to complete dead. Such cell line specific difference can also potentially help design treatment protocols in which neural cells are selectively killed within the same target region where other types of cells (e.g. cardiac muscle cells) are present.

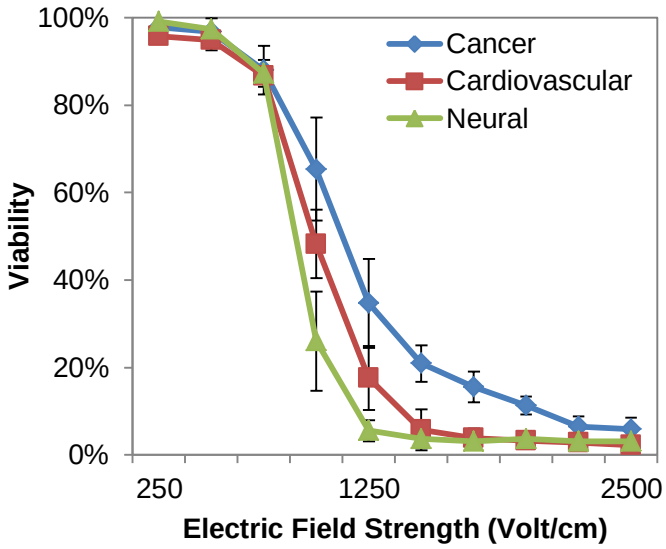

Figure 4.6. *In vitro IRE treatments on cancer (LNCaP Pro5), Cardiovascular (HL-1) and neural (CLU-172) cells with various E-field strength and 50 of 50µs pulses at 10Hz*

4.3.4 Summary

Although further experiments are needed to confirm these findings, our preliminary results support the idea that IRE can be used to preferentially deactivate nerves in patients with neural disorders. Effective injury can be achieved with appropriate combination of E-field strength, pulse number and pulse duration. Further characterization and testing of other IRE parameters and on advanced neural models will be needed to fully translate this finding.

Chapter 5. *Future Directions*

5.1 IRE Mechanisms

IRE therapy has been used in both pre-clinical and clinical environments for almost a decade (Table 1.2 and 1.3). Although many encouraging results have been reported and unique benefits have been observed compared to other focal therapies (See Chapter 1), several essential aspects of IRE mechanisms are still lacking.

For instance, the principle effect that defines IRE is the irreversible change of membrane permeability. However, the connection between permeability change and cell injury is still unclear. In our previous sessions (1.2 and 1.3.1.3), two classes of injury mechanisms have been introduced at the cellular level: direct irreversible membrane defect and secondary cellular responses. To model the irreversible membrane defect, a nucleation based energy model (Eqn 1.3) has been used and supported by the majority of people in the field [51], [54]. The secondary cell injury effects are more complicated and difficult to model. Several different processes could contribute to the secondary cell injuries, including protein denaturation [34], osmotic imbalance, flush in/out of ions, depletion of ATP [61], or uptake of toxic/foreign molecules [14], etc. The questions whether these secondary effects contribute to the final cell death and how to model these effects are ongoing areas of study.

The IRE injury mechanism in the tissue environment *in vivo* is even more complicated because of the live organism's response to injury as a system. Only a limited number of studies have investigated the living body's systematic response to IRE, and the conclusions are contradictive. Al-Sakere et. al. [98] reported that IRE does not induce an

infiltration of immune cells to the tumor because of the destruction of infiltration routes, therefore the immune response is not instrumental in IRE efficacy. In contrast, Onik et. al. [25] observed a significant immunologic reaction in the lymph nodes draining the treatment area. Li et. al. [152] also reported that IRE modified the cellular immune response compared with surgical resection.

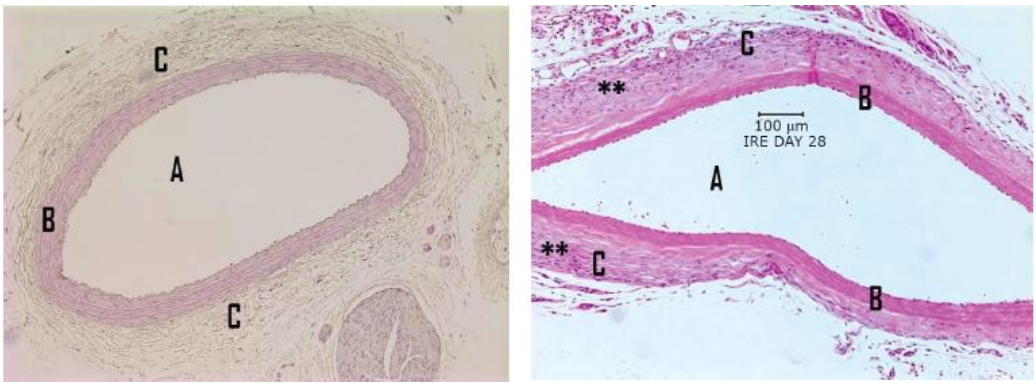

Figure 5.1. *IRE on rat artery after 28 days (H&E X100 magnification). Top picture shows a normal right common carotid artery. Bottom picture shows a left common carotid artery 28 days after irreversible electroporation. There are almost no vascular smooth muscle cells in the tunica media, compared with control artery. The thickness of the tunica media is reduced. There is no neointimal formation. There is marked fibrosis and hypercellularity in the adventitia layer of the IRE artery, compared with the control. (A, intraarterial lumen; B, tunica media; C, tunica adventitia; **, area of fibrosis and hypercellularity).* [105] Published with permission from: "The effect of irreversible electroporation on blood vessels," *Technol. Cancer Res. Treat.*, vol. 6, no. 4, pp. 307–312, Aug. 2007, Adenine press, http://www.tcrt.org.

In addition, the impact of IRE on the vasculature system requires further study *in vivo*. One of the major claimed benefits of IRE is its ability to spare major blood vessels and ducts within the treatment zone [24]. However, while the vessel structure may remain,

the cells will often be injured. In fact, studies on direct IRE application on blood vessels have shown that IRE kills most of the cells to the margin of the blood vessel including the vascular smooth muscle cells (Figure 5.1) [105]. What IRE apparently does not compromise are the internal lamina and endothelial layers. Importantly, an intact endothelial layer is essential for the physiological function of blood vessels. This selective killing effect of IRE may explain why the blood vessel matrix is preserved after IRE [105].

5.2 IRE Treatment Planning

Currently, the most popular approach researchers use to predict treatment outcome in pre-clinical and clinical IRE is predicting the distribution of electric field within the tissue and comparing it with an electric field threshold obtained either from modeling or previous experience (Table 1.2). However, several critical factors need to be considered with this treatment planning method.

Firstly, it has been widely recognized that different cell types respond differently to IRE injury. For instance, Bao et. al. [18] treated lung cancer, red blood cells, and white blood cells using the same IRE system, and found the threshold for red blood cells (1100~1200V/cm) to be significantly higher than lung cancer (300~400V/cm) and white blood cells (400~500V/cm). Maor et. al. also found that when IRE is directly applied to the rate artery, the number of vascular smooth muscle cells is significantly reduced while endothelial cells are mostly preserved [105]. Further, we compared the responses of cancer, cardiovascular, and neural cells to IRE treatment (Chapter 4.3), and found that neural cells have a lower threshold for IRE destruction compared to the other two cell lines (Figure 4.6). It is thus of great interest to investigate what properties of the different

cell types contribute to their differences in IRE response. And more importantly, it is necessary to characterize the specific IRE thresholds when performing treatment planning for different therapeutic targets.

In addition, the heterogeneity of injury response within the target treatment zone also needs to be considered. It is now becoming appreciated with a few studies [29], [101] that incomplete treatment (live tumor patches in a target treated zone) have been found after IRE. This phenomenon is a real concern for cancer treatments due to the likelihood of recurrence, and if unresolved, represents a threat to the eventual translation of IRE. Having studied pre-clinical lesions for IRE, heat and cryo in an identical animal model, the appearance of live tumor patches within the treated tumor volume (rather than at the boundary) appears to be unique for electroporation (although more work is needed) [101], [133]. It is possible that the live cell patches are a result of local electrical property heterogeneity within the tumor tissue thereby lowering the effective electric field in the target region [134]. Thus, methods that can ensure the electric field distribution over the entire target region is above the IRE threshold is needed to improve the reliability of IRE cancer therapy.

Another topic in IRE treatment planning is the influence of pulse duration and pulse number on the outcome of IRE. It has been shown in our (Figure 1.6) and other studies [17], [31] that when electric field is kept the same, viability after IRE treatment can vary depending on the pulse duration and number delivered. The influences of pulse duration and pulse timing are similar to the “thermal dose” concept in thermal therapies (i.e. radiofrequency [151]). Therefore, it is important for people to report the pulse duration and pulse number used along with the electric field when determining the threshold for

treating a specific type of tissue. And careful consideration needs to be given to the pulse duration and number during treatment planning.

5.3 Enhancement Potentials

The two IRE enhancement approaches we proposed in Chapter 2 and 3, directly DMSO application and change of pulse timing, have both demonstrated significant cell destruction enhancement effect in various cancer models *in vitro* (cell suspension) and *in vivo* (DSFC and hindlimb tumors). However, our results are still limited in terms of experiment parameter range and the following future work is proposed as useful.

5.3.1 Adjuvant Delivery (DMSO)

The challenge of drug delivery in tumor has long been recognized in cancer treatment, and is a main motivation for people to introduce electroporation to chemo therapy [8], [9], [13]. There is the potential for non-uniform DMSO distribution in tissue to affect IRE enhancement. In our DSFC model, the local tissue conductivity is assumed to be elevated homogeneously as the fluid (saline + DMSO) is added topically and allowed to diffuse throughout a relatively thin tumor layer (0.5mm). We can then argue that the distribution of electric field within the tumor should remain relatively constant. It is, however, highly possible that if the solution were injected locally into the tissue, as in a solid tumor case, there could be conductivity variations that would change the overall electric field distribution. This could add to the risk of incomplete treatment and local occurrence in clinical applications.

5.3.2 Pulse Timing Optimization

It is also interesting to explore what other pulse timing delivery patterns can provide enhancement to IRE, and whether there is an optimum delivery pattern. The 30 seconds delay in our proposed approach was selected based on our previous study [136] which showed that other delay periods (10s, 1min, and 2mins) yield equivalent or less benefit in our experiment setup. However, the range we studied was limited and further testing on other delay period selections are still needed to fully characterize the potential of the pulse timing approach. Similarly, in our study the pulses were divided into three trains, but other or better possibilities may exist. It may also be helpful to develop a model to characterize the effect of pulse timing. To achieve that, a better understanding of the pore recovery time frame and IRE injury mechanism is highly needed.

[1] J. C. Weaver, “Electroporation of cells and tissues,” *Plasma Sci. IEEE Trans. On*, vol. 28, no. 1, pp. 24–33, 2000.

[2] A. Ivorra and B. Rubinsky, “Irreversible Electroporation,” Springer Berlin Heidelberg, 2010, pp. 1–21.

[3] R. Stampfli, “Reversible electrical breakdown of the excitable membrane of a Ranvier node,” *Acad Bras Cienc*, vol. 30, pp. 57–63, 1958.

[4] A. J. H. Sale and W. A. Hamilton, “Effects of high electric fields on microorganisms: I. Killing of bacteria and yeasts,” *Biochim. Biophys. Acta BBA - Gen. Subj.*, vol. 148, no. 3, pp. 781–788, Dec. 1967.

[5] M. J. Jaroszeski, R. Gilbert, C. Nicolau, and R. Heller, “In vivo gene delivery by electroporation,” *Adv. Drug Deliv. Rev.*, vol. 35, no. 1, pp. 131–137, Jan. 1999.

[6] L. M. Mir, “Therapeutic perspectives of in vivo cell electropermeabilization,” *Bioelectrochemistry Amst. Neth.*, vol. 53, no. 1, pp. 1–10, Jan. 2001.

[7] J. Gehl, “Electroporation: theory and methods, perspectives for drug delivery, gene therapy and research,” *Acta Physiol. Scand.*, vol. 177, no. 4, pp. 437–447, Apr. 2003.

[8] M. Okino and H. Mohri, “Effects of a high-voltage electrical impulse and an anticancer drug on in vivo growing tumors.,” *Jpn. J. Cancer Res. Gann*, vol. 78, no. 12, p. 1319, 1987.

[9] L. M. Mir, M. Belehradek, C. Domenge, S. Orlowski, B. Poddevin, J. Belehradek Jr, G. Schwaab, B. Luboinski, and C. Paoletti, “Electrochemotherapy, a new antitumor treatment: first clinical trial,” *CR Acad Sci III*, vol. 313, no. 13, pp. 613–618, 1991.

[10] R. Heller, M. J. Jaroszeski, L. F. Glass, J. L. Messina, D. P. Rapaport, R. C. DeConti, N. A. Fenske, R. A. Gilbert, L. M. Mir, and D. S. Reintgen, “Phase I/II trial for the treatment of cutaneous and subcutaneous tumors using electrochemotherapy,” *Cancer*, vol. 77, no. 5, pp. 964–971, 1998.

[11] L. M. Mir, L. F. Glass, G. Sersa, J. TeissiÃ, C. Domenge, D. Miklavcic, M. J. Jaroszeski, S. Orlowski, D. S. Reintgen, and Z. Rudolf, “Effective treatment of cutaneous and subcutaneous malignant tumours by electrochemotherapy.,” *Br. J. Cancer*, vol. 77, no. 12, p. 2336, 1998.

[12] G. A. Hofmann, S. B. Dev, S. Dimmer, and G. S. Nanda, “Electroporation therapy: a new approach for the treatment of head and neck cancer,” *IEEE Trans. Biomed. Eng.*, vol. 46, no. 6, pp. 752–759, Jun. 1999.

[13] A. Gothelf, L. M. Mir, and J. Gehl, “Electrochemotherapy: results of cancer treatment using enhanced delivery of bleomycin by electroporation,” *Cancer Treat. Rev.*, vol. 29, no. 5, pp. 371–387, Oct. 2003.

[14] G. Sersa, T. Jarm, T. Kotnik, A. Coer, M. Podkrajsek, M. Sentjurc, D. Miklavcic, M. Kadivec, S. Kranjc, A. Secerov, and M. Cemazar, “Vascular disrupting action of electroporation and electrochemotherapy with bleomycin in murine sarcoma,” *Br. J. Cancer*, vol. 98, no. 2, pp. 388–398, Jan. 2008.

[15] L. M. Mira, J. Gehld, G. Sersae, C. G. Collinsf, J. R. Garbaya, V. Billarda, P. F. Geertsend, Z. Rudolfe, G. C. O'Sullivanf, and M. Martya, "Standard operating procedures of the electrochemotherapy: Instructions for the use of bleomycin or cisplatin administered either systemically or locally and electric pulses delivered by the Cliniporator TM by means of invasive or non-invasive electrodes," *CR Acad Sci Paris*, vol. 313, pp. 613–8, 2006.

[16] R. V. Davalos, I. L. M. Mir, and B. Rubinsky, "Tissue ablation with irreversible electroporation," *Ann. Biomed. Eng.*, vol. 33, no. 2, pp. 223–231, Feb. 2005.

[17] J. Rubinsky, G. Onik, P. Mikus, and B. Rubinsky, "Optimal parameters for the destruction of prostate cancer using irreversible electroporation," *J. Urol.*, vol. 180, no. 6, pp. 2668–2674, Dec. 2008.

[18] N. Bao, T. T. Le, J.-X. Cheng, and C. Lu, "Microfluidic electroporation of tumor and blood cells: observation of nucleus expansion and implications on selective analysis and purging of circulating tumor cells," *Integr. Biol. Quant. Biosci. Nano Macro*, vol. 2, no. 2–3, pp. 113–120, Mar. 2010.

[19] L. Miller, J. Leor, and B. Rubinsky, "Cancer cells ablation with irreversible electroporation," *Technol. Cancer Res. Treat.*, vol. 4, no. 6, pp. 699–705, Dec. 2005.

[20] H. Shafiee, P. A. Garcia, and R. V. Davalos, "A preliminary study to delineate irreversible electroporation from thermal damage using the arrhenius equation," *J. Biomech. Eng.*, vol. 131, no. 7, p. 074509, Jul. 2009.

[21] J. F. Edd, L. Horowitz, R. V. Davalos, L. M. Mir, and B. Rubinsky, "In vivo results of a new focal tissue ablation technique: irreversible electroporation," *Biomed. Eng. IEEE Trans. On*, vol. 53, no. 7, pp. 1409 –1415, Jul. 2006.

[22] B. Al-Sakere, F. André, C. Bernat, E. Connault, P. Opolon, R. V. Davalos, B. Rubinsky, and L. M. Mir, "Tumor Ablation with Irreversible Electroporation," *PLoS ONE*, vol. 2, no. 11, p. e1135, Nov. 2007.

[23] P. A. Garcia, J. H. Rossmeisl Jr, R. E. Neal 2nd, T. L. Ellis, J. D. Olson, N. Henao-Guerrero, J. Robertson, and R. V. Davalos, "Intracranial nonthermal irreversible electroporation: in vivo analysis," *J. Membr. Biol.*, vol. 236, no. 1, pp. 127–136, Jul. 2010.

[24] B. Rubinsky, G. Onik, and P. Mikus, "Irreversible electroporation: a new ablation modality--clinical implications," *Technol. Cancer Res. Treat.*, vol. 6, no. 1, pp. 37–48, Feb. 2007.

[25] G. Onik, P. Mikus, and B. Rubinsky, "Irreversible electroporation: implications for prostate ablation," *Technol. Cancer Res. Treat.*, vol. 6, no. 4, pp. 295–300, Aug. 2007.

[26] T. L. Ellis, P. A. Garcia, J. H. Rossmeisl, N. Henao-Guerrero, J. Robertson, and R. V. Davalos, "Nonthermal irreversible electroporation for intracranial surgical applications," *J. Neurosurg.*, vol. 114, no. 3, pp. 681–688, Mar. 2011.

[27] A. Deodhar, S. Monette, G. W. Single Jr., W. C. Hamilton Jr., R. Thornton, M. Maybody, J. A. Coleman, and S. B. Solomon, "Renal Tissue Ablation With

Irreversible Electroporation: Preliminary Results in a Porcine Model," *Urology*, vol. 77, no. 3, pp. 754–760, Mar. 2011.
[28] C. R. Tracy, W. Kabbani, and J. A. Cadeddu, "Irreversible electroporation (IRE): a novel method for renal tissue ablation," *BJU Int.*, vol. 107, no. 12, pp. 1982–1987, Jun. 2011.
[29] Y. Guo, Y. Zhang, R. Klein, G. M. Nijm, A. V. Sahakian, R. A. Omary, G.-Y. Yang, and A. C. Larson, "Irreversible electroporation therapy in the liver: longitudinal efficacy studies in a rat model of hepatocellular carcinoma," *Cancer Res.*, vol. 70, no. 4, pp. 1555–1563, Feb. 2010.
[30] A. Golberg and M. L. Yarmush, "Nonthermal Irreversible Electroporation: Fundamentals, Applications, and Challenges," *IEEE Trans. Biomed. Eng.*, vol. 60, no. 3, pp. 707–714, 2013.
[31] J. C. Weaver, K. C. Smith, A. T. Esser, R. S. Son, and T. R. Gowrishankar, "A brief overview of electroporation pulse strength–duration space: A region where additional intracellular effects are expected," *Bioelectrochemistry*, vol. 87, no. 0, pp. 236–243, Oct. 2012.
[32] C. Chen, S. W. Smye, M. P. Robinson, and J. A. Evans, "Membrane electroporation theories: a review," *Med. Biol. Eng. Comput.*, vol. 44, no. 1–2, pp. 5–14, Mar. 2006.
[33] J. C. Weaver and Y. A. Chizmadzhev, "Theory of electroporation: a review," *Bioelectrochem. Bioenerg.*, vol. 41, no. 2, pp. 135–160, 1996.
[34] R. C. Lee, D. Zhang, and J. Hannig, "Biophysical Injury Mechanisms in Electrical Shock Trauma," *Annu. Rev. Biomed. Eng.*, vol. 2, no. 1, pp. 477–509, 2000.
[35] A. Ben-Or and B. Rubinsky, "Irreversible Electroporation," Springer Berlin Heidelberg, 2010, pp. 63–83.
[36] E. Neumann and K. Rosenheck, "Permeability changes induced by electric impulses in vesicular membranes," *J. Membr. Biol.*, vol. 10, no. 1, pp. 279–290, 1972.
[37] I. G. Abiror, V. B. Arakelyan, L. V. Chernomordik, Y. A. Chizmadzhev, V. F. Pastushenko, and M. R. Tarasevich, "246 - Electric breakdown of bilayer lipid membranes I. The main experimental facts and their qualitative discussion," *Bioelectrochem. Bioenerg.*, vol. 6, no. 1, pp. 37–52, Mar. 1979.
[38] V. F. Pastushenko, Y. A. Chizmadzhev, and V. B. Arakelyan, "247 - Electric breakdown of bilayer lipid membranes II. Calculation of the membrane lifetime in the steady-state diffusion approximation," *Bioelectrochem. Bioenerg.*, vol. 6, no. 1, pp. 53–62, Mar. 1979.
[39] Y. A. Chizmadzhev, V. B. Arakelyan, and V. F. Pastushenko, "248 - Electric breakdown of bilayer lipid membranes III. Analysis of possible mechanisms of defect origination," *Bioelectrochem. Bioenerg.*, vol. 6, no. 1, pp. 63–70, Mar. 1979.
[40] V. F. Pastushenko, Y. A. Chizmadzhev, and V. B. Arakelyan, "249 - Electric breakdown of bilayer lipid membranes IV. Consideration of the kinetic stage in the case of the single-defect membrane," *Bioelectrochem. Bioenerg.*, vol. 6, no. 1, pp. 71–79, Mar. 1979.

[41] V. B. Arakelyan, Y. A. Chizmadzhev, and V. F. Pastushenko, “250 - Electric breakdown of bilayer lipid membranes V. Consideration of the kinetic stage in the case of the membrane containing an arbitrary number of defects,” *Bioelectrochem. Bioenerg.*, vol. 6, no. 1, pp. 81–87, Mar. 1979.

[42] V. F. Pastushenko, V. B. Arakelyan, and Y. A. Chizmadzhev, “251 - Electric breakdown of bilayer lipid membranes VI. A stochastic theory taking into account the processes of defect formation and death: Membrane lifetime distribution function,” *Bioelectrochem. Bioenerg.*, vol. 6, no. 1, pp. 89–95, Mar. 1979.

[43] K. Kinosita Jr, I. Ashikawa, N. Saita, H. Yoshimura, H. Itoh, K. Nagayama, and A. Ikegami, “Electroporation of cell membrane visualized under a pulsed-laser fluorescence microscope,” *Biophys. J.*, vol. 53, no. 6, pp. 1015–1019, Jun. 1988.

[44] K. Kinosita, M. Hibino, H. Itoh, M. Shigemori, K. Hirano, Y. Kirino, and T. Hayakawa, “Events of membrane electroporation visualized on a time scale from microsecond to seconds,” *Guide Electroporation Electrofusion*, pp. 29–46, 1992.

[45] R. Susil, D. \vSemrov, and D. Miklavcic, “Electric Field-Induced Transmembrane Potential Depends on Cell Density and Organizatio,” *Electromagn. Biol. Med.*, vol. 17, no. 3, pp. 391–399, 1998.

[46] W. Krassowska and P. D. Filev, “Modeling Electroporation in a Single Cell,” *Biophys. J.*, vol. 92, no. 2, pp. 404–417, Jan. 2007.

[47] G. Pucihar, D. Miklavcic, and T. Kotnik, “A Time-Dependent Numerical Model of Transmembrane Voltage Inducement and Electroporation of Irregularly Shaped Cells,” *IEEE Trans. Biomed. Eng.*, vol. 56, no. 5, pp. 1491–1501, May 2009.

[48] J. M. Crowley, “Electrical Breakdown of Bimolecular Lipid Membranes as an Electromechanical Instability,” *Biophys. J.*, vol. 13, no. 7, pp. 711–724, Jul. 1973.

[49] J. D. Litster, “Stability of lipid bilayers and red blood cell membranes,” *Phys. Lett. A*, vol. 53, no. 3, pp. 193–194, Jun. 1975.

[50] C. Taupin, M. Dvolaitzky, and C. Sauterey, “Osmotic pressure-induced pores in phospholipid vesicles,” *Biochemistry (Mosc.)*, vol. 14, no. 21, pp. 4771–4775, Oct. 1975.

[51] J. C. Weaver and R. A. Mintzer, “Decreased bilayer stability due to transmembrane potentials,” *Phys. Lett. A*, vol. 86, no. 1, pp. 57–59, Oct. 1981.

[52] C. Jiang, Z. Qin, and J. Bischof, “Membrane-Targeting Approaches for Enhanced Cancer Cell Destruction with Irreversible Electroporation,” *Ann. Biomed. Eng.*, pp. 1–12, Aug. 2013.

[53] K. T. Powell and J. C. Weaver, “Transient aqueous pores in bilayer membranes: A statistical theory,” *Bioelectrochem. Bioenerg.*, vol. 15, no. 2, pp. 211–227, Apr. 1986.

[54] M. Toner and E. G. Cravalho, “Kinetics and likelihood of membrane rupture during electroporation,” *Phys. Lett. A*, vol. 143, no. 8, pp. 409–412, Jan. 1990.

[55] D. C. Chang and T. S. Reese, “Changes in membrane structure induced by electroporation as revealed by rapid-freezing electron microscopy,” *Biophys. J.*, vol. 58, no. 1, pp. 1–12, Jul. 1990.

[56] R. Benz, F. Beckers, and U. Zimmermann, “Reversible electrical breakdown of lipid bilayer membranes: A charge-pulse relaxation study,” *J. Membr. Biol.*, vol. 48, no. 2, pp. 181–204, Jun. 1979.
[57] O. Tovar and L. Tung, “Electroporation and Recovery of Cardiac Cell Membrane with Rectangular Voltage Pulses,” *Am. J. Physiol. - Heart Circ. Physiol.*, vol. 263, no. 4, pp. H1128–H1136, Oct. 1992.
[58] A. Ivorra and B. Rubinsky, “In vivo electrical impedance measurements during and after electroporation of rat liver,” *Bioelectrochemistry Amst. Neth.*, vol. 70, no. 2, pp. 287–295, May 2007.
[59] Y. Granot, A. Ivorra, E. Maor, and B. Rubinsky, “In vivo imaging of irreversible electroporation by means of electrical impedance tomography,” *Phys. Med. Biol.*, vol. 54, no. 16, pp. 4927–4943, Aug. 2009.
[60] R. Shirakashi, V. L. Sukhorukov, I. Tanasawa, and U. Zimmermann, “Measurement of the permeability and resealing time constant of the electroporated mammalian cell membranes,” *Int. J. Heat Mass Transf.*, vol. 47, no. 21, pp. 4517–4524, Oct. 2004.
[61] S. K. Frandsen, H. Gissel, P. Hojman, T. Tramm, J. Eriksen, and J. Gehl, “Direct Therapeutic Applications of Calcium Electroporation to Effectively Induce Tumor Necrosis,” *Cancer Res.*, vol. 72, no. 6, pp. 1336–1341, Mar. 2012.
[62] H. Schoellnast, S. Monette, P. C. Ezell, M. Maybody, J. P. Erinjeri, M. D. Stubblefield, G. Single, and S. B. Solomon, “The delayed effects of irreversible electroporation ablation on nerves,” *Eur. Radiol.*, vol. 23, no. 2, pp. 375–380, Feb. 2013.
[63] G. L. Andreason and G. A. Evans, “Optimization of electroporation for transfection of mammalian cell lines,” *Anal. Biochem.*, vol. 180, no. 2, pp. 269–275, Aug. 1989.
[64] S. Y. Ho and G. S. Mittal, “Electroporation of cell membranes: a review,” *Crit. Rev. Biotechnol.*, vol. 16, no. 4, pp. 349–362, 1996.
[65] B. Alberts, D. Bray, K. Hopkin, A. Johnson, J. Lewis, M. Raff, K. Roberts, and P. Walter, *Essential cell biology*. Garland Science, 2013.
[66] G. C. Troiano, L. Tung, V. Sharma, and K. J. Stebe, “The reduction in electroporation voltages by the addition of a surfactant to planar lipid bilayers,” *Biophys. J.*, vol. 75, no. 2, pp. 880–888, Aug. 1998.
[67] G. C. Troiano, K. J. Stebe, R. M. Raphael, and L. Tung, “The Effects of Gramicidin on Electroporation of Lipid Bilayers,” *Biophys. J.*, vol. 76, no. 6, pp. 3150–3157, Jun. 1999.
[68] D. K. L. Cheng, L. Tung, and E. A. Sobie, “Nonuniform responses of transmembrane potential during electric field stimulation of single cardiac cells,” *Am. J. Physiol.-Heart Circ. Physiol.*, vol. 277, no. 1, pp. H351–H362, 1999.
[69] A. V. Somlyo and A. P. Somlyo, “Electromechanical and Pharmacomechanical Coupling in Vascular Smooth Muscle,” *J. Pharmacol. Exp. Ther.*, vol. 159, no. 1, pp. 129–145, Jan. 1968.
[70] McMahon J.M. and Wells D.J., “Electroporation for Gene Transfer to Skeletal Muscles: Current Status,” *BioDrugs*, vol. 18, no. 3, pp. 155–165, 2004.

[71] A. Lau, C. Ionescu-Zanetti, J. Seo, and L. P. Lee, “A single cell electroporation chip,” *Lab. Chip*, vol. 5, no. 1, pp. 38–43, 2005.
[72] J. Olofsson, K. Nolkrantz, F. Ryttsén, B. A. Lambie, S. G. Weber, and O. Orwar, “Single-cell electroporation,” *Curr. Opin. Biotechnol.*, vol. 14, no. 1, pp. 29–34, 2003.
[73] J. L. Rae and R. A. Levis, “Single-cell electroporation,” *Pflüg. Arch. Eur. J. Physiol.*, vol. 443, no. 4, pp. 664–670, 2002.
[74] M. Wang, O. Orwar, J. Olofsson, and S. G. Weber, “Single-cell electroporation,” *Anal. Bioanal. Chem.*, vol. 397, no. 8, pp. 3235–3248, 2010.
[75] R. Ziv, Y. Steinhardt, G. Pelled, D. Gazit, and B. Rubinsky, “Micro-electroporation of mesenchymal stem cells with alternating electrical current pulses,” *Biomed. Microdevices*, vol. 11, no. 1, pp. 95–101, Feb. 2009.
[76] A. Kaner, I. Braslavsky, and B. Rubinsky, “Model of pore formation in a single cell in a flow-through channel with micro-electrodes,” *Biomed. Microdevices*, Oct. 2013.
[77] T. Y. Tsong, “Electroporation of cell membranes,” *Biophys. J.*, vol. 60, no. 2, pp. 297–306, 1991.
[78] K. A. DeBruin and W. Krassowska, “Modeling electroporation in a single cell. I. Effects of field strength and rest potential,” *Biophys. J.*, vol. 77, no. 3, pp. 1213–1224, 1999.
[79] M. Hibino, M. Shigemori, H. Itoh, K. Nagayama, and K. Kinosita Jr, “Membrane conductance of an electroporated cell analyzed by submicrosecond imaging of transmembrane potential,” *Biophys. J.*, vol. 59, no. 1, pp. 209–220, Jan. 1991.
[80] D. Gross, L. M. Loew, and W. W. Webb, “Optical imaging of cell membrane potential changes induced by applied electric fields,” *Biophys. J.*, vol. 50, no. 2, pp. 339–348, 1986.
[81] Y. Rosemberg and R. Korenstein, “Electroporation of the photosynthetic membrane: A study by intrinsic and external optical probes,” *Biophys. J.*, vol. 58, no. 4, pp. 823–832, 1990.
[82] E. H. Serpersu, K. Kinosita Jr, and T. Y. Tsong, “Reversible and irreversible modification of erythrocyte membrane permeability by electric field,” *Biochim. Biophys. Acta BBA-Biomembr.*, vol. 812, no. 3, pp. 779–785, 1985.
[83] R. V. Davalos, B. Rubinsky, and D. M. Otten, “A feasibility study for electrical impedance tomography as a means to monitor tissue electroporation for molecular medicine,” *IEEE Trans. Biomed. Eng.*, vol. 49, no. 4, pp. 400–403, Apr. 2002.
[84] R. V. Davalos, D. M. Otten, L. M. Mir, and B. Rubinsky, “Electrical impedance tomography for imaging tissue electroporation,” *IEEE Trans. Biomed. Eng.*, vol. 51, no. 5, pp. 761–767, May 2004.
[85] R. E. Neal, P. A. Garcia, J. L. Robertson, and R. V. Davalos, “Experimental Characterization and Numerical Modeling of Tissue Electrical Conductivity during Pulsed Electric Fields for Irreversible Electroporation Treatment Planning,” *IEEE Trans. Biomed. Eng.*, vol. 59, no. 4, pp. 1076 –1085, Apr. 2012.

[86] K. Kinosita Jr and T. Y. Tsong, “Voltage-induced conductance in human erythrocyte membranes,” *Biochim. Biophys. Acta BBA-Biomembr.*, vol. 554, no. 2, pp. 479–497, 1979.
[87] E. W. Lee, D. Wong, S. V. Prikhodko, A. Perez, C. Tran, C. T. Loh, and S. T. Kee, “Electron Microscopic Demonstration and Evaluation of Irreversible Electroporation-Induced Nanopores on Hepatocyte Membranes,” *J. Vasc. Interv. Radiol.*, vol. 23, no. 1, pp. 107–113, Jan. 2012.
[88] C. S. Djuzenova, U. Zimmermann, H. Frank, V. L. Sukhorukov, E. Richter, and G. Fuhr, “Effect of medium conductivity and composition on the uptake of propidium iodide into electropermeabilized myeloma cells,” *Biochim. Biophys. Acta BBA - Biomembr.*, vol. 1284, no. 2, pp. 143–152, Oct. 1996.
[89] C. Jiang, J. Choi, P. Patana-anake, and J. C. BISCHOF, “Comparison of Irreversible Electroporation, Cryo, and Thermal Ablations on Cardiovascular Cells,” presented at the Design of Medical Devices Conference, 2014.
[90] Y. Guo, Y. Zhang, G. M. Nijm, A. V. Sahakian, G.-Y. Yang, R. A. Omary, and A. C. Larson, “Irreversible electroporation in the liver: contrast-enhanced inversion-recovery MR imaging approaches to differentiate reversibly electroporated penumbra from irreversibly electroporated ablation zones,” *Radiology*, vol. 258, no. 2, pp. 461–468, Feb. 2011.
[91] D. Miklavčič, D. Šemrov, H. Mekid, and L. M. Mir, “A validated model of in vivo electric field distribution in tissues for electrochemotherapy and for DNA electrotransfer for gene therapy,” *Biochim. Biophys. Acta BBA - Gen. Subj.*, vol. 1523, no. 1, pp. 73–83, Sep. 2000.
[92] M. B. Sano, R. E. Neal 2nd, P. A. Garcia, D. Gerber, J. Robertson, and R. V. Davalos, “Towards the creation of decellularized organ constructs using irreversible electroporation and active mechanical perfusion,” *Biomed. Eng. Online*, vol. 9, p. 83, 2010.
[93] M. A. Phillips, R. Narayan, T. Padath, and B. Rubinsky, “Irreversible electroporation on the small intestine,” *Br. J. Cancer*, vol. 106, no. 3, pp. 490–495, Jan. 2012.
[94] C. B. Arena, M. B. Sano, J. H. Rossmeisl Jr, J. L. Caldwell, P. A. Garcia, M. N. Rylander, and R. V. Davalos, “High-frequency irreversible electroporation (H-FIRE) for non-thermal ablation without muscle contraction,” *Biomed. Eng. Online*, vol. 10, p. 102, 2011.
[95] P. A. Garcia, J. H. Rossmeisl Jr, R. E. Neal 2nd, T. L. Ellis, and R. V. Davalos, “A parametric study delineating irreversible electroporation from thermal damage based on a minimally invasive intracranial procedure,” *Biomed. Eng. Online*, vol. 10, p. 34, 2011.
[96] A. Deodhar, T. Dickfeld, G. W. Single, W. C. Hamilton, R. H. Thornton, C. T. Sofocleous, M. Maybody, M. Gónen, B. Rubinsky, and S. B. Solomon, “Irreversible Electroporation Near the Heart: Ventricular Arrhythmias Can Be Prevented With ECG Synchronization,” *Am. J. Roentgenol.*, vol. 196, no. 3, pp. W330–W335, Mar. 2011.

[97] J. J. Wendler, M. Pech, S. Blaschke, M. Porsch, A. Janitzky, M. Ulrich, O. Dudeck, J. Ricke, and U. B. Liehr, "Angiography in the Isolated Perfused Kidney: Radiological Evaluation of Vascular Protection in Tissue Ablation by Nonthermal Irreversible Electroporation," *Cardiovasc. Intervent. Radiol.*, pp. 1–8, 2011.

[98] B. Al-Sakere, C. Bernat, F. Andre, E. Connault, P. Opolon, R. V. Davalos, and L. M. Mir, "A study of the immunological response to tumor ablation with irreversible electroporation," *Technol. Cancer Res. Treat.*, vol. 6, no. 4, pp. 301–306, Aug. 2007.

[99] A. Ivorra, B. Al-Sakere, B. Rubinsky, and L. M. Mir, "In vivo electrical conductivity measurements during and after tumor electroporation: conductivity changes reflect the treatment outcome," *Phys. Med. Biol.*, vol. 54, no. 19, pp. 5949–5963, Oct. 2009.

[100] R. E. Neal 2nd, R. Singh, H. C. Hatcher, N. D. Kock, S. V. Torti, and R. V. Davalos, "Treatment of breast cancer through the application of irreversible electroporation using a novel minimally invasive single needle electrode," *Breast Cancer Res. Treat.*, vol. 123, no. 1, pp. 295–301, Aug. 2010.

[101] Z. Qin, J. Jiang, G. Long, B. Lindgren, and J. C. Bischof, "Irreversible Electroporation: An In Vivo Study with Dorsal Skin Fold Chamber," *Ann. Biomed. Eng.*, pp. 1–11, Nov. 2012.

[102] P. A. Garcia, T. Pancotto, J. H. Rossmeisl Jr, N. Henao-Guerrero, N. R. Gustafson, G. B. Daniel, J. L. Robertson, T. L. Ellis, and R. V. Davalos, "Non-thermal irreversible electroporation (N-TIRE) and adjuvant fractionated radiotherapeutic multimodal therapy for intracranial malignant glioma in a canine patient," *Technol. Cancer Res. Treat.*, vol. 10, no. 1, pp. 73–83, Feb. 2011.

[103] P. A. Garcia, J. H. Rossmeisl Jr, and R. V. Davalos, "Electrical conductivity changes during irreversible electroporation treatment of brain cancer," *Annu. Int. Conf. IEEE Eng. Med. Biol. Soc.*, vol. 2011, pp. 739–742, 2011.

[104] R. E. Neal 2nd, J. H. Rossmeisl Jr, P. A. Garcia, O. I. Lanz, N. Henao-Guerrero, and R. V. Davalos, "Successful treatment of a large soft tissue sarcoma with irreversible electroporation," *J. Clin. Oncol.*, vol. 29, no. 13, pp. e372–377, May 2011.

[105] E. Maor, A. Ivorra, J. Leor, and B. Rubinsky, "The effect of irreversible electroporation on blood vessels," *Technol. Cancer Res. Treat.*, vol. 6, no. 4, pp. 307–312, Aug. 2007.

[106] E. Maor, A. Ivorra, and B. Rubinsky, "Intravascular irreversible electroporation: theoretical and experimental feasibility study," *Conf. Proc. Annu. Int. Conf. IEEE Eng. Med. Biol. Soc. IEEE Eng. Med. Biol. Soc. Conf.*, vol. 2008, pp. 2051–2054, 2008.

[107] E. Maor, A. Ivorra, and B. Rubinsky, "Non Thermal Irreversible Electroporation: Novel Technology for Vascular Smooth Muscle Cells Ablation," *PLoS ONE*, vol. 4, no. 3, p. e4757, Mar. 2009.

[108] M. Phillips, E. Maor, and B. Rubinsky, "Nonthermal irreversible electroporation for tissue decellularization," *J. Biomech. Eng.*, vol. 132, no. 9, p. 091003, Sep. 2010.

[109] M. Phillips, E. Maor, and B. Rubinsky, “Principles of Tissue Engineering With Nonthermal Irreversible Electroporation,” *J. Heat Transf.*, vol. 133, no. 1, p. 011004, 2011.
[110] J. Lavee, G. Onik, P. Mikus, and B. Rubinsky, “A novel nonthermal energy source for surgical epicardial atrial ablation: irreversible electroporation,” in *The heart surgery forum*, 2007, vol. 10, pp. 162–167.
[111] J. F. Edd and R. V. Davalos, “Mathematical modeling of irreversible electroporation for treatment planning,” *Technol. Cancer Res. Treat.*, vol. 6, no. 4, pp. 275–286, 2007.
[112] R. Goel, D. Swanlund, J. Coad, G. F. Paciotti, and J. C. Bischof, “TNF-α–based accentuation in cryoinjury—dose, delivery, and response,” *Mol. Cancer Ther.*, vol. 6, no. 7, pp. 2039–2047, Jul. 2007.
[113] R. E. Neal II, “Spectrum of imaging and characteristics for liver tumors treated with irreversible electroporation,” *J. Biomed. Sci. Eng.*, vol. 05, no. 12, pp. 813–818, 2012.
[114] L. Ew, L. Ct, and K. St, “Imaging guided percutaneous irreversible electroporation: ultrasound and immunohistological correlation.,” *Technol. Cancer Res. Treat.*, vol. 6, no. 4, pp. 287–294, Aug. 2007.
[115] L. Appelbaum, E. Ben-David, J. Sosna, Y. Nissenbaum, and S. N. Goldberg, “US Findings after Irreversible Electroporation Ablation: Radiologic-Pathologic Correlation,” *Radiology*, vol. 262, no. 1, pp. 117–125, Jan. 2012.
[116] J. E. Coad and J. C. Bischof, “Histologic differences between cryothermic and hyperthermic therapies,” in *Biomedical Optics 2003*, 2003, pp. 27–36.
[117] C. C. Rupp, N. E. Hoffmann, F. R. Schmidlin, D. J. Swanlund, J. C. Bischof, and J. E. Coad, “Cryosurgical changes in the porcine kidney: histologic analysis with thermal history correlation,” *Cryobiology*, vol. 45, no. 2, pp. 167–182, 2002.
[118] N. Z. Wu, B. Klitzman, G. Rosner, D. Needham, and M. W. Dewhirst, “Measurement of Material Extravasation in Microvascular Networks Using Fluorescence Video-Microscopy,” *Microvasc. Res.*, vol. 46, no. 2, pp. 231–253, Sep. 1993.
[119] K. Thomson, “Human Experience with Irreversible Electroporation,” in *Irreversible Electroporation*, B. Rubinsky, Ed. Springer Berlin Heidelberg, 2010, pp. 249–254.
[120] M. Pech, A. Janitzky, J. J. Wendler, C. Strang, S. Blaschke, O. Dudeck, J. Ricke, and U. B. Liehr, “Irreversible electroporation of renal cell carcinoma: a first-in-man phase I clinical study,” *Cardiovasc. Intervent. Radiol.*, vol. 34, no. 1, pp. 132–138, 2011.
[121] K. R. Thomson, W. Cheung, S. J. Ellis, D. Federman, H. Kavnoudias, D. Loader-Oliver, S. Roberts, P. Evans, C. Ball, and A. Haydon, “Investigation of the Safety of Irreversible Electroporation in Humans,” *J. Vasc. Interv. Radiol.*, vol. 22, no. 5, pp. 611–621, May 2011.
[122] T. P. Kingham, A. M. Karkar, M. I. D’Angelica, P. J. Allen, R. P. DeMatteo, G. I. Getrajdman, C. T. Sofocleous, S. B. Solomon, W. R. Jarnagin, and Y. Fong,

"Ablation of Perivascular Hepatic Malignant Tumors with Irreversible Electroporation," *J. Am. Coll. Surg.*, vol. 215, no. 3, pp. 379–387, Sep. 2012.
[123] R. Cannon, S. Ellis, D. Hayes, G. Narayanan, and R. C. G. Martin, "Safety and early efficacy of irreversible electroporation for hepatic tumors in proximity to vital structures," *J. Surg. Oncol.*, vol. 107, no. 5, pp. 544–549, Apr. 2013.
[124] P. Philips, D. Hays, and R. C. G. Martin, "Irreversible Electroporation Ablation (IRE) of Unresectable Soft Tissue Tumors: Learning Curve Evaluation in the First 150 Patients Treated," *PLoS ONE*, vol. 8, no. 11, p. e76260, Nov. 2013.
[125] Cheung, "Irreversible Electroporation for Unresectable Hepatocellular Carcinoma: Initial Experience and Review of Safety and Outcomes," *Technol. Cancer Res. Treat.*, 2013.
[126] R. C. G. Martin II, K. McFarland, S. Ellis, and V. Velanovich, "Irreversible Electroporation Therapy in the Management of Locally Advanced Pancreatic Adenocarcinoma," *J. Am. Coll. Surg.*, vol. 215, no. 3, pp. 361–369, Sep. 2012.
[127] R. E. Neal, J. L. Millar, H. Kavnoudias, P. Royce, F. Rosenfeldt, A. Pham, R. Smith, R. V. Davalos, and K. R. Thomson, "In vivo characterization and numerical simulation of prostate properties for non-thermal irreversible electroporation ablation," *The Prostate*, vol. 74, no. 5, pp. 458–468, May 2014.
[128] R. C. G. Martin II, K. McFarland, S. Ellis, and V. Velanovich, "Irreversible Electroporation in Locally Advanced Pancreatic Cancer: Potential Improved Overall Survival," *Ann. Surg. Oncol.*, vol. 20, no. 3, pp. 443–449, Dec. 2013.
[129] B. Mali, T. Jarm, S. Corovic, M. S. Paulin-Kosir, M. Cemazar, G. Sersa, and D. Miklavcic, "The effect of electroporation pulses on functioning of the heart," *Med. Biol. Eng. Comput.*, vol. 46, no. 8, pp. 745–757, Aug. 2008.
[130] L. Solbiati, T. Livraghi, S. N. Goldberg, T. Ierace, F. Meloni, M. Dellanoce, L. Cova, E. F. Halpern, and G. S. Gazelle, "Percutaneous Radio-frequency Ablation of Hepatic Metastases from Colorectal Cancer: Long-term Results in 117 Patients1," *Radiology*, vol. 221, no. 1, pp. 159–166, Oct. 2001.
[131] E. K. Abdalla, J.-N. Vauthey, L. M. Ellis, V. Ellis, R. Pollock, K. R. Broglio, K. Hess, and S. A. Curley, "Recurrence and Outcomes Following Hepatic Resection, Radiofrequency Ablation, and Combined Resection/Ablation for Colorectal Liver Metastases," *Ann. Surg.*, vol. 239, no. 6, pp. 818–827, Jun. 2004.
[132] A. S. Pearson, F. Izzo, R. Y. D. Fleming, L. M. Ellis, P. Delrio, M. S. Roh, J. Granchi, and S. A. Curley, "Intraoperative radiofrequency ablation or cryoablation for hepatic malignancies," *Am. J. Surg.*, vol. 178, no. 6, pp. 592–598, Dec. 1999.
[133] R. Goel, K. Anderson, J. Slaton, F. Schmidlin, G. Vercellotti, J. Belcher, and J. C. Bischof, "Adjuvant Approaches to Enhance Cryosurgery," *J. Biomech. Eng.*, vol. 131, no. 7, p. 074003, 2009.
[134] C. Daniels and B. Rubinsky, "Electrical field and temperature model of nonthermal irreversible electroporation in heterogeneous tissues," *J. Biomech. Eng.*, vol. 131, no. 7, p. 071006, Jul. 2009.

[135] C. B. Arena, M. B. Sano, M. N. Rylander, and R. V. Davalos, “Theoretical Considerations of Tissue Electroporation With High-Frequency Bipolar Pulses,” *IEEE Trans. Biomed. Eng.*, vol. 58, no. 5, pp. 1474–1482, May 2011.
[136] C. Jiang, Z. Qin, G. Long, and J. C. Bischof, “An in vitro study on adjuvant enhanced irreversible electroporation,” presented at the Summer Bioengineering Conference, Farjardo, Puerto Rico, USA, 2012.
[137] S. N. Murthy, A. Sen, and S. W. Hui, “Surfactant-enhanced transdermal delivery by electroporation,” *J. Controlled Release*, vol. 98, no. 2, pp. 307–315, Aug. 2004.
[138] S. N. Murthy, Y.-L. Zhao, A. Sen, and S. W. Hui, “Cyclodextrin enhanced transdermal delivery of piroxicam and carboxyfluorescein by electroporation,” *J. Controlled Release*, vol. 99, no. 3, pp. 393–402, Oct. 2004.
[139] I. van Uitert, S. Le Gac, and A. van den Berg, “The influence of different membrane components on the electrical stability of bilayer lipid membranes,” *Biochim. Biophys. Acta BBA - Biomembr.*, vol. 1798, no. 1, pp. 21–31, Jan. 2010.
[140] J. C. Weaver, R. Vanbever, T. E. Vaughan, and M. R. Prausnitz, “Heparin Alters Transdermal Transport Associated with Electroporation,” *Biochem. Biophys. Res. Commun.*, vol. 234, no. 3, pp. 637–640, May 1997.
[141] T. E. Zewert, U. F. Pliquett, R. Vanbever, R. Langer, and J. C. Weaver, “Creation of transdermal pathways for macromolecule transport by skin electroporation and a low toxicity, pathway-enlarging molecule,” *Bioelectrochem. Bioenerg.*, vol. 49, no. 1, pp. 11–20, Oct. 1999.
[142] J. T. Au, T. P. Kingham, K. Jun, D. Haddad, S. Gholami, K. Mojica, S. Monette, P. Ezell, and Y. Fong, “Irreversible electroporation ablation of the liver can be detected with ultrasound B-mode and elastography,” *Surgery*, vol. 153, no. 6, pp. 787–793, Jun. 2013.
[143] R. V. Davalos, B. Rubinsky, and L. M. Mir, “Theoretical analysis of the thermal effects during in vivo tissue electroporation,” *Bioelectrochemistry Amst. Neth.*, vol. 61, no. 1–2, pp. 99–107, Oct. 2003.
[144] Long, “Histological and Finite Element Analysis of Cell Death due to Irreversible Electroporation,” *TCRT Express*, 2013.
[145] D. S. Lu, S. S. Raman, D. J. Vodopich, M. Wang, J. Sayre, and C. Lassman, “Effect of Vessel Size on Creation of Hepatic Radiofrequency Lesions in Pigs Assessment of the ‘Heat Sink’ Effect,” *Am. J. Roentgenol.*, vol. 178, no. 1, pp. 47–51, 2002.
[146] E. Karatekin, O. Sandre, H. Guitouni, N. Borghi, P.-H. Puech, and F. Brochard-Wyart, “Cascades of Transient Pores in Giant Vesicles: Line Tension and Transport,” *Biophys. J.*, vol. 84, no. 3, pp. 1734–1749, Mar. 2003.
[147] L. Tung, G. C. Troiano, V. Sharma, R. M. Raphael, and K. J. Stebe, “Changes in electroporation thresholds of lipid membranes by surfactants and peptides,” *Ann. N. Y. Acad. Sci.*, vol. 888, no. 1, pp. 249–265, 1999.
[148] D. Moldovan, D. Pinisetty, and R. V. Devireddy, “Molecular dynamics simulation of pore growth in lipid bilayer membranes in the presence of edge-active agents,” *Appl. Phys. Lett.*, vol. 91, no. 20, pp. 204104 –204104–3, Nov. 2007.

[149] R. V. Devireddy, “Statistical thermodynamics of biomembranes,” *Cryobiology*, vol. 60, no. 1, pp. 80–90, Feb. 2010.
[150] S. A. Isbell, C. A. Fyfe, R. L. M. Ammons, and B. Pearson, “Measurement of Cryoprotective Solvent Penetration into Intact Organ Tissues Using High-Field NMR Microimaging,” *Cryobiology*, vol. 35, no. 2, pp. 165–172, Sep. 1997.
[151] S. A. Sapareto and W. C. Dewey, “Thermal dose determination in cancer therapy,” *Int. J. Radiat. Oncol. Biol. Phys.*, vol. 10, no. 6, pp. 787–800, Apr. 1984.
[152] X. Li, K. Xu, W. Li, X. Qiu, B. Ma, Q. Fan, and Z. Li, “Immunologic response to tumor ablation with irreversible electroporation,” *PloS One*, vol. 7, no. 11, p. e48749, 2012.
[153] H. Schoellnast, S. Monette, P. C. Ezell, A. Deodhar, M. Maybody, J. P. Erinjeri, M. D. Stubblefield, G. W. Single, W. C. Hamilton, and S. B. Solomon, “Acute and Subacute Effects of Irreversible Electroporation on Nerves: Experimental Study in a Pig Model,” *Radiology*, vol. 260, no. 2, pp. 421–427, Aug. 2011.
[154] P. A. Heidenreich, J. G. Trogdon, O. A. Khavjou, J. Butler, K. Dracup, M. D. Ezekowitz, E. A. Finkelstein, Y. Hong, S. C. Johnston, A. Khera, D. M. Lloyd-Jones, S. A. Nelson, G. Nichol, D. Orenstein, P. W. F. Wilson, and Y. J. Woo, “Forecasting the Future of Cardiovascular Disease in the United States A Policy Statement From the American Heart Association,” *Circulation*, vol. 123, no. 8, pp. 933–944, Mar. 2011.
[155] H. Calkins, P. Yong, J. M. Miller, B. Olshansky, M. Carlson, J. P. Saul, S. K. S. Huang, L. B. Liem, L. S. Klein, S. A. Moser, D. A. Bloch, P. Gillette, and E. Prystowsky, “Catheter Ablation of Accessory Pathways, Atrioventricular Nodal Reentrant Tachycardia, and the Atrioventricular Junction Final Results of a Prospective, Multicenter Clinical Trial,” *Circulation*, vol. 99, no. 2, pp. 262–270, Jan. 1999.
[156] W. C. Claycomb, N. A. Lanson, B. S. Stallworth, D. B. Egeland, J. B. Delcarpio, A. Bahinski, and N. J. Izzo, “HL-1 cells: A cardiac muscle cell line that contracts and retains phenotypic characteristics of the adult cardiomyocyte,” *Proc. Natl. Acad. Sci.*, vol. 95, no. 6, pp. 2979–2984, Mar. 1998.
[157] M. P. Schlaich, P. A. Sobotka, H. Krum, E. Lambert, and M. D. Esler, “Renal Sympathetic-Nerve Ablation for Uncontrolled Hypertension,” *N. Engl. J. Med.*, vol. 361, no. 9, pp. 932–934, 2009.
[158] C. N. Shealy, “Percutaneous radiofrequency denervation of spinal facets: treatment for chronic back pain and sciatica,” *J. Neurosurg.*, vol. 43, no. 4, pp. 448–451, 1975.
[159] H. Krum, M. Schlaich, R. Whitbourn, P. A. Sobotka, J. Sadowski, K. Bartus, B. Kapelak, A. Walton, H. Sievert, S. Thambar, W. T. Abraham, and M. Esler, “Catheter-based renal sympathetic denervation for resistant hypertension: a multicentre safety and proof-of-principle cohort study,” *The Lancet*, vol. 373, no. 9671, pp. 1275–1281, 11.
[160] H.-F. Tse, S. Reek, C. Timmermans, K. L.-F. Lee, J. C. Geller, L.-M. Rodriguez, B. Ghaye, G. M. Ayers, H. J. G. . Crijns, H. U. Klein, and C.-P. Lau, “Pulmonary vein isolation using transvenous catheter cryoablation for treatment of atrial

fibrillation without risk of pulmonary vein stenosis," *J. Am. Coll. Cardiol.*, vol. 42, no. 4, pp. 752–758, Aug. 2003.
[161] T. Neumann, J. Vogt, B. Schumacher, A. Dorszewski, M. Kuniss, H. Neuser, K. Kurzidim, A. Berkowitsch, M. Koller, J. Heintze, U. Scholz, U. Wetzel, M. A. E. Schneider, D. Horstkotte, C. W. Hamm, and H.-F. Pitschner, "Circumferential Pulmonary Vein Isolation With the Cryoballoon TechniqueResults From a Prospective 3-Center Study," *J. Am. Coll. Cardiol.*, vol. 52, no. 4, pp. 273–278, Jul. 2008.
[162] D. D. Belsham, F. Cai, H. Cui, S. R. Smukler, A. M. F. Salapatek, and L. Shkreta, "Generation of a Phenotypic Array of Hypothalamic Neuronal Cell Models to Study Complex Neuroendocrine Disorders," *Endocrinology*, vol. 145, no. 1, pp. 393–400, Jan. 2004.
[163] D. L. Hoyert, "Deaths: Preliminary data for 2011," National Vital Stat Report, 2011.
[164] C. Jiang, R. Goff, P. Patana-anake, P. A. Iaizzo, and J. Bischof, "Irreversible Electroporation of Cardiovascular Cells and Tissues," *J. Med. Devices*, vol. 7, no. 3, pp. 030903–030903, Jul. 2013.
[165] X. He and J. C. Bischof, "The kinetics of thermal injury in human renal carcinoma cells," *Ann. Biomed. Eng.*, vol. 33, no. 4, pp. 502–510, Apr. 2005.

Appendix A1. *Comparison of Irreversible Electroporation, Cryo, and Thermal Ablations on Cardiovascular Cells*

Contributing Authors: Chunlan Jiang, Jeunghwan Choi, Dushyant Mehra, Pong Patana-anake, and John C. Bischof

The following chapter appeared in publications:
C. Jiang, J. Choi, D. Mehra, P. Patana, and J. C. Bischof, “Comparison of Irreversible Electroporation, Cryo, and Thermal Ablations on Cardiovascular Cells”, presented at the ASME Design of Medical Device Conference, April, 2014.

A1.1 Introduction

Cardiovascular disease remains the number one cause of death in the United States, and was responsible for approximately 6 million deaths of men and women in 2011 [163] Many acquired cardiovascular diseases are associated with abnormal proliferation of vascular smooth muscle cells (e.g. heart attack) or irregular electrical pathways (e.g. arrhythmia). Of the various methods applied to manage cardiovascular diseases, using energy-based technologies to create myocardial lesions (i.e. “ablation”) has gained increasing popularity due to their effectiveness, short treatment times, and minimal surgical damages.

Thermal energy was one of the earliest technologies used for catheter ablation and currently has the greatest patient-year experience [155]. Various modalities, such as radiofrequency, high-intensity focused ultrasound (HIFU), catheter-based cryoablation,

focused laser, and microwaves, have been proposed as potential sources for cardiovascular ablation.

Irreversible Electroporation (IRE), an emerging focal ablation modality that has attracted much interest in cancer research, may also provide new opportunities for treatments of cardiovascular diseases. Unlike thermal technologies, IRE is based on the electrical field distribution rather than diffusion, and induces cell death by increasing permeability, thus leaving long-term defects within cell membranes [1]. Although there have been several studies on IRE ablation of cardiovascular cells [164] and tissues (i.e. artery [107] and myocardial [110]), direct comparison between IRE and thermal ablation has yet to be done on the same biological model.

In this report, we evaluated the ability of IRE to destroy cardiovascular cells and compared the results with those of cryo and thermal ablations on the same model. To do so, we use an atrial cardiac muscle cell line (HL-1 [156]) in order to characterize the biophysical effects and efficacy of these therapies. Specific influences of applied therapeutic variables for each modality (IRE: electric field (E-field), pulse duration and number, cryo and thermal: cooling/heating rate, end temperature and holding time) were studied and compared based on a common measure of injury (i.e., cell membrane integrity). The results presented here will likely aid in the selection of the best singular or combinatorial approach to treat cardiovascular diseases among the three studied modalities.

A1.2 Materials and Methods

A1.2.1 Cardiac muscle cell cultures

A HL-1 cell line was cultured as adherent monolayers [156]. More specifically, cells were grown in T-75 flasks with Claycomb medium (51800C, Sigma-Aldrich, St. Louis, MO) supplemented with 10% fetal bovine serum, 2mM L-Glutamine, 100U/ml of Penicillin/Streptomycin, and 0.1mM Norepinephrine. When 90% confluence was reached and spontaneous beating was elicited (observed under the microscope), the cells were detached by adding 0.05% Trypsin-EDTA (Invitrogen, CA) and then formed into a single cell suspension (0.5~0.6 million cells/ml).

A1.2.2 Irreversible Electroporation Treatment

400µl volumes of the prepared HL-1 suspensions were pipetted into electroporation cuvettes (Fisher Scientific), which were then placed in an external electrical field created by an electrical pulse generator (BTX ECM 830, Harvard Apparatus). The output voltages and currents were monitored by an oscilloscope (Tektronix TDS 2002).

A1.2.3 Cryoablation Treatment

10µl volumes of the prepared HL-1 suspensions were pipetted into a crucible which was placed on a controlled temperature stage in conjunction with a light microscope to observe freezing of the samples. Before cooling, samples were pre-nucleated by applying a chilled needle on the outer edge of the sample. The end temperature (-5 to -60 ^{o}C), and hold time (0 to 5 min) were varied among experiment groups, while cooling rate was kept constant at 5^{o}C/min. This constant cooling rate was chosen best on preliminary results (data not shown) that suggest peak survival at this rate compared to faster or slower rates.

A1.2.4 Thermal (Heat) Treatment

10µl volumes of the prepared HL-1 suspensions were placed in a sample pan then placed in a differential scanning calorimeter which controls the heating rate and end temperature. The cells were first held at 25^{o}C for 1 min before being heated to end temperatures between 40 to 70^{o}C at 5^{o}C/min, then immediately cooled to 25^{o}C at 130^{o}C/min. After heating, the cells were kept at 37^{o}C for 3 hours before injury evaluation.

A1.2.5 Injury Evaluations

After treatments, aliquots of the treated cell suspensions were incubated with Hoechst 33342 (10µM) and Propidium iodide (PI) dyes (7.5µM) for 15mins. These samples were then observed under a fluorescent microscope and photos were taken to calculate relative cell viability.

A1.3 Results

All treatment methods in our experiment were able to achieve complete (more than 95%) cell destruction with appropriate combination of therapeutic parameters. Specifically, for IRE the electric field required for complete cell destruction is 1250V/cm with 99 of 50µs long pulses. Pulse number has significant impact on E-field threshold. With 50 pulses, the E-field threshold increased to 1500V/cm. With 10 pulses, we were unable to achieve viability lower than 20% with even the highest E-field. For cryo, with a cooling rate of 5^{o}C/min, the end temperature required for complete cell destruction is lower than -40^{o}C. Changing holding time from 1 to 5 minutes appears not to be a deterministic factor for cell viability in this cell line. For heating at 5^{o}C/min and no holding time at the end temperature, the injury started to occur when end temperature went over 45^{o}C. However, complete cell destruction was not achieved until end temperature reached

60°C. The heating injury kinetics has been characterized with more details from previous studies in our lab [165].

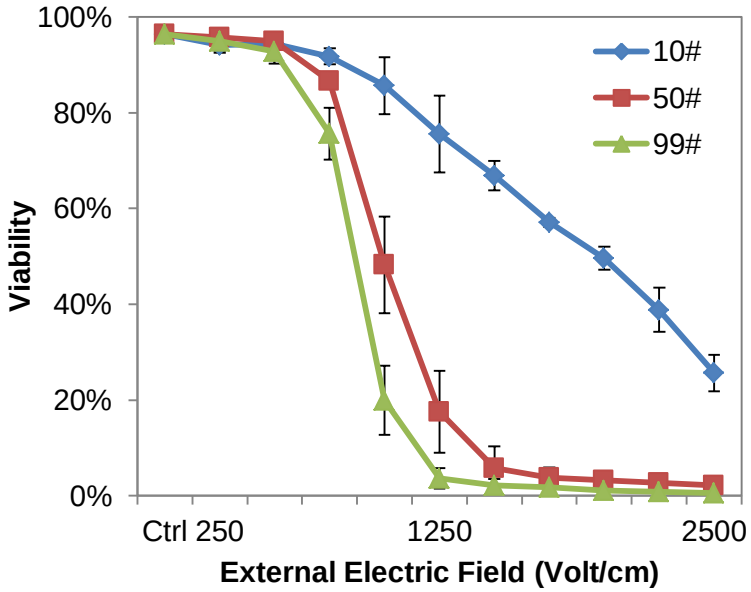

(a)

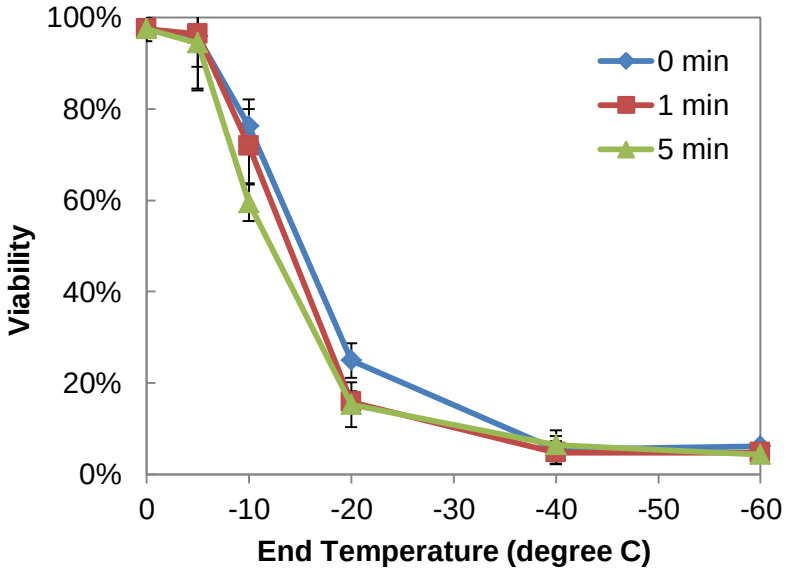

(b)

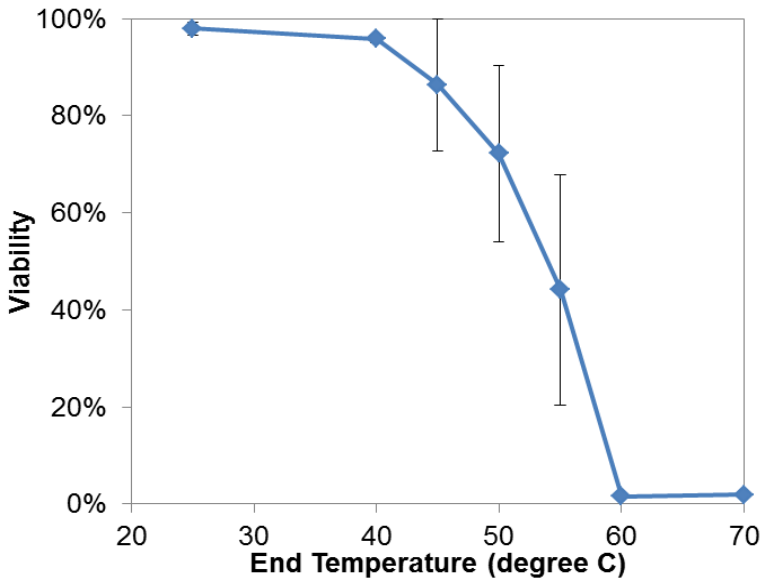

Figure A1.1. *Viability results of the HL-1 cell line after treatments of (a) IRE with E-field of 50~500V, 50μs pulse duration and 10~99 number of pulses, (b) Cryoablation with end temperatures of 0~-60oC, 5oC/min cooling rate and 0~5min holding times, (c) Heating with end temperatures of 40~70oC, 5oC/min heating rate and no holding times. (N=4, error bars represent standard deviations)*

Our experiment results indicate that IRE is capable of destroying cardiovascular cells as well as cryo and heat ablations. The critical therapeutic factors for IRE are E-field, pulse duration and numbers, verses end temperature, cooling rate for cryo or holding time for heating. Over 98% cell destruction was achieved with 99 of 50μs IRE pulses over 1250V/cm. However, the time required for IRE to deliver treatment is significantly shorter than that of cryo and heating (Table A1.1). Although all three modalities suffer from a "transition zone" from initial to complete injury, it is likely that in vivo it is more important an issue for heating and cryo since there will be diffusional limitations that would slow heat and cold down. However, further modeling and experimental characterization are necessarily to confirm these arguments.

Table A1.1. *Treatment comparison*

	IRE	Cryo	Heat
Duration	<10s	>10min	>10min
Critical Factors	Electric field, pulse duration, pulse number	End temperature, Cooling rate	End temperature, holding time
Initial Injury Threshold	750V/cm, 100 of 50us pulses	-10^{o}C at 5^{o}C/min	40^{o}C for 0 min
Complete Injury Threshold	1250V/cm, 100 of 50us pulses	-40^{o}C at 5^{o}C/min	60^{o}C for 0 min
Issues	Muscle contraction	Heat diffusion from blood vessels	Heat diffusion from blood vessels

Appendix A2. *Possibility of Protein Denaturation during Irreversible Electroporation*

A2.1 Introduction

One of the major benefits claimed for IRE compared to other traditional focal therapies (radiofrequency heating or cryosurgery) is that IRE does not rely on thermal effect to create injury. Many theoretical and experimental studies [52], [101], [111] have confirmed that although tissue heating does exist during IRE due to Joule heating, the temperature rise and thermal dose are too low to induce significant thermal injury. Therefore, other mechanisms primarily associated with lipid membrane poration or permeabilization are thought to be responsible for cell injury during IRE as reviewed in previous chapters (Chapter 1.3.3, Chapter 3, Chapter 5.1). While these mechanisms are generally accepted, there is also the possibility that IRE could cause protein denaturation and that too can contribute to cell injury. This appendix shows some preliminary results that begin to address whether IRE has an impact of cellular proteins.

A2.2 Materials and Methods

A2.2.1 Cardiac muscle cell cultures

A HL-1 cell line was cultured as adherent monolayers [156]. More specifically, cells were grown in T-75 flasks with Claycomb medium (51800C, Sigma-Aldrich, St. Louis, MO) supplemented with 10% fetal bovine serum, 2mM L-Glutamine, 100U/ml of Penicillin/Streptomycin, and 0.1mM Norepinephrine. When 90% confluence was reached and spontaneous beating was elicited (observed under the microscope), the cells were detached by adding 0.05% Trypsin-EDTA (Invitrogen, CA) and then formed into a single cell suspension (0.5~0.6 million cells/ml).

A2.2.2 Irreversible Electroporation Treatment

400µl volumes of the prepared HL-1 suspensions were pipetted into electroporation cuvettes (Fisher Scientific), which were then placed in an external electrical field created by an electrical pulse generator (BTX ECM 830, Harvard Apparatus). The IRE parameters were chosen to be 300V, 50µs, 50#, and 10Hz. The output voltages and currents were monitored by an oscilloscope (Tektronix TDS 2002).

A2.2.4 Thermal (Heat) Treatment

10µl volumes of the prepared HL-1 cells were placed in a sample pan then placed in a differential scanning calorimeter (DSC) which controls the heating rate and end temperature. The cells were first held at 25^{o}C for 1 min before being heated to end temperature of 85^{o}C at 5^{o}C/min, after being held at 85^{o}C for 1 min, the cells were cooled to 25^{o}C at 5^{o}C/min and then the first step was repeated. These protocols have been previously established to insure a controlled and uniform denaturation of the cellular proteins in a cell type of interest [165]. The difference between the excess specific heat in the initial and final heating protocol is a measure of available protein denaturation within that cell system. Anything that reduces the protein available for denaturation in the first step will reduce the overall excess specific heat due to protein denaturation. This in turn can then be further interrogated as a source of protein denaturation prior to heating (i.e. potentially IRE).

A2.2.5 Protein Denaturation Assay

The IRE treated cell suspension was centrifuged and transferred to the DSC machine for protein denaturation assay as described in [165]. The protein denaturation is measured by comparing the apparent specific heats between the initial and final heating cycles.

The cell concentrations of both the IRE and heat treated cells are standardized so that the initial protein concentration per cell population was the same and hence a change in the excess specific heat would imply the amount of protein that was available to denature in the two cases (IRE VS. heat alone).

A2.2.6 Data Analysis

The second heating curve in each Cp graph was corrected using a baseline correction protocol [165]. The difference in the area under the first heating and second heating corrected was obtained from each graph and averaged in order to create the total denaturation plots. The IRE, post heating, and control curves were normalized using the corresponding control curve for that set of experiments. The average of the normalizations was used in order to obtain the fractional denaturation plots.

A2.3 Results and Discussion

Both the IRE and heating protocols were chosen at levels that would induce 100% cell destruction (Figure 1.6, [165]). As can be seen from Figure A2.1, almost 100% protein has denatured post heating treatment. This result is expected since protein denaturation is a major mechanism of heat injury. However, despite the fact that IRE does not cause injurious heating at our chosen level, only a fraction (~33%) of the protein was left undenatured after IRE.

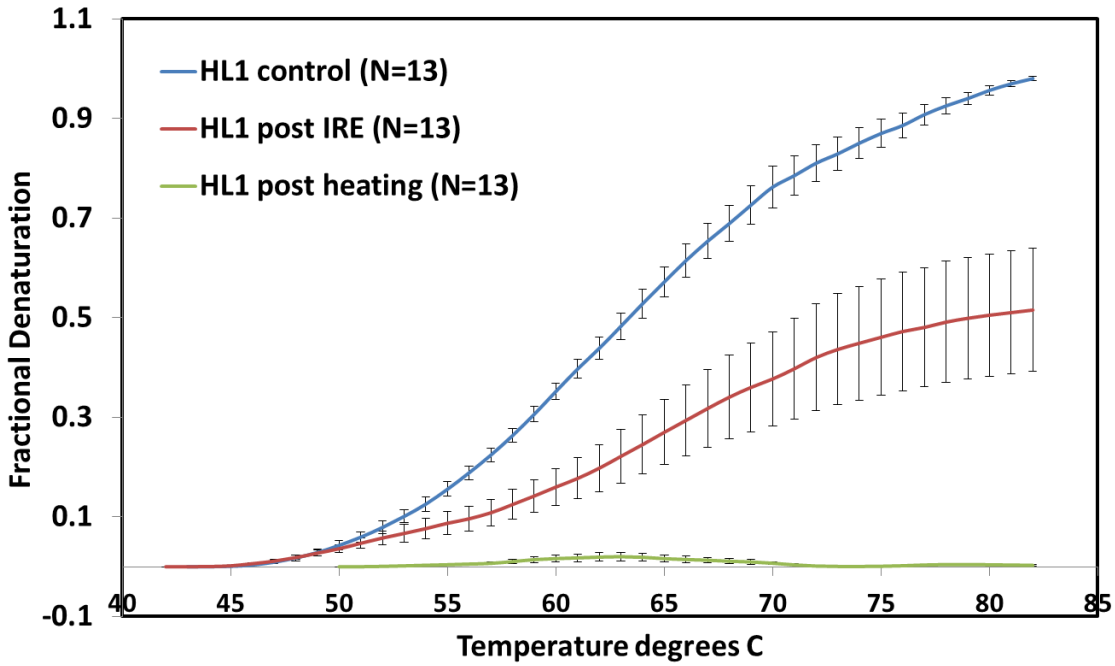

Figure A2.1. *Fraction of protein denaturation post IRE and heating. (N=10 error bars represent standard errors)*

At least two possible mechanisms can explain why the amount of protein that denatured was significantly lowered after IRE. Firstly, although our chosen IRE level does not cause heat induced protein denaturation, it is possible that some proteins in the cells were electrically denatured due to intensive electric shock. This mechanism was first proposed by Lee. et. al. [34] and was named “electro-conformational denaturation” of proteins, many of which are related to the iron channels or pumps on the cell membrane. In addition, because of the permeability change during and shortly after IRE, intercellular proteins could leak out of the cell membrane and be washed out with the medium during centrifugation. Further study is still needed to characterize what portion of the protein loss was due to denaturation versus membrane leakage. Nevertheless, these initial

results clearly indicate that protein loss by denaturation or leakage is likely a real and underappreciated event that may contribute to injury during IRE.

Appendix A3. *Electroporation with Low Electric Fields and Extra Large Pulse Numbers*

A3.1 Introduction

The role of the three critical IRE parameters has been discussed previously in Chapter 1.3.4. In brief, the electric field appears to be the deterministic factor of injury post IRE. For the LNCaP cell line, when the electric field is lower than 500V/cm, simply increasing the pulse number or pulse duration cannot induce cell injury from IRE (Figure 1.5). Moreover, the pulse number and pulse duration appears to act as treatment dosage of IRE. When the electric field exceeds a specific threshold, the number and duration of the pulses can affect how much percentage of cells can be killed.

However, this appears to be contradictory to the findings from a study by Rubinsky's group [17], in which complete cell death (100%) can be achieved for an E-field as low as 125V/cm. As this result is in direct conflict with most of the field [Weaver], we set out to repeat the study and test if complete cell death can be achieved by low E-field (lower than 500V/cm) given sufficient pulse number and duration.

A3.2 Materials and Methods

The cell line we used for this study is LNCaP Pro 5, a prostate cancer cell line we have used in Chapter 2. The cell culture procedure, IRE protocol, and viability assessment methods are exactly the same as described in Chapter 2.

A3.3 Results and Discussions

Our results (titled UM results) are summarized and compared with Rubinsky's [17] in Table A3.1. The pulse duration and frequency are the same in both studies. Only pulse

number and electric field and cell type have been changed for each data point. Both of our results achieved around 54% viability after IRE for 17 of 1500V/cm IRE pulses. However, the results start to diverge for cases with 1000V/cm and 750V/cm. The biggest difference happens with electric fields lower than 500V/cm. In our results, increasing the pulse number to extreme large numbers (e.g. 3840 at 125V/cm) did not induce significant cell destruction (<10%), while in Rubinsky's results, complete cell destruction (100%) was achieved for the same parameter combo.

Table A3.1. *Comparison of viability results after IRE treatment in vitro. (pulse duration is 100μs, frequency is 10Hz for all cases)*

Pulse #	**3840**	**960**	**240**	**106**	**60**	**17**
E-field	**125**	**250**	**500**	**750**	**1000**	**1500**
UM results (n=3, ave±SD%)	93±0.2	88±2	90±2	46±8	43±8	54±14
Rubinsky's results (n=12, ave±SD%)	0	0	0	12±4	27±9	56±12

Although variations of some experimental conditions could cause differences in the viability results, such as cell type, medium component, and viability assay, the huge differences between our studies (10% versus 100% cell destruction) is hard to be accounted for with these variations.

Another factor that might cause significantly higher cell destruction in Rubisky's study is the possibility of introducing delays between pulse trains when applying the large pulse numbers (240~3840). The pulse number that can be delivered in one train with their pulse generator (ECM 830, Harvard Apparatus) is 99. To deliver up to 3840 pulses in one treatment, at least 39 pulse trains need to be applied. If the researcher introduced seconds of delays between these pulse trains, the injury can be significantly enhanced

due to the pulse timing enhancement effect introduced in Chapter 2 and 3. In summary, our attempts to repeat the findings in Rubinsky's study [17] that complete cell destruction can be achieved with ultra-low electric fields (<500V/cm) and large pulse numbers was not successful. This suggests, based on our results and the literature we have reviewed in Chapter 1, that E-fields of >500V/cm are needed for IRE.